DOE/CS/52059-1
Dist. Categories UC-4,
94a, 94c, 94d, and 96.

Development of Lightweight Hydrides

DOE/CS/52059--1

DE83 004227

July 1982

Prepared by:
J.F. Nachman, David A. Rohy, and
T.A. Argabright
Solar Turbines, Inc.
San Diego, CA 92138
Under Contract No. DE-AC03-78CS52059

Prepared for:
U.S. Department of Energy
Assistant Secretary, Conservation
and Renewable Energy
Office of Vehicle and Engine R&D
Washington, D.C. 20585

Alternative Fuels Utilization Program

TABLE OF CONTENTS

TABLE OF CONTENTS (Contd)

LIST OF FIGURES

LIST OF FIGURES (Contd)

LIST OF FIGURES (Contd)

LIST OF FIGURES (Contd)

LIST OF TABLES

LIST OF TABLES (Contd)

ACKNOWLEDGEMENTS

The authors express their appreciation to Mr. E. E. Ecklund and the Alternative Fuels Utilization Program (AFUP) of the U.S. Department of Energy for their support of this work. Thanks are also due Mr. W. J. D. Escher of E:F Technology, Inc., for his critical review and helpful comments on the manuscript for the final report.

GLOSSARY OF TERMS

a/o	Atomic percent
Acicular (hydrides)	Elongated or needle-like
Comminution	The progressive reduction to minute particles of materials as during reported hydriding/dehydriding cycles
ΔT	The change in temperature (°C) experienced during the hydriding and dehydriding cycle
Disproportionation	The transformation of a substance into two or more dissimilar substances usually by simultaneous oxidation and reduction
EDX	Energy Dispersive X-ray
Hypereutectic	An alloy with more of a given element than is contained in the eutectic composition
Isotypic	Exhibiting the same type of crystal structure
Master Alloy	An alloy, rich in one or more desired addition elements that can be added to a melt to adjust the percentage of a desired constituent
Mini-PC Isotherm	An abbreviated form of pressure-composition isotherm based upon three or four data points
Proeutectic (intermetallic)	The express intermetallic phase (eutectic constituent) that precipitates before the eutectic composition is reached during the solidification of an alloy
SEM	Scanning Electron Microscope
T_D	Temperature at which pressure of fully hydrided alloys equals 1 atmosphere
Temperature of Stability	Temperature to which intermetallic compound remains stable to decompositon or melting
w/o	Weight percent

x-ray dot pattern	X-ray concentration photographs or X-ray dot maps show the qualitative distribution of individual elements within a particular field of view on the Scanning Electron Microscope. Concentrations of specific elements in different phases or particles can be shown with a high of resolution. In conjunction with SEM secondary electron image photographs, X-ray dot maps provide a pictorial view of elemental distributions.

ABSTRACT

Automotive use of hydrogen as a fuel (energy carrier) is a future option in a world with low petroleum reserves. Hydrogen has a high energy content per pound and produces relatively few emissions when burned. Two basic problems restrict the exercise of that option; methods must be developed to produce hydrogen economically from renewable or solid fossil fuel sources and the need for practical onboard systems to store hydrogen in a safe, dense and relatively lightweight configuration. The authors have concentrated their efforts on the development of the metal hydride approach for hydrogen storage.

Metal hydrides can store more hydrogen per unit volume than normal high pressure or even cryogenic hydrogen techniques. Little energy is required to store the hydrogen in the hydride, and high stability at room temperature ensures low losses over long storage periods. Safety features of metal hydride storage are favorable. Because of its low weight and high hydrogen storage densities, modified magnesium alloy-based hydrides appear to offer the greatest potential for automotive storage of hydrogen. Recent experimental and analytical work has been directed toward the optimization of this storage system. Due to the relative stability of MgH_2, modifications of the form MgMHx (M = metal atom) have been made to decrease the dissociation temperature while retaining high hydrogen capacity. This parameter is crucial since vehicle exhaust will supply the thermal energy to dissociate the hydride in an automobile. System studies indicate that hydride dissociation temperature should be 200°C or lower to ensure uninterrupted fuel flow at all driving and idle conditions.

This report describes the authors' modifications to magnesium hydride based families of materials and is presented with a review of other relevent research on magnesium alloy hydrides to provide a comprehensive treatise to allow the reader to better understand the direction and contribution of this newly reported work.

1

EXECUTIVE SUMMARY

This report summarizes the authors' study of magnesium alloy hydrides for use as hydrogen fuel storage in future automobiles. The work was sponsored by the Alternative Fuels Utilization Program, U.S. Department of Energy. Mr. Eugene Ecklund was the technical monitor. The activities leading up to the results reported here took place from August 1978 to January 1982 in the Research Laboratories of Solar Turbines Incorporated in San Diego, California.

Hydrogen is considered to be an excellent energy carrier and automotive fuel for use in a predominantly, non-petroluem, future period. Many non-portable energy resources such as solar and nuclear can be transformed into hydrogen which can be used efficienctly and cleanly in engines very similar to those in production today. Unfortunately, storing the hydrogen aboard a vehicle is not a simple feat. To obtain sufficient range for the vehicle, about 5 to 15 kg of hydrogen must be contained in a readily available form. Cryogenics, compressed gas, chemical carriers and metal hydrides have been considered as candidate hydrogen storage means. This study addreses one means thought by the authors to offer an attractive potential for low weight, energy conservation and safety -- metal hydrides.

The metal hydrides studied and discussed in this report are all based on magnesium. The hydrides of magnesium have high hydrogen contents and low weight densities leading to hydrogen capacities of 4 to 7 percent by weight. Alloys existing at the beginning of this work were not acceptable because of high dissociation temperatures or high contents of strategic elements, e.g. nickel. The goals of this program effort were directed to the reduction of the hydrogen dissociation temperature and the formulation of alloys with almost no rare or strategic elements. Thus the program was metallurgical in nature. Alloys were formulated and tested in small batches. If the screening criteria were not met, no further work was done on an alloy. More complex and time consuming tests were performed on alloys that appeared to meet the technical objectives. Consequently, the authors did not build an automobile fueling system nor conduct engine tests. All work was centered on achieving an acceptable magnesium based hydrogen storage alloy.

Small (15 to 30 gm) samples of over 200 alloys were prepared and tested in this program. The alloys were divided into several families or classes shown in the next chapter. Usually the results of one set of alloys yielded information that led the authors to investigate the following set of alloys. Each alloy was prepared according to a strict laboratory procedure which included x-ray analysis. A minimum set of pressure-temperature-composition measurements was taken and the hydrogen capacity of the alloy was determined. The alloys that met some of the conditions required for automotive fuel storage were subjected to additional tests such as metallurgical analysis, chemical analysis, comminution studies and more complete isotherm recording.

About four of the most favorable alloys were subjected to a larger scale test in which 450 grams of the alloy were subjected to a long term cycling with hydrogen gas. This test simulated the problems encountered in refueling a hydride system over the life of a vehicle.

The alloys selected as being the best candidates for an automotive hydrogen fuel system are listed in Table 1. Some of the properties of the chosen alloys are shown in the same table along with section references for further reading. No one alloy met all the prescribed conditions. The work presented in this report should aide future researchers in this area.

Table 1

Comparative Properties of Hydride Alloys

Authors Alloy Designation	Composition	Alloy Density g/cc	Weight Percent H_2 Absorbed	Section Reference In This Report
	SELECTED ALLOYS			
149	$Mg_{0.845}Ni_{0.05}Cu_{0.1}Y_{0.005}$	2.37	4.42	3.1
14L	$Mg_{0.7}Li_{0.1}Ni_{0.1}Sn_{0.1}$	3.36	2.32	3.2.4
14A	$Mg_{0.56}Al_{0.34}Y_{0.1}$	2.56	3.6	3.3.1
23A	$Mg_{0.8}Al_{0.1}La_{0.1}$	2.41	4.22	3.3.2
	REFERENCE ALLOYS			
Fe-Mn-Ti	$Fe_{0.5}Mn_{0.5}Ti$	5.44		--
$LaNi_5$	--	8.43	1.5	--
Mg_2Ni	--	3.44	4.2	Appendix A
Mg	--	1.74*	7.6	--

*ASM Metals Handbook, 8th Edition, Vol. 1, 1961. All other values were measured in the Solar Laboratories.

2

INTRODUCTION

2.1 BACKGROUND

Hydrogen is a candidate fuel for transportation in the long term (post 2000) period. While it is not a primary energy resource but rather an energy carrier, it offers several advantages. It is reasonably easy to produce. It can be consumed in heat engines or fuel cells without costly fuel preparation devices. If NOx is controlled, hydrogen can be consumed with very low emissions. There are two major drawbacks for this fuel. Hydrogen is neither inexpensive to produce nor easy to store. The production problem is presently being approached by the research community, e.g., by looking at thermochemical water-splitting processes driven by the heat of a nuclear reactor. Four major methods have been advanced for hydrogen storage. They are shown in Table 2 with some advantages and disadvantages. E. E. Ecklund and F. L. Lester (Ref. 1) have analyzed these storage options and concluded that further research is warranted on lightweight metal hydrides. Appendix A provides an overview on lightweight hydride research status in general, as background.

2.1.1 Physical Description of Hydrides

Many metals (e.g., Ti, V, Nb, Pd, Sc, etc.) and alloys have the ability to absorb large amounts of hydrogen into interstitial crystal locations (see Fig. 1). the resulting material is a metal hydride. The hydrogen can be readily dissociated from some of these alloys by the application of thermal energy. The original alloy remains after the hydrogen has been removed. Hydrogen can be re-introduced into the metal and removed from it indefinitely with little change in the parent material.

The metal hydrides have several common features:

- Hydrogen is stored in interstitial sites in the metal lattice.
- Hydrogen density is equal to or greater than that of liquid hydrogen (0.07 g/cc).
- The heat of formation is relatively low (ΔH_f = -73.7 x 10^3 joules/mole).
- Hydriding and dehydrding can be performed indefinitely.

The amount of hydrogen absorbed into the lattice of the material varies with electronic and lattice structure of the material. With knowledge of materials

Table 2

Hydrogen Storage Concept

Concept	Advantages	Disadvantages
Metal Hydrides	High storage density Room temperature storage	High temperatures required to dissociate
Cryogenic	High storage density	Safety Energy required to liquefy
Compressed Gas	Proven technology	Low storage density
Chemical	Good kinetics	High weight

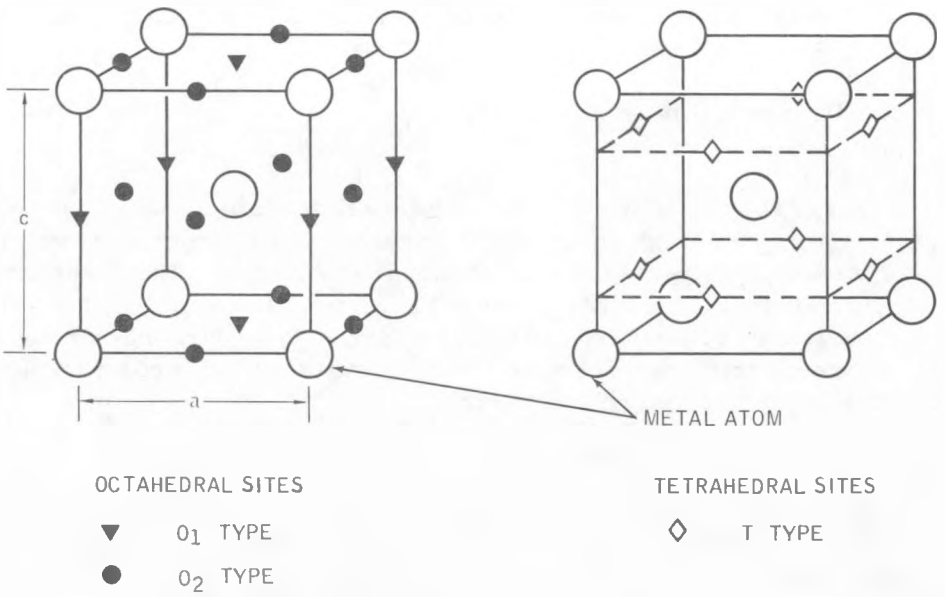

Octahedral (O) and tetrahedral (T) sites in a body-centered tetragonal (bct) lattice. Metal atoms show as the large open circles. In a body-centered cubic (bcc) lattice, O_1 and O_2 sites are indistinguishable. C and A are Lattice Parameters of Tetragonal Cell.

Figure 1. Interstitial Sites for Hydrogen in a Body-Centered Tetragonal Crystal Lattice.

in this regard, one can select combinations of elements that are more likely to form hydrides with a high H/M (hydrogen/metal atom) ratio. Figure 2 shows the temperature pressure relationships for several metal hydrides. The hydrogen is absorbed into the metal through a multistep process. In the first step, the H_2 molecule must be adsorbed and then reduced to atomic hydrogen at the surface of the material. The hydrogen is then adsorbed and diffused into the material. The hydrogen diffuses rapidly in the metal lattice occupying the interstitial locations.

The formation of the hydride in this manner is almost always exothermic once a threshold temperature or pressure has been obtained. The threshold level depends to a great extent on the condition of the metal surface. Oxide films inhibit the formation of the hydride, while small particle size is desirable for the rapid production of metal hydrides with a high H/M ratio. Since the lattice constants often expand by ten percent or more upon the introduction of hydrogen, many metals crumble, crack or become extremely brittle when hydrided, resulting in a pulverizing or comminution effect. Cyclic absorption and desorption of the hydrogen in a metal increases and cleans the surface area, resulting in the formation of the hydride at a lower threshold temperature. Maximum concentrations of one, two, or three hydrogens per metal atom are common with some ternary systems displaying higher H/M ratios under special conditions.

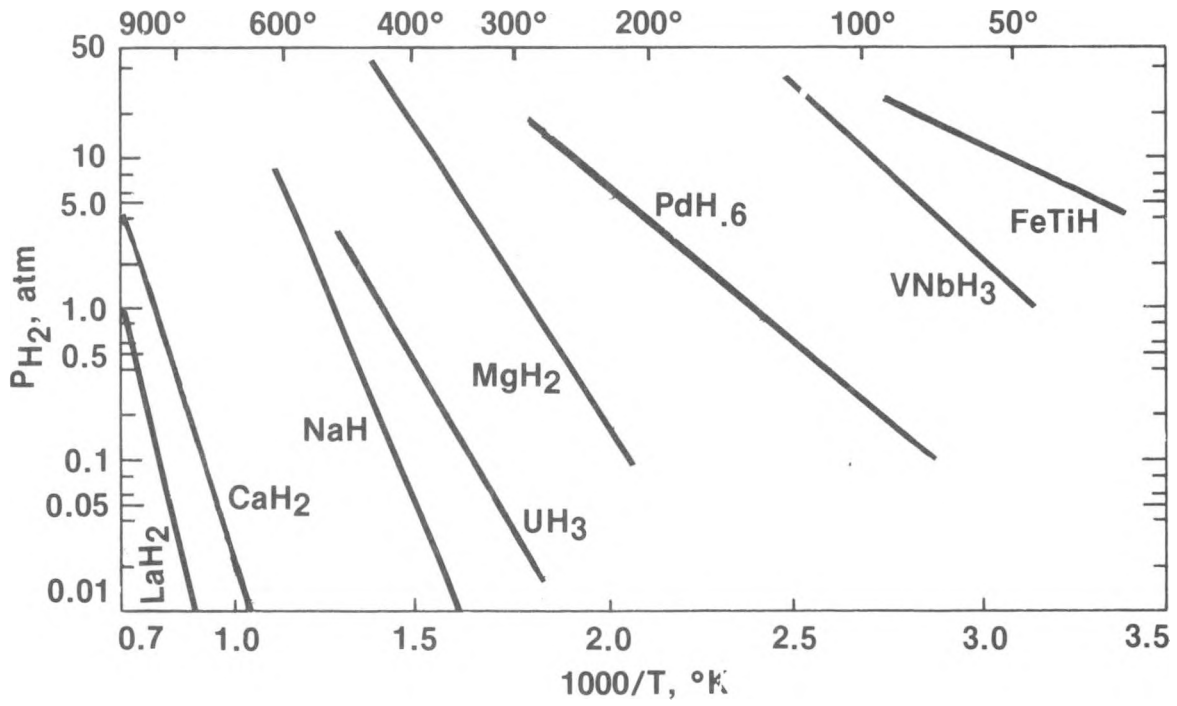

Figure 2. Dissociation Pressure-Temperature of Hydrides

2.1.2 Selection of Hydride Forming Alloys

Since so many alloys do form hydrides, criteria were developd to limit the scope of investigation to the most practical alloys. The criteria are:

- inexpensive nonstrategic material
- low mass density
- high hydrogen mass-fraction
- moderate dissociation temperature
- good kinetics

A comparison of the mass and volumetric densities with storage capacity is shown in Table 3 for several hydrides. The data for the hydrides are the highest reported values and may not represent performance in an actual hydrogen storage system.

Table 3

Comparisons of Various Metal Hydrides With Cryogenic Storage of Hydrogen

	Wt % Hydrogen	Relative* Mass Storage	Volumetric Storage of H_2 g/ml	Relative** Volumetric Storage
LH_2	100	1	0.07	1.0
MgH_2	7.6	13	0.132	0.53
TiH_2	4.0	25	0.187	0.37
VH_2	3.8	26	0.234	0.30
$FeTiH_2$	1.9	53	0.123	0.569
$LaNi_5H_{6.7}$	1.5	67	0.126	0.555

*Weight of metal hydride required to store one unit of hydrogen compared with LH_2. Container weight not included for hydrides or LH_2.

**Volume required to store one unit of hydrogen compared with LH_2 storage.

The two alloys that best satisfy the screening criteria are the magnesium based alloys and the iron-titanium alloys.

These two hydrides are compared in Table 4. FeTi has been used in experimental vehicles by The Billings Corporation of Independence, Missouri, and Daimler Benz. It has an advantage of low dissociation temperature. The magnesium alloy hydrides offer considerably greater storage capacity per pound but suffer from a high dissociation temperature. Due to the favorable storage density for magnesium hydrides, the reported work was directed at reducing the dissociation temperature of the magnesium based alloys.

Table 4

Metal Hydride Comparison (Theoretical Basis)

	FeTi	Mg Alloys
Weight for 320 km (200 mile) range (kg)	577	191
Cost per Vehicle ($) for hydride material only	1300	420
Hydrogen Capacity (%)	2	7
Dissociation Temperature (°C)	0	220

2.1.3 Description of a Hydrogen Storage System

A hydrogen storage system for automotive use might resemble that shown in Figure 3. That figure illustrates the general components of such a system but does not represent an actual system. The hydride bed shown in Figure 3 would contain between 48 and 382 kg of metal hydride depending on the range of the vehicle and its energy requirements. This added weight penalty is small in comparison with battery systems. Figure 4 illustrates the difference in weight for fuel systems composed of magnesium hydride, iron-titanium hydride and NiCad batteries* for the same vehicle range. While none can compare favorably with gasoline, magnesium hydrides are clearly superior to battery storage and the iron titanium alloys on a storage system weight basis.

---

*Nickel cadmium batteries, used extensively in aircraft electrical systems since they are relatively lightweight, are not usually taken to be acceptable for battery-electric vehicles because of their high cost.

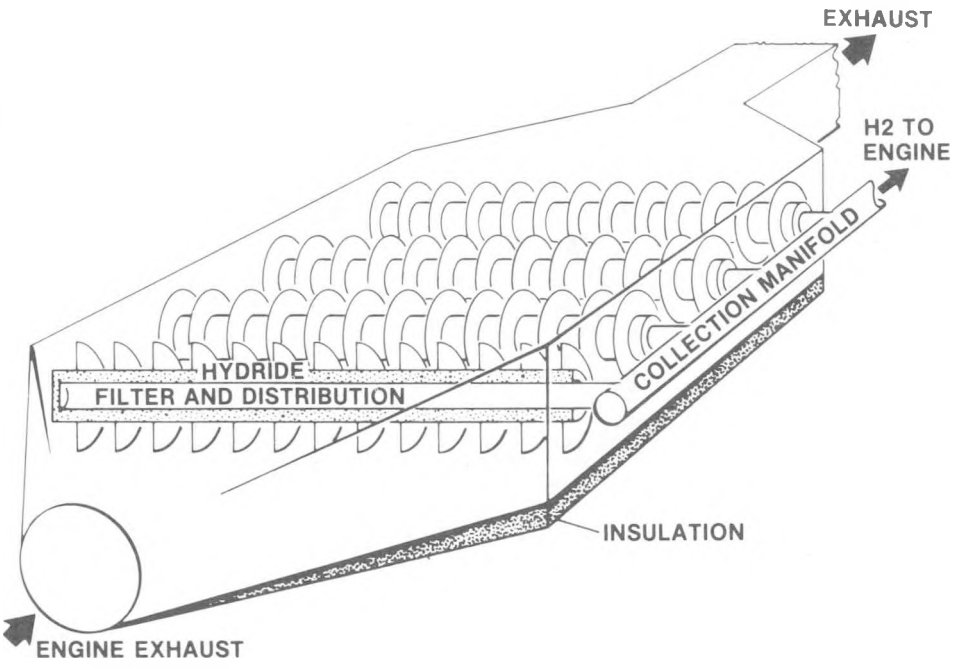

Figure 3. Automotive Hydrogen Storage System

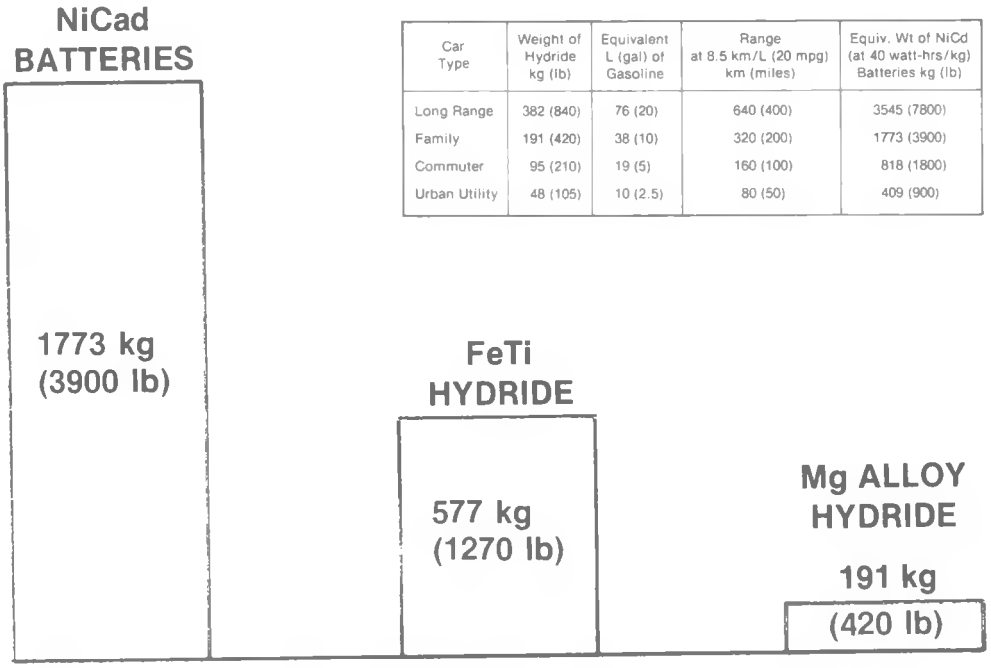

Car Type	Weight of Hydride kg (lb)	Equivalent L (gal) of Gasoline	Range at 8.5 km/L (20 mpg) km (miles)	Equiv. Wt of NiCd (at 40 watt-hrs/kg) Batteries kg (lb)
Long Range	382 (840)	76 (20)	640 (400)	3545 (7800)
Family	191 (420)	38 (10)	320 (200)	1773 (3900)
Commuter	95 (210)	19 (5)	160 (100)	818 (1800)
Urban Utility	48 (105)	10 (2.5)	80 (50)	409 (900)

Figure 4. Energy Storage Weight for 200 Mile Range
(see footnote, page 7)

The cost of the alloy for a 191 kg magnesium alloy hydride bed is approximately $695 in 1981 dollars. This is equivalent to $3.64/kg ($1.65/lb). The cost of tankage, heat exchangers, and systems components is not included in this estimate. Minimizing the hydrogen pressure and the mass of the hydride material will reduce the cost of the tankage and heat exchangers.

2.2 PROGRAM GOALS

On-board fuel storage is a basic limitation to the use of hydrogen as an automotive fuel. Metal hydrides can store hydrogen at the same volumetric density as cryogenic methods, but generally incur serious weight penalties. Among the relatively common materials, magnesium-base alloys offer the best (lowest) weight density. The objective of the reported work was to characterize several magnesium-base alloys to store hydrogen that meet the operating constraints of a conventional automobile with a spark ignition engine. Specific design criteria include:

- Dissociation Temperature - The dissociation temperature of the magnesium hydride must be 200°C or less (see Section 2.3). The hydride bed must provide hydrogen at one atmosphere pressure or more when heated to that temperature.

- Weight - It must store 9 to 23 kg (20 to 50 pounds) of hydrogen with total weight of hydride metal plus containment tank and heat exchanger system sufficiently low to not seriously impair vehicle performance.

- Storage Density - The volume/pound of hydrogen must be sufficiently low to allow installation in a vehicle and, nominally, must be close to the density of liquid hydrogen [0.07 g/cm^3 (4.4 lbs/ft^3)].

- Waste Heat Utilization - The heat of dissociation and temperature/pressure relationship of the metal hydride must be in a range that allows waste heat of the engine, alone, to be utilized for hydrogen generation.

- Rate of Dissociation - The hydride must dissociate at a rate high enough to supply a continuous flow of hydrogen for steady state [0.62 g/sec to 1.25 g/sec (5 to 10 lb/hr)] and transient [3.15 to 6.3 g/sec (25 to 50 lb/hr)] fuel flow rates. The system must be designed to handle virtually instantaneous flow transients from engine idle to full power (i.e., maximum flow).

- Startup - A startup system to supply hydrogen immediately from a cold condition must be provided.

- Cost - The cost of the basic hydride must be compatible with typical automotive materials cost requirements of approximately $2.20/kg ($1.00/lb) (1976 dollars).

2.3 DISSOCIATION TEMPERATURE GOALS

The dissociation temperature goals calculations are shown in this section. The original goal was 200°C as reported in Solar's earlier document for ERDA/DOE, report TEC-75/002 (Ref. 2). This goal was based on a minimum exhaust gas temperature of 866°K derived from a gasoline fueled internal combustion engine. The calculations presented here are based on the data from King and Mogens (Ref. 3) as presented in report TEC-75/003 (Ref. 4) as Figure 5.1. Two operating points were chosen: Equivalence Ratio = 0.5 and Equivalence Ratio = 1.0. The temperatures measured 7.6 cm from the exhaust valve were recorded as 640°K and 825°K (see Fig. 5). Using the equation on page 46 of Reference 2, we find for the higher temperature, 825°K.

$$59.9 \text{ J/kg} \times \frac{(825°K - z)}{(825°K - 293°K)} = 27.4 \times 10^6 \text{ J/kg}$$

$$z = 493°K \ (220°C)$$

and for the lower temperature, 640°K:

$$59.5 \text{ J/kg} \times \frac{(640°K - z)}{(640°K - 293°K)} \quad 37.4 \times 10^6 \text{ J/kg}$$

$$z = 423°K \ (150°C)$$

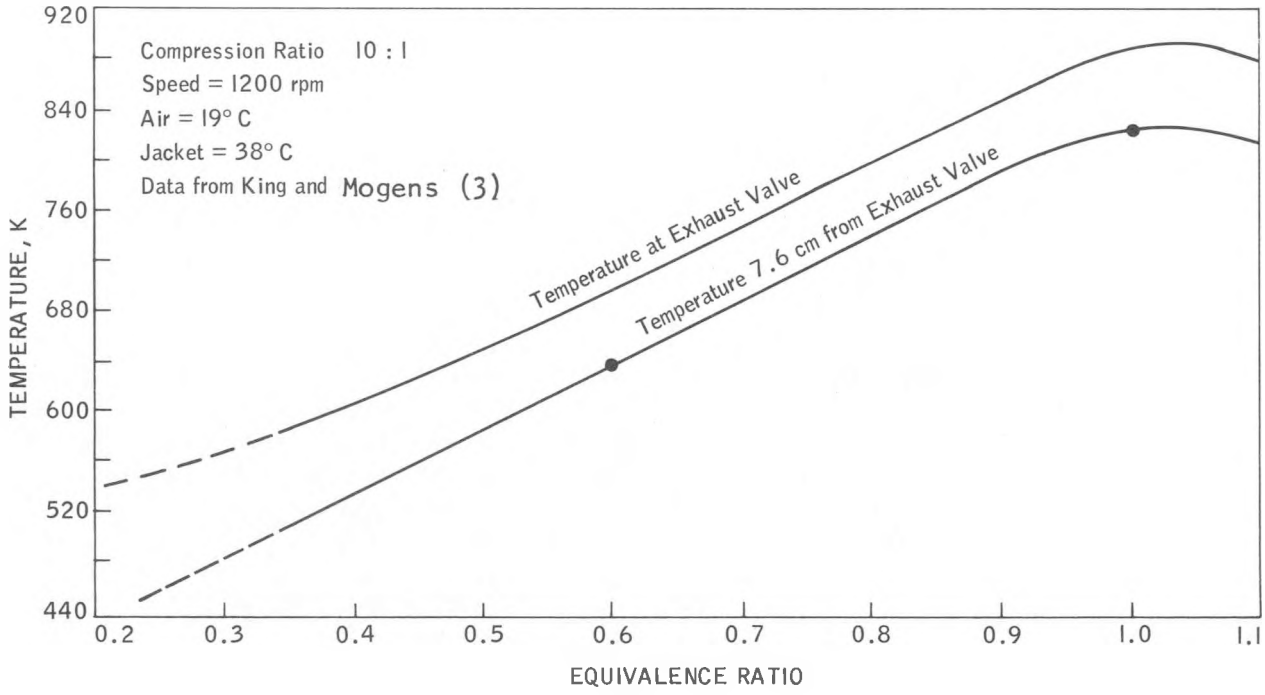

Figure 5. Exhaust Gas Temperature for CFR Engine Fueled With Hydrogen (Ref. 4). Two Selected, Representative Operating Points are Shown With Dots

To minimize the size and cost of heat exchangers it is common to utilize a 28°C (50°F) temperature difference between fluids in the heat exchanger. thus the maximum temperature of the hydride will be:

$T_{hydride}$ = 220 - 28 = 192°C (for Equivalence Ratio = 1.0)

$T_{hydride}$ = 150 - 28 = 122°C (for Equivalence Ratio = 0.6)

The first number is essentially the same as our past goal of 200°C. The second number is significantly lower, hence, more difficult to meet.

2.4 METALLURGICAL DEVELOPMENT

These system constraints and dissociation temperature goals were well recognized at the inception of this work. It was also accepted that magnesium hydride or its then-known alloy hydrides could not meet the dissociation temperature goals. Since the magnesium hydrides offered the potential of lightweight hydride hydrogen storage, the research efforts were concentrated on developing new or modifying known magnesium alloy hydrides that would have significantly lower dissociation temperatures while maintaining high hydrogen storage densities. A secondary goal was to minimize or eliminate any expensive or strategic alloying element from the selected alloys. The metallurigical development work to achieve these goals is described in detail in Section 3. The reader can achieve a sense of overview of that work in Figures 6 through 10. Each of the families of alloys investigated is shown in these figures. The alloys that best met the program goals are surrounded by the heavy boxes. While no one single alloy met program goals, the investigators believe that significant progress has been made and a detailed foundation laid for future efforts.

2.5 CYCLE TESTS

As a part of the metallurgical work several of the most promising alloys were made in quantity (454 grams, one pound) and subjected to cyclic tests. The tests simulated up to 2000 refueling cycles. New hydrogen was introduced for each cycle to simulate refueling with "fresh" hydrogen. In this way cummulative effects of gas impurities could be studied. Hydride samples were removed on a regular basis and studied for hydrogen capacity and particle size distribution. The information on these tests is reported in Section 4. It should form the basis for future investigations of hydride storage systems. The authors suggest that such tests be an integral part of any future alloy development effort since those tests reveal information concerning bulk properties of hydrides in a realistic operating mode.

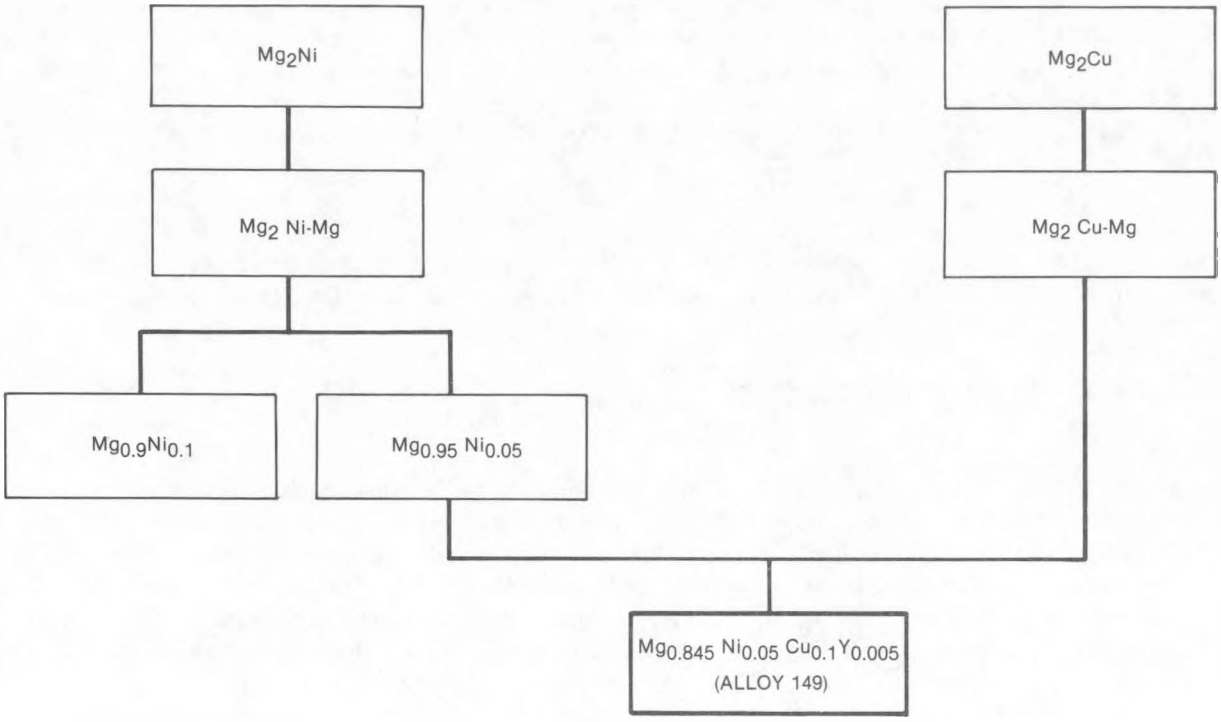

Figure 6. Magnesium Alloy Groups Evaluated and Reported in This Report

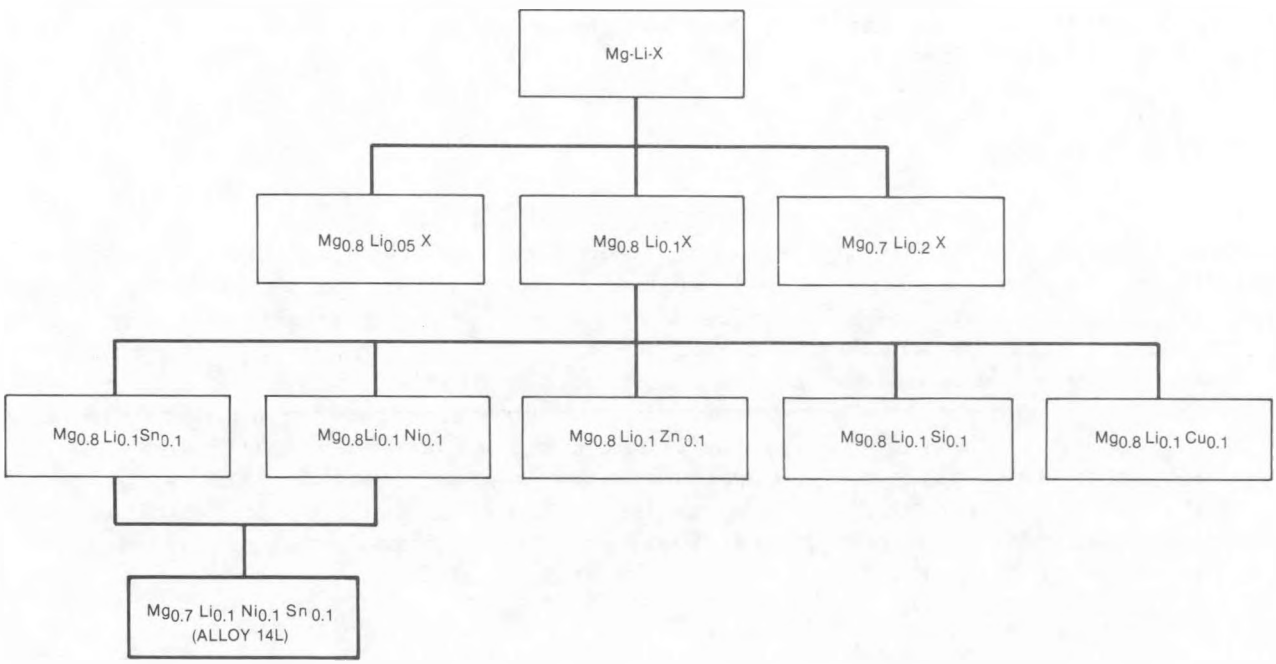

Figure 7. Magnesium Alloy Groups Evaluated and Reported in This Report

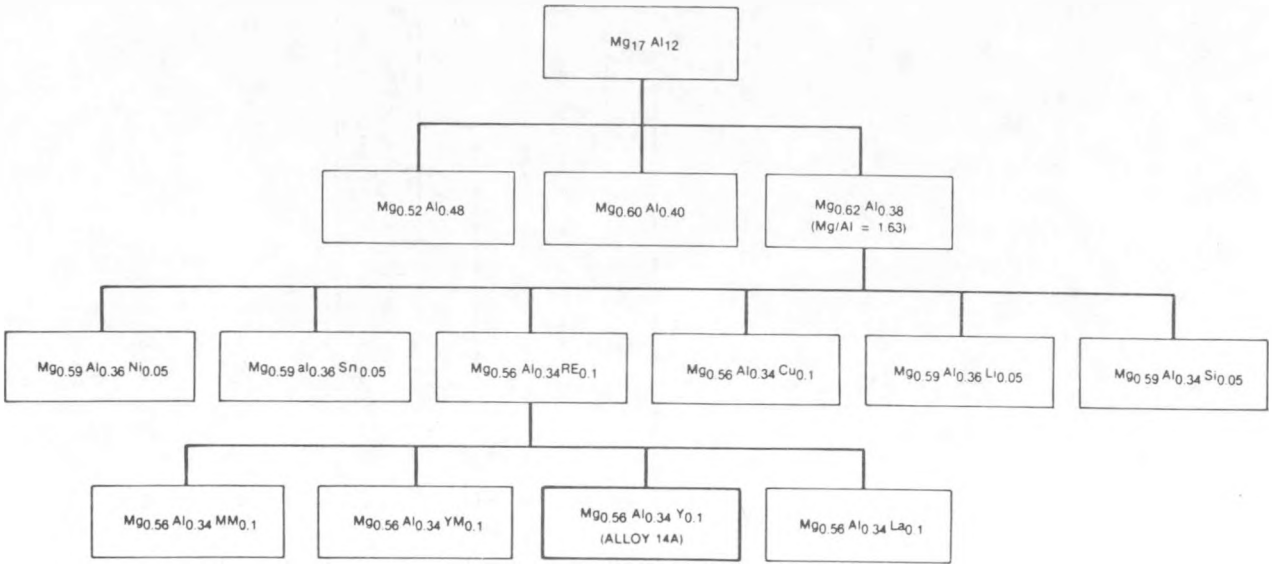

Figure 8. Magnesium Alloy Groups Evaluated and Reported in This Report

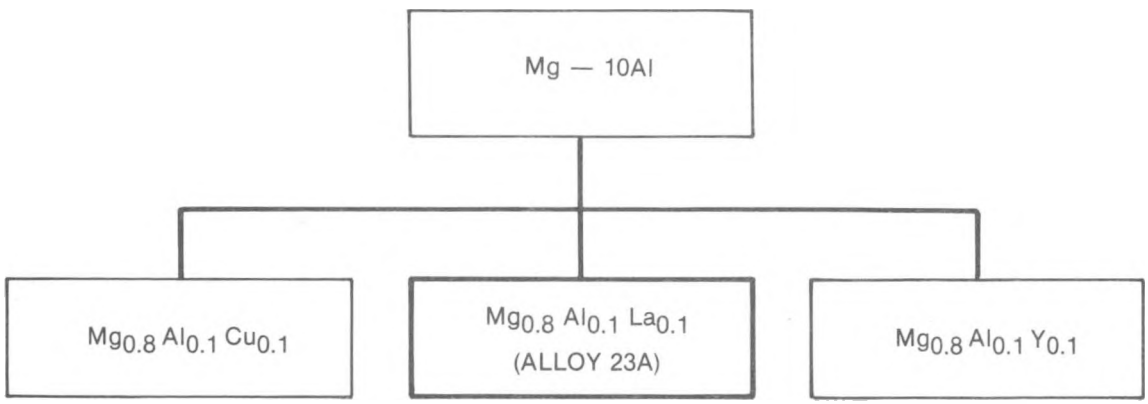

Figure 9. Magnesium Alloy Groups Evaluated and Reported in This Report

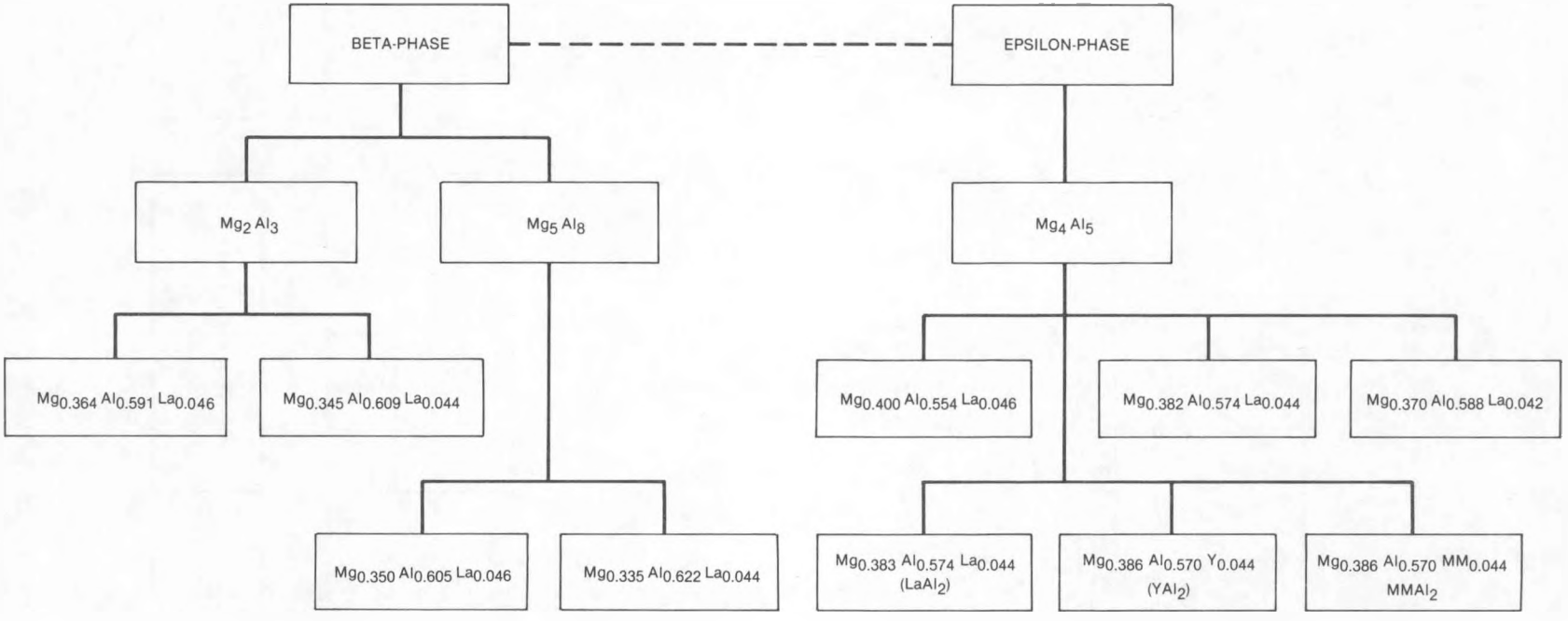

Figure 10. Magnesium Alloy Groups Evaluated and Reported in This Report

3

ALLOY STUDIES

This section of the report describes in some detail the extensive alloying program undertaken by the authors for the development of Mg-base alloy hydrides suitable for lightweight automotive hydrogen storage (refer to flowcharts in Figs. 6 through 10; also see Ref. 5 and Appendix A for previous work). One of the major objectives was to reduce the dissociation temperature of magnesium hydride without substantially decreasing hydrogen capacity. At the inception of this work, the Mg-Ni system, especially the Mg_2Ni phase, represented the best available alloy from the standpoint of favorable dissociation temperatures (plateau pressure of one atmosphere at 250°C) and good hydriding and dehydriding kinetics. Since the Mg_2Ni phase contains 54.6 weight percent Ni, another important objective of this investigation was to use as little as possible of this strategic and heavy metal.

Hydrides of magnesium and lithium both have many desirable characteristics for automotive applications. Their densities are very low and both contain substantial quantities of hydrogen on a theoretical basis: 7.55 weight percent for MgH_2 and 12.68 percent for LiH. Investigation of alloys combining the two elements appeared to be a logical step.

Likewise, alloys in the Mg-Al system as the Mg-10Al, gamma-phase ($Mg_{17}Al_{12}$), and the beta (Mg_2Al_3)- and epsilon (Mg_4Al_5)-phases indicated the potential of this system for higher plateau pressures and resistance to comminution, especially the Mg-10Al alloys. However, the very poor hydriding-dehydriding kinetics of these alloys prompted the authors to conduct a comprehensive alloying program to remedy these shortcomings.

The results of these alloy studies are described in detail under their respective alloy categories. Described also are studies involving effects of impurities and cycling upon the hydriding characteristics of these alloys.

3.1 MAGNESIUM-NICKEL-COPPER ALLOYS

The Mg-Ni-Cu hydride alloys were the result of an extensive alloying program at Solar (supported by DOE), which was based upon the investigation of ternary and multicomponent alloy additions to the basic $Mg_{0.9}Ni_{0.1}$ and $Mg_{0.95}Ni_{0.05}$ compositions.* Alloying additions consisted of Cu, Zn, Sn, Ga, V, Sn , B, Al, In, and rare-earth and related elements.

---

*Alloy compositions in this report are generally expressed in terms of atom fractions and atomic percent.

3.1.1 Preparation of Alloys

Experimental alloy preparation was conducted with a 30 kW Tocco motor generator, which because of its relatively low induction frequency produces a vigorous stirring in the melt. (Typically, induction furnaces operate at frequencies of ~3,000 to 10,000 Hz.) Except for the rare earths, high-purity elemental metals of better than 99.9 percent were used in the alloy preparation. The rare-earth metal additions were of 99+ percent purity. Certain elements were prepared as master alloys prior to addition to the induction melt.

Induction melting was conducted in an argon atmosphere in a low carbon steel crucible which also serves as a susceptor. (A susceptor absorbs the induced electromagnetic waves and converts them to heat energy.) The melt was allowed to solidify and cool within the crucible before removal to air. The ingots were radiographically examined and those which showed undissolved elements, evidenced by less dense areas of the radiograph were remelted.

3.1.2 Hydriding-Dehydriding

The sample, about 15 grams, was placed in an Inconel 600 reactor, evacuated and backfilled at least three times with ultra high purity hydrogen to purge the system, and finally pressurized to 300 psig. The reactor was heated, under pressure to 400°C, and then alternately evacuated and pressurized with hydrogen, about five minutes per cycle, for five cycles. The sample was held at temperature and pressure for one to two hours, and then cooled under pressure to room temperature. The reactor with a total capacity of 71 cc was evacuated, sealed, and reheated to the temperature of interest.

After allowing the temperature to come to equilibrium for at least one hour, hydrogen was allowed to escape into evacuated known volumes. The system pressure was measured after an equilibrium was obtained in approximately one hour. Temperature was controlled to within $\pm$1°C during equilibration. The quantity of gas withdrawn for each increment was calculated according to the ideal gas law. Weight of desorbed hydrogen in each increment was recalculated in terms of H/M ratio.

3.1.3 Screening of Alloys

In order to screen the many alloy combinations, only abbreviated or "mini-PC" (see glossary) isotherms were determined so that a maximum number of alloy combinations could be covered in a minimum amount of time. Three or four points were usually sufficient for the mini-PC isotherms to show the trend in plateau pressures.

After alloy optimization studies, Alloy 149 emerged as representing the best effort for low dissociation temperature combined with a low nickel content. The composition of Alloy 149 is $Mg_{0.845}Ni_{0.05}Cu_{0.10}Y_{0.005}$, in terms of the atomic fractions of the elements present. Characterization studies of Alloy 149 are discussed in the following sections.

3.1.4 Dissociation Characteristics

PC isotherms were determined for many alloys at 271, 299, and 310°C according to the procedures described above. The three isotherms for Alloy 149 are shown in Figures 11, 12, and 13, respectively. Comparing the isotherm in Figure 11 with that in Figure A-2 of Appendix A, one can see that the dissociation pressures of Alloy 149, with less than 10 weight percent Ni, are somewhat higher than those of the 25 weight percent Ni alloy at the same temperature.

A Van't Hoff plot of dissociation pressure versus 1/T yields the following relationship:

$$\log P_{atm} = -4225/T + 7.582 \quad (1)$$

3.1.5 Metallurgical Analysis

Extensive metallurgical studies were conducted on Alloy 149 in both unhydrided (as-cast) and partially hydrided forms. Main objectives of the Scanning Electron Microscopy (SEM) and microprobe analyses were (1) to identify visually the constituent phases showing greatest propensity for hydriding and (2) to determine the chemical compositions of these and all other phases through Scanning Electron Microscope/Energy Dispersive X-ray (SEM/EDX) analysis.

Alloy 149 exhibits a hypereutectic (see glossary) as-cast microstructure; with approximately 10 volume percent consisting of primary proeutectic (see glossary) hard needle-like intermetallic(s). SEM analysis (uncorrected) indicates these spikes or needles are an Mg-Cu-Ni intermetallic; probably of the general type $Mg(Cu,Ni)_{1.5}$ to Mg(CuNi), with copper the predominant species. Yttrium levels are typically very low in this phase, probably $<<0.1$ percent. The exact ratios of Mg-Cu-Ni are difficult to establish with a SEM/EDX program uncorrected for mutual absorption, but it is clear the proeutectic (and eutectic) intermetallics identified in this work are not stoichiometric, possibly due to rather rapid and nonequilibrium cooling rates during solidification.

The balance of the cast structure (~90 percent by volume) consists of a complex cellular or Chinese script eutectic, comprised of three distinct phases (see Fig. 14). The most readily identified eutectic phase, because it is essentially a physical outgrowth with common boundaries of the above proeutectic intermetallic, is again $Mg(Cu,Ni)_{1.5}$ to Mg(Cu,Ni). To facilitate discussion, this eutectic intermetallic phase is called Phase A. Phase A differs principally from its proeutectic variant (i.e., the needles noted above) in appearing to have appreciably more copper. Phase A provides the outline or network for the cellular eutectic structure in the form of an interconnected thin-wall maze. This intermetallic phase (Phase A) does not appear to hydride preferentially.

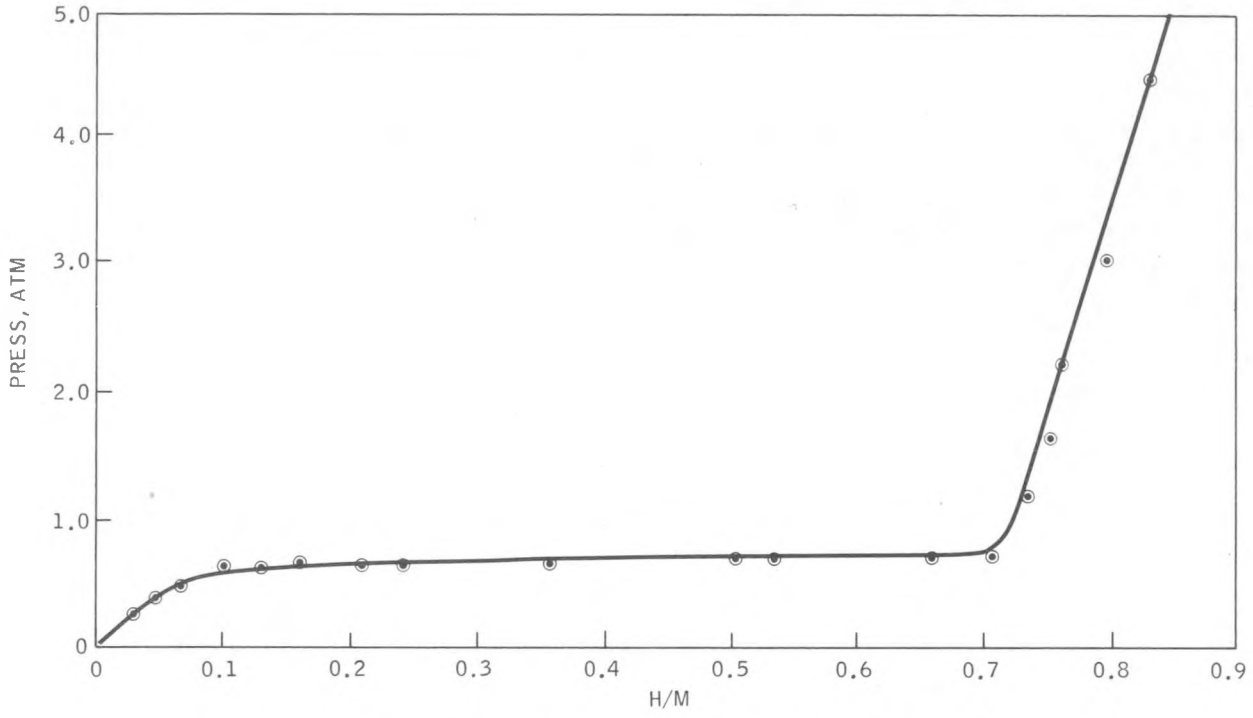

Figure 11. PCT Isotherms at 271°C for Alloy 149

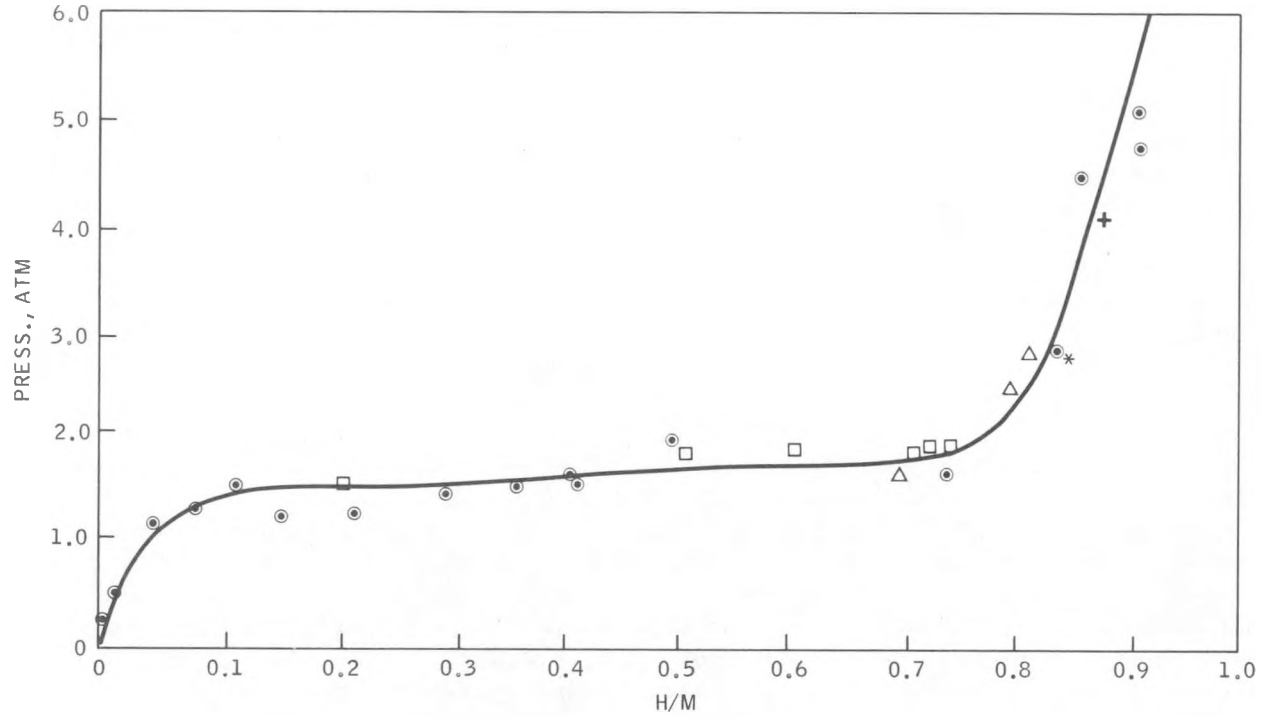

Figure 12. PCT Isotherms at 299°C for Alloy 149. Different Points Represent Different Hydriding-Dehydriding Runs

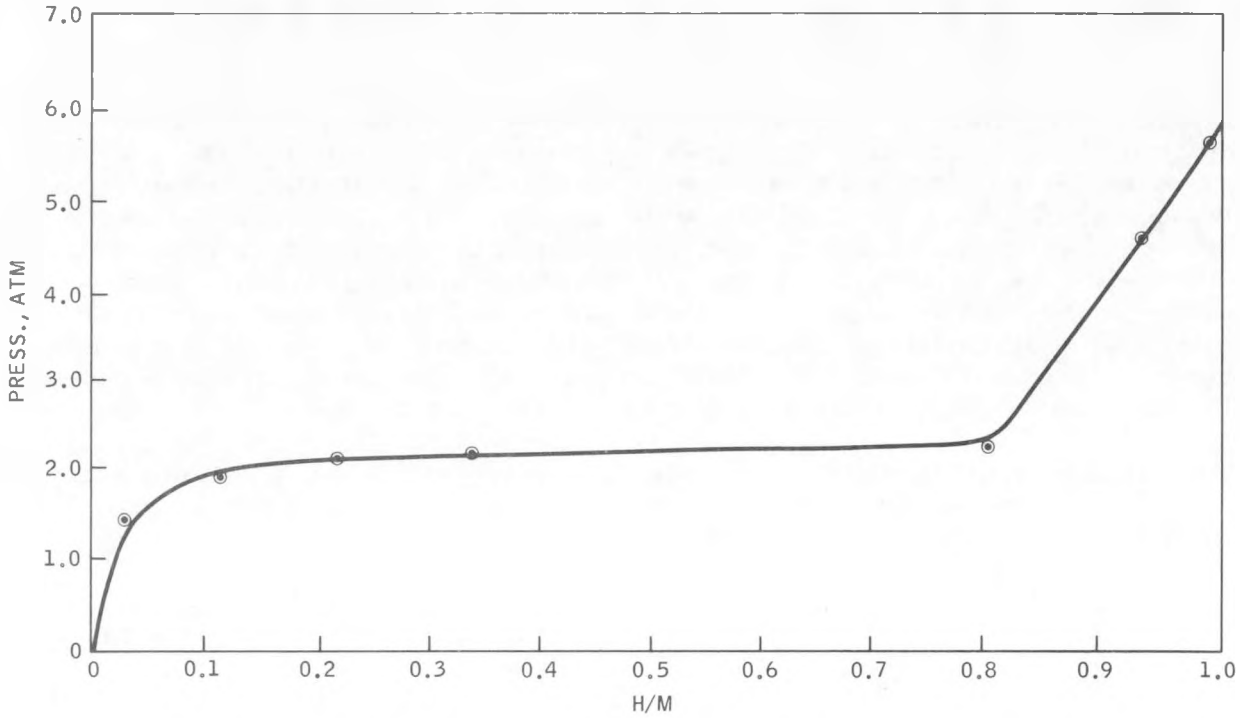

Figure 13. PCT Isotherms at 310°C for Alloy 149

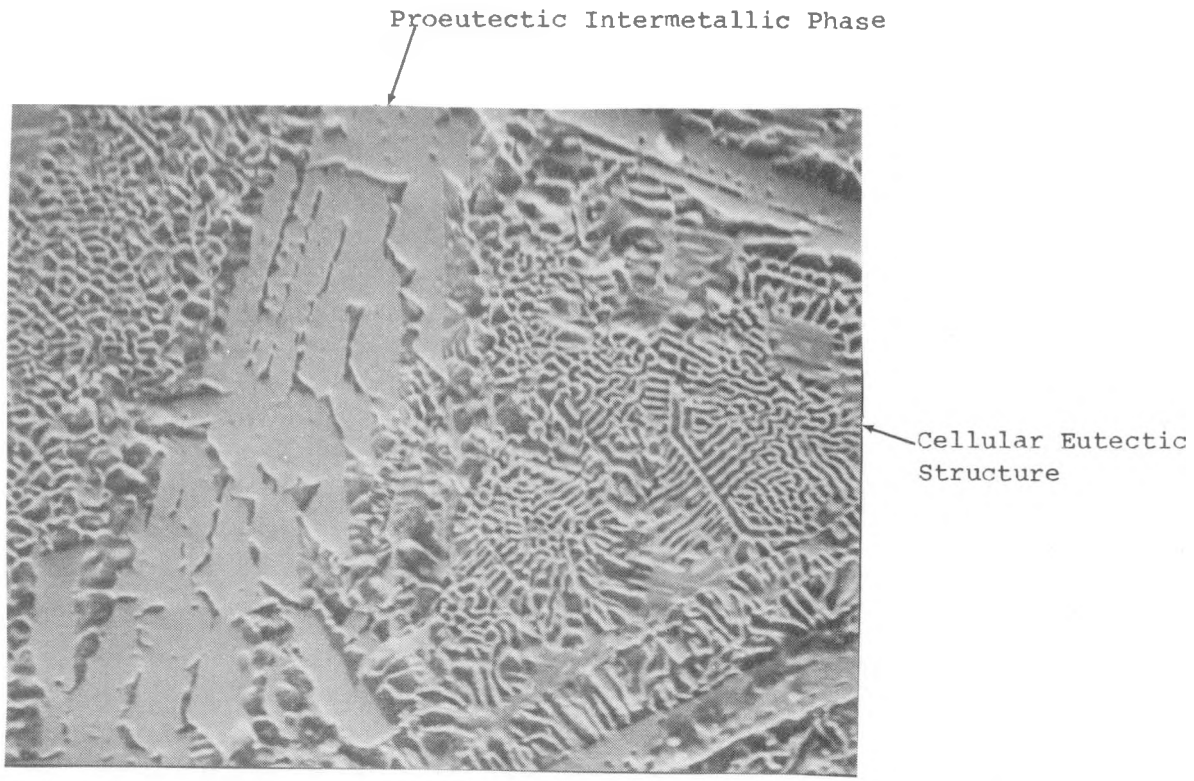

Figure 14. SEM Photomicrograph of $Mg_{0.845}Cu_{0.1}Ni_{0.05}Y_{0.005}$ (Alloy 149) Before Hydriding (200X)

The second eutectic phase consists of the Mg-rich terminal solid solution, predominantly Mg metal, occupying intercellular position in narrow bands typically parallel to the proeutectic needles discussed above. Total volume of this phase in banded form does not exceed 10 percent. This metallic phase in banded form appears to be a secondary proeutectic network called Phase B (refer to Fig. 15). Phase B appears to be the major reservoir for yttrium; but copper, nickel, and yttrium levels are all low; probably $\leq$1.0 at. percent on an individual basis. Existing binary phase diagrams for Mg alloys would tend to support this. Phase B, which is essentially impure Mg metal, in addition to its banded form, also occurs in intimate mixture with the third eutectic phase (C), described below. In total, Phase B probably is the single, most voluminous phase in the microstructure of Alloy 149.

The third eutectic phase (Phase C) is a relatively fragile and friable intermetallic, occupying (with Phase B in intimate mixture) the balance of the intercellular spaces.

Phase C appeared to have a probable intermetallic formula of $Mg_2(Cu,Ni)$, with copper almost twice the level of nickel. Yttrium levels are negligibly low. Partial hydriding of Alloy 149 surfaces cause expansion and volume-induced cracking of the intimate mixture of Phase B and C, which appears to be hydriding preferentially (Fig. 16). Because Phases B and C are so intimately mixed, it was difficult to determine which of the two phases were hydriding initially. Based on other studies of the $Mg-Mg_2Ni$ system (Ref. 6) in which it was determined that the magnesium phase hydrided preferentially, it is presumed that Phase B (impure Mg) is the preferentially hydriding phase in this case also. Note the build-up of hydride nodules on the surface of Alloy 149.

3.1.6 Sensitivity to Oxygen Contamination

Pure oxygen in increments of 0.1 weight percent was introduced to the reactor, containing dehydrided Alloy 149, at ambient temperature and allowed to remain for about 12 hours. Upon introduction of the oxygen, an immediate reaction was indicated by a slight rise in the temperature and drop in pressure within the reaction chamber. To make certain the alloy reacted completely with the oxygen, the reactor was heated to about 200°C before the hydriding procedure was resumed. The effect of oxygen contamination upon the hydriding parameters is summarized in Table 5.

After each increment of oxygen was added, the temperature of dissociation (T_D) increased by 45 to 50°C, and the ΔT decreased to a level of about 80°C. However, recovery (as indicated by T_D) of hydriding characteristics appeared to be fairly complete after three or four normal hydriding cycles (alternate pressure and vacuum) at a temperature of 340 to 370°C.

The general conclusion is that, although some deterioration occurs, the hydride can continue to function usefully. There appears to be no obvious explanation at this time for the increase in the H/M ratio of the alloy containing 0.4 percent oxygen. It is possible that the large number of hydriding-dehydriding cycles could have some effect upon the H/M ratio through increased comminution and therefore increased surface area.

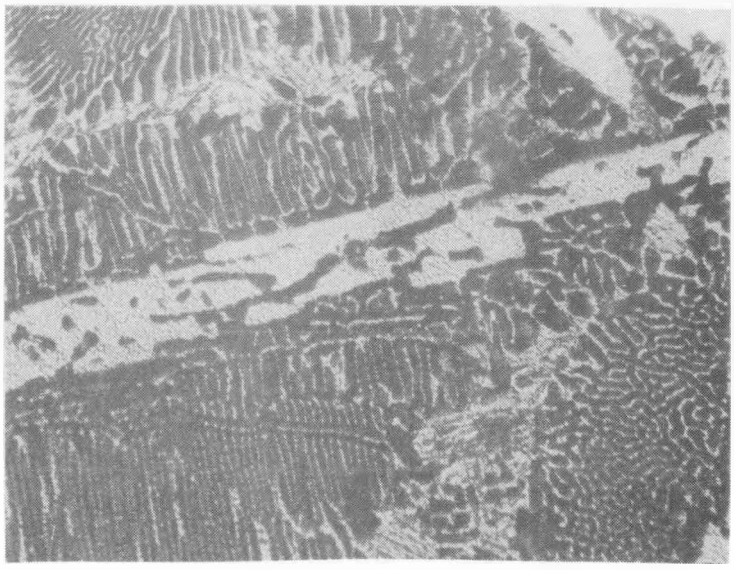

Figure 15. Optical Photograph of Alloy 149 Before Hydriding (250X)

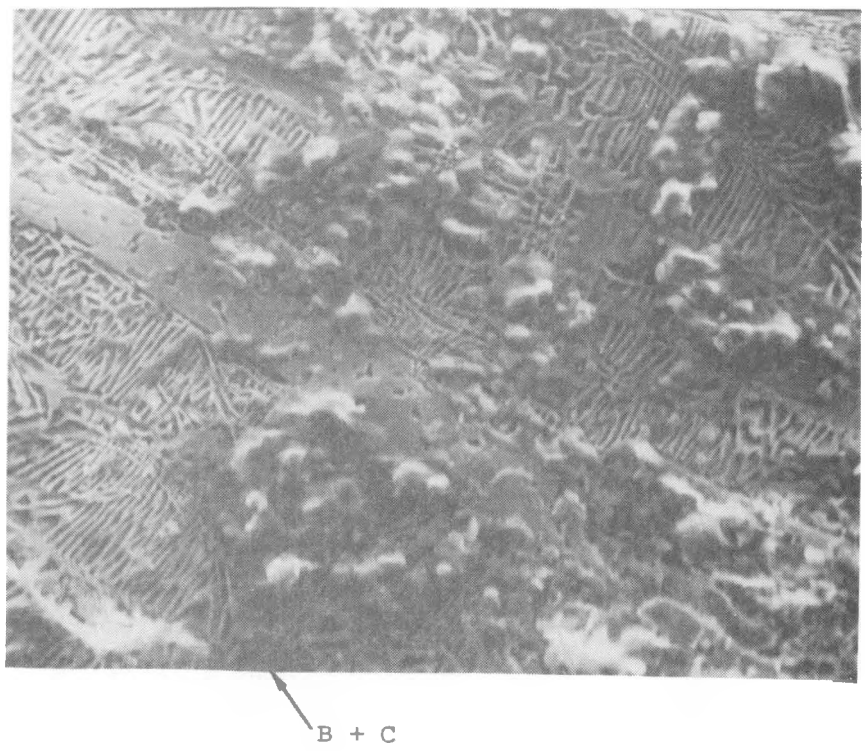

Figure 16. SEM Photograph of Alloy 149, Partially Hydrided (200X) (Note build-up of hydrided material nodules)

Table 5

Effect of Oxygen Contamination Upon Hydriding Properties of Alloy 149

Oxygen Increments, w/o*	Total Added Oxygen, w/o	T_D, °C**	H/M Ratio	*** ΔT, °C
0	0	228	1.09***	108
0.1	0.1	238	--	97
0.1	0.2	232	--	97
0.2	0.4	235	1.23	94

*w/o, weight percent
**Temperature at which pressure of fully hydrided alloy equals 1 atm.
***Previous hydriding run for Alloy 149.
****ΔT in °C is the change in temperature experienced during the hydriding and dehydriding cycle. It is felt to be qualitatively related to the kinetics and hydrogen capacity of each alloy.

3.1.7 Effect of Commercial Hydrogen

Since in all probability, hydriding on a large scale in a commercial application will be carried out with commercial gas, Alloy 149 was hydrided with Linde Commercial hydrogen, 99.95 percent minimum purity to determine the effect of these impurities on hydriding characteristics. Maximum moisture content of this gas is reported as 32 ppm.

After the normal five hydriding cycles, the hydride appeared to behave in a normal manner. To determine the effect of repeated cycling, thereby increasing contamination, fourteen hydriding cycles were completed before an equilibrium dissociation temperature was measured. A T_D of 227°C was observed after this sequence. After the 26th and 30th hydriding cycle, dissociation temperatures of 224 and 227°C were obtained, respectively. New hydrogen gas was introduced for each hydriding cycle. The H/M ratio was observed to be 1.21 after the 30th cycle. Thus the alloy appears to be affected very little by the minor amounts of impurities in commercial grade hydrogen over a limited number of cycles. Subsequently, extensive cycling tests were conducted with commercial hydrogen. With 2,000 cycles, considerable deterioration of Alloy 149 took place. The H/M ratio dropped from 1.16 to 0.44 and the hydrogen absorption decreased from 3.71 to 1.46 percent (see section on cycling). Apparently a sufficient amount of impurities are present in commercial gas to cause substantial deterioration during cycling.

3.1.8 Sensitivity to Nitrogen Contamination

Another contamination sensitivity experiment was performed using nitrogen in place of oxygen. A new sample of Alloy 149 was prepared in the normal manner. Several hydriding cycles were accomplished using ultra-pure hydrogen. A dissociation temperature (T_D) of 226°C was established for this sample. All hydrogen was removed by pumping at elevated temperatures. Then nitrogen was introduced at room temperature. No temperature increase was noted as was the case with oxygen additions. After approximately 12 hours of exposure to nitrogen the sample was heated to approximately 325°C in the presence of the nitrogen. Any nitrogen not absorbed was removed and the sample rehydrided. A summary of the results is shown in Table 6.

The effect of nitrogen on the dissociation temperature and hydrogen capacity was expected to be relatively minor. In fact the dissociation temperature (T_D) changed only slightly. The hydrogen capacity also showed only minor changes after the nitrogen additions.

Table 6

Effect of Nitrogen Contamination Upon Hydriding Properties of Alloy 149

Nitrogen Increments w/o	Total Added Nitrogen w/o	T_D, °C*	H/M Ratio
0	0	226	1.09
0.1	0.1	226	--
0.1	0.2	229	--
0.2	0.4	231	1.14

*Temperature at which pressure of fully hydrided alloy equals 1 atm

3.2 MAGNESIUM-LITHIUM BASE ALLOYS

As stated earlier, the hydrides of magnesium and lithium have many desirable characteristics for automotive applications. Their densities are very low and both can contain substantial quantities of hydrogen, 7.55 weight percent for MgH_2 and 12.68 percent for LiH (theoretical basis). Investigation of alloys combining the two elements appeared to be a logical step. The greatest disadvantage of both hydrides is their relatively high thermodynamic stability, with LiH exhibiting even a higher stability than MgH_2.

One of the purposes of this study was to attempt to decrease the thermodynamic stability of a Mg-Li base alloy hydride by the addition of ternary alloying elements consisting of Zn, Sn, Si, Ni, and Cu. Large differences in electronegativities between Li and the addition elements favor formation of stable compounds which in turn influence the interstitial hole size. Again, the smaller the interstitial hole size the less stable the hydride (Ref. 7). The electronegativities of the alloy elements and possible compounds that might be formed are given in Table 7.

Table 7

Electronegativities of Alloy Elements and Possible Compounds

Element	Electronegativity (Reference 8)	Possible Compounds (Reference 9)	Temperature of Stability, °C
Li	0.95	--	--
Zn	1.50	Li_2Zn_3	520
Sn	1.61	Li_7Sn_2	783
Si	1.82	Li_2Si	752

3.2.1 Preparation of Alloys

Melting and preparation procedures of the Mg alloys have been described under Magnesium-Nickel-Copper Alloys. The only change in procedure was the addition of Li just prior to solidification of the melt, to minimize oxidation. By plunging the Li below the molten surface, both oxidation and vaporization losses were held to a minimum.

Homogeneity on a macroscale was not a problem except in a few isolated instances. One of these instances was Alloy 9L ($Mg_{0.67}Li_{0.2}Si_{0.125}$), where apparently the higher Li and Si contents caused the solubility limit to be exceeded, leading to formation of highly insoluble and refractory silicides.

Other problems of homogeneity were encountered with the Ni-containing alloys. In the case of the ternary $Mg_{0.7}Li_{0.2}Ni_{0.1}$ immiscibility appears to be the problem, which was not evident with alloys containing 10 atomic percent Li. This is not entirely unexpected as the binary system of Li-Ni exhibits essentially complete immiscibility (Ref. 9). Lowering the Li to 17.5 atomic percent did not appear to improve the immiscibility of the system to any great extent.

Those alloys containing 5 to 10 atomic percent Si appeared to have unmelted pieces present, indicating presence of some refractory silicides, possibly Ni_2Si or Ni_5Si_2. The presence of unmelted refractory silicides was noted even though the NiSi master alloy was used, and the Si addition was reduced to 2.5 atomic percent.

Ingots free of macrosegregation were given a homogenization anneal at 400°C for a period of 48 to 72 hours to remove or minimize any microsegregation or coring. Homogeneous ingots were then pulverized to -12 mesh with a steel mortar and pestle under argon.

3.2.2 Hydriding and Mini-PC Isotherms

Approximately 15 g of the pulverized alloy were placed in the Inconel 600 reactor and subjected to the standard hydriding procedure, except that the pressure was increased to 600 psi, instead of the usual 300 psi, to improve the hydriding kinetics.

After hydriding, mini-PC isotherms were determined on each alloy at 310°C. As mentioned earlier in the Mg-Ni-Cu section, this procedure was adopted to permit screening large numbers of prospective alloys. Four points appear to be sufficient to indicate the plateau region and the general shape of the pressure-composition isotherm for each alloy. For convenience, the alloy hydrides and their characteristics are discussed in separate categories, beginning with ternary and ending with multicomponent systems.

3.2.3 Mg-Li-X (X = Ni, Zn, Sn, Si, Cu) (see Table 8)

$\underline{Mg}_{0.8}\underline{Li}_{0.1}\underline{X}_{0.1}$

The PC relationships are plotted in Figure 17. Highest plateau pressures at 310°C were attained with $Mg_{0.8}Li_{01}Ni_{0.1}$ followed by $Mg_{0.8}Li_{0.1}Si_{0.1}$. Kinetics of hydrogen release were not as rapid as anticipated so that each point was equilibrated for 1.5 to 2 hours.

Hydriding characteristics of the ternary systems containing 10 atomic percent of the various addition elements are summarized in Table 8. The highest hydrogen content in this series (2.04 percent) was achieved with Alloy 1L, containing 10 atomic percent Ni, followed by 1.70 percent for Alloy 3L ($Mg_{0.8}Li_{0.1}Sn_{0.1}$).

$\underline{Mg}_{0.7}\underline{Li}_{0.2}\underline{X}_{0.1}$

This series of alloys was designed to study the effect of doubling the Li content from 10 to 20 atomic percent on the ternary systems. The resulting mini-PC isotherms are shown in Figure 18. For the Si-containing alloy, doubling of the Li content to 20 atomic percent appears to increase the decomposition pressure abruptly.

In general, other than decreasing the density of the alloy, there appears to be no advantage in doubling the Li content. The hydriding-dehydriding kinetics are impaired, as indicated by the long time required for equilibration

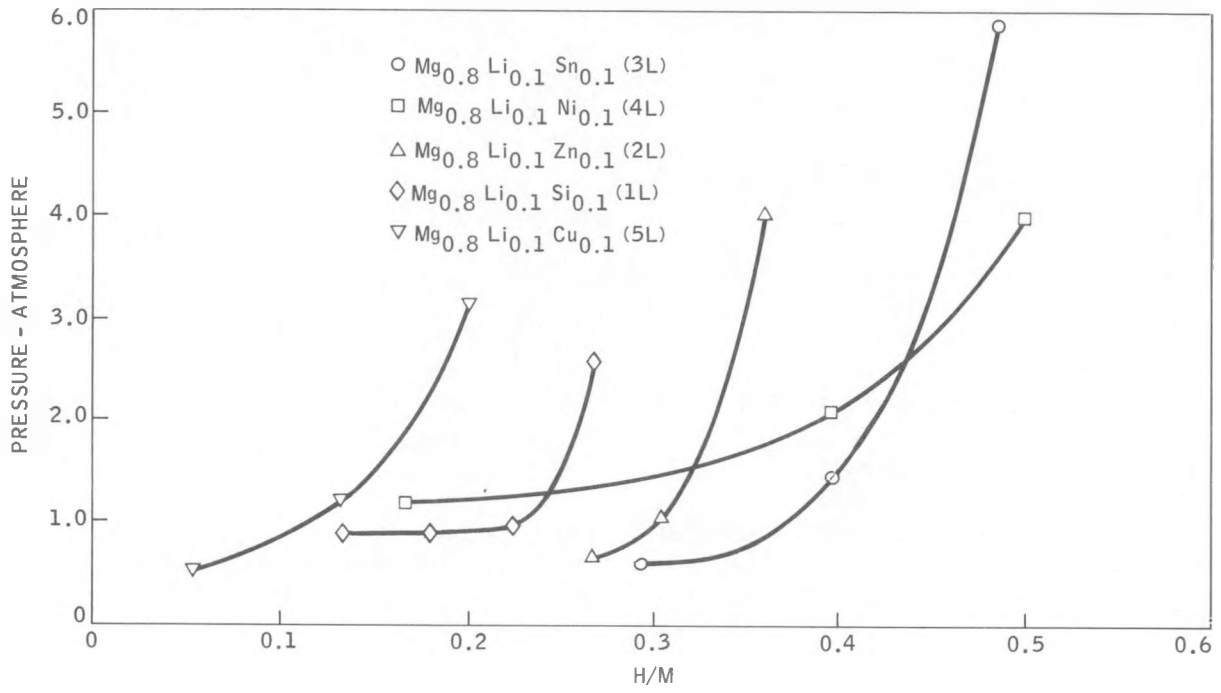

Figure 17. Pressure-Composition Isotherms of Mg-Li-X at 310°C

(approx. 2 hours), and the total hydrogen absorbed is considerably less than that of the ternary alloys containing 10 atomic percent Li. See Table 8 for a comparison of the hydriding characteristics of the various ternary alloys. No data are available for Ni-containing alloys with 20 atomic percent Li because of the immiscibility of Ni in the presence of Li contents in excess of 10 atomic percent.

$\underline{Mg}_{0.85}\underline{Li}_{0.05}\underline{X}_{0.1}$

To determine the basic effect of the lower Li content and to have a direct comparison with the 10 atomic percent Li ternary series, a ternary series containing 5 atomic percent Li was investigated. Figure 19 shows the mini-PC. isotherms obtained with the lower Li content. These can be directly compared with the isotherms shown in Figure 17. The hydrogen contents are about half and the decomposition pressures are considerably lower than the 10 atomic percent Li ternary series. See Table 8 for the hydriding characteristics of both the 5 and 10 atomic percent Li systems.

3.2.4 Mg-Li-Ni-X (X = Cu, Zn, Sn, Si) (see Table 9)

$\underline{Mg}_{0.7}\underline{Li}_{0.1}\underline{Ni}_{0.1}\underline{X}_{0.1}$

Since the best ternary hydride results were attained with $Mg_{0.8}Li_{0.1}Ni_{0.1}$, Alloy 1L was used as a base for the quaternary alloy hydrides which are

Table 8

Hydriding Characteristics of Mg-Li-X

Alloy	Composition	ΔT, °C	% H_2 Absorbed	Approximate Plateau Pressure @ 310°C (atm)
1L	$Mg_{0.8}Li_{0.1}Ni_{0.1}$	44	2.04	1.2
2L	$Mg_{0.8}Li_{0.1}Zn_{0.1}$	19	1.63	0.6
3L	$Mg_{0.8}Li_{0.1}Sn_{0.1}$	10	1.70	0.8
4L	$Mg_{0.8}Li_{0.1}Si_{0.1}$	18	1.26	0.8
5L	$Mg_{0.8}Li_{0.1}Cu_{0.1}$	14	0.86	0.6
9L	$Mg_{0.675}Li_{0.2}Si_{0.125}$	11	1.64	0.4
20L	$Mg_{0.7}Li_{0.2}Zn_{0.1}$	11	1.10	0.6
21L	$Mg_{0.7}Li_{0.2}Sn_{0.1}$	22	0.60	0.5
22L	$Mg_{0.7}Li_{0.2}Cu_{0.1}$	18	0.69	0.5
38L	$Mg_{0.85}Li_{0.05}Ni_{0.1}$	44	1.38	1
39L	$Mg_{0.85}Li_{0.05}Zn_{0.1}$	9	0.59	0.3
40L	$Mg_{0.85}Li_{0.05}Sn_{0.1}$	14	0.77	0.5
41L	$Mg_{0.85}Li_{0.05}Cu_{0.1}$	9	0.51	0.4

shown in Figure 20. It should be noted that the addition of 0.1 atomic fraction of Cu increased the decomposition pressure materially. The most dramatic improvement in hydriding characteristics was achieved by the addition of 0.1 atom fraction of Sn. A plateau pressure greater than two atmospheres and an H/M ratio greater than 0.8 were observed for this hydride. Hydriding characteristics of all the alloys studied are summarized in Table 9. Note the much higher ΔT (89°C) for $Mg_{0.7}Li_{0.1}Ni_{0.1}Sn_{0.1}$. The temperature rise, ΔT, observed during hydriding is felt to be a good qualitative measure of hydriding kinetics.

$\underline{Mg}_{0.75}\underline{Li}_{0.1}\underline{Ni}_{0.1}\underline{X}_{0.05}$

Although encouraging results were obtained with the 10 atomic percent Sn quaternary system, the heavy metal content is rather high. This particular

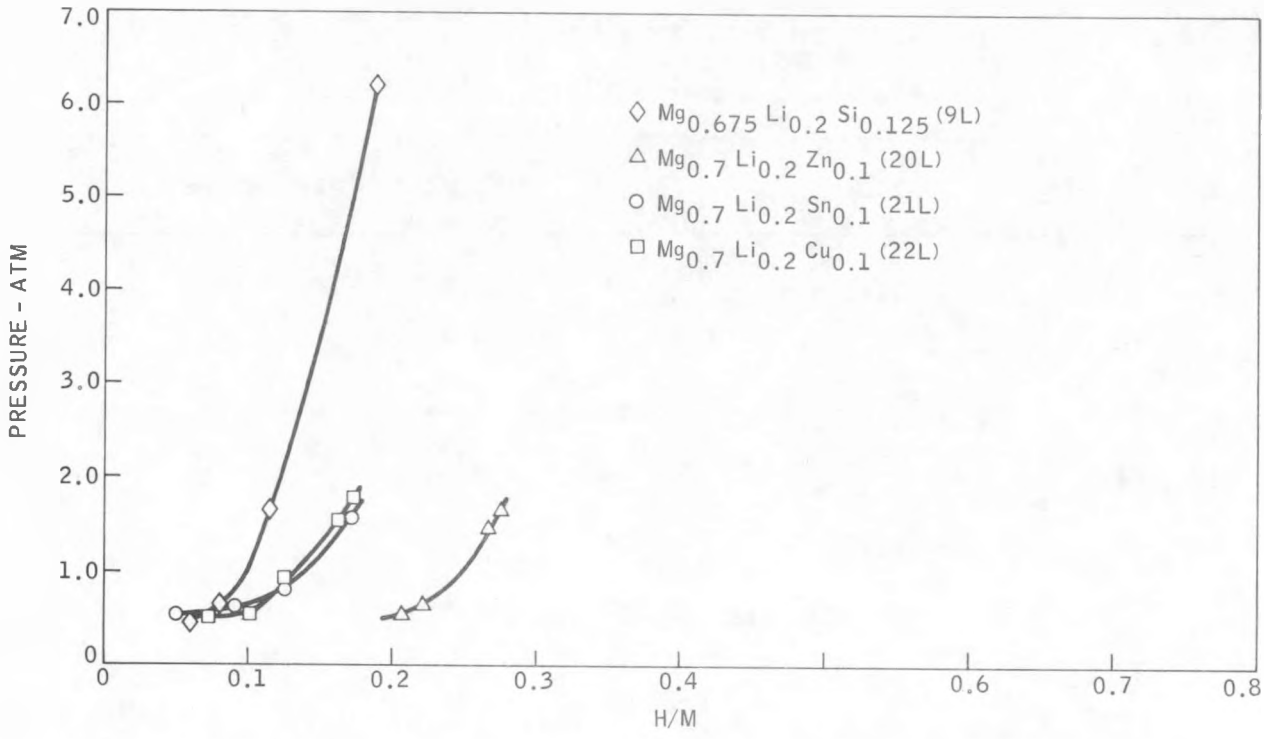

Figure 18. Pressure-Composition Isotherms of $Mg\text{-}Li_{0.2}\text{-}X$ at 310°C

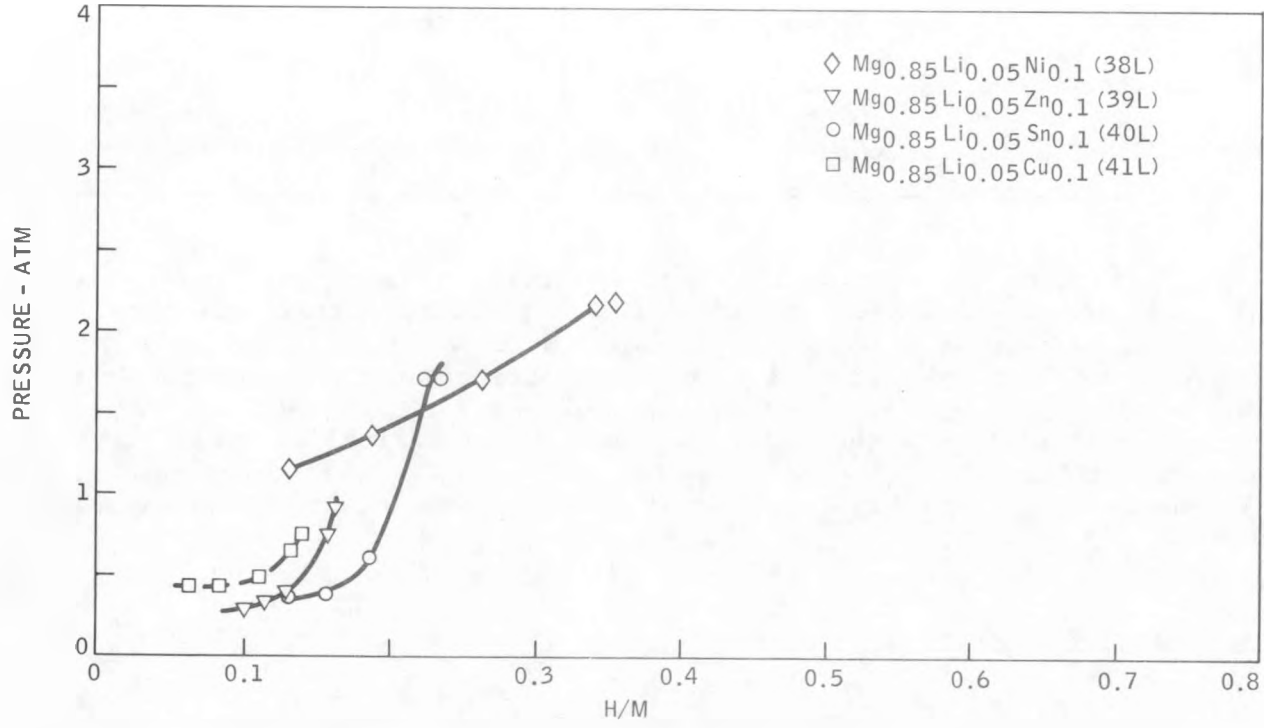

Figure 19. Pressure-Composition Isotherms of $Mg_{0.85}Li_{0.05}X_{0.1}$ Systems at 310°C

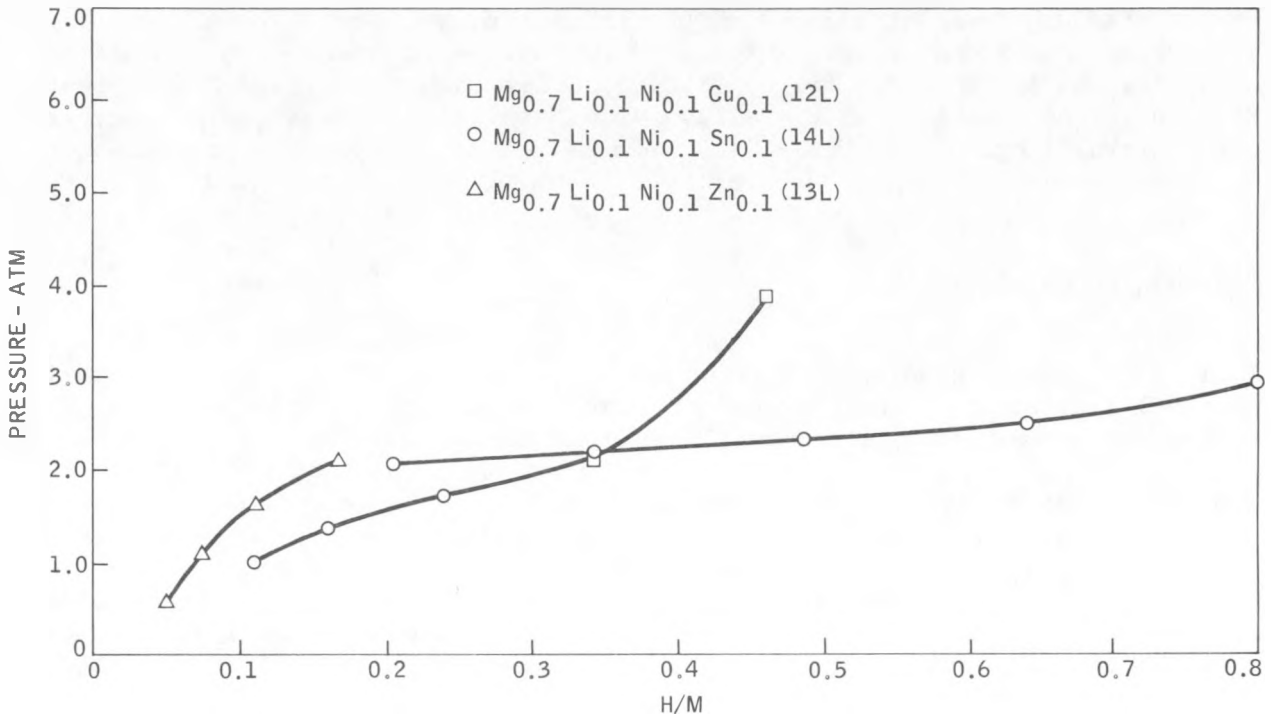

Figure 20. Pressure-Composition Isotherms of Mg-Li-Ni-X at 310°C

Table 9

Hydriding Characteristics of Mg-Li-Ni-X

Alloy	Composition	ΔT, °C	% H_2 Absorbed	Approximate Plateau Pressure @ 310°C (atm)
11L	$Mg_{0.75}Li_{0.1}Ni_{0.1}Cu_{0.05}$	60	1.95	1.6
12L	$Mg_{0.7}Li_{0.1}Ni_{0.1}Cu_{0.1}$	45	1.64	1.0
13L	$Mg_{0.7}Li_{0.1}Ni_{0.1}Zn_{0.1}$	48	0.95	--
14L	$Mg_{0.7}Li_{0.1}Ni_{0.1}Sn_{0.1}$	89	2.32	2.4
28L	$Mg_{0.75}Li_{0.1}Ni_{0.1}Sn_{0.05}$	91	1.92	1.8
29L	$Mg_{0.75}Li_{0.1}Ni_{0.1}Zn_{0.05}$	41	1.03	--
35L	$Mg_{0.8}Li_{0.05}Ni_{0.1}Sn_{0.05}$	81	2.48	2.0
36L	$Mg_{0.8}Li_{0.05}Ni_{0.1}Cu_{0.05}$	40	1.11	0.9
37L	$Mg_{0.8}Li_{0.05}Ni_{0.1}Zn_{0.05}$	37	1.63	1.8

series of alloys was an attempt to limit the Cu, Sn, and Zn additions to 5 atomic percent. Hydriding results on this series of quaternary alloys are summarized in Table 9. The alloy (35L) containing 5 atomic percent Sn appears to give better results than the alloys with Cu and Zn additions. The isotherm for 5 atomic percent Cu (Alloy 11L) exhibits a higher plateau pressure, and a higher hydrogen content than Alloy 12L containing 10 atomic percent Cu.

$\underline{Mg}_{0.8}\underline{Li}_{0.05}\underline{Ni}_{0.1}\underline{X}_{0.05}$

Earlier hydriding studies indicated that larger amounts of Li (20 atomic percent) limited the total amount of hydrogen absorbed. To check this out further, a series of quaternary alloys were investigated. They were based on $Mg_{0.8}Li_{0.05}Ni_{0.1}X_{0.05}$, where X represents Sn, Cu, or Zn. Figure 21 summarizes the pressure-composition relationships obtained with this system. The hydriding characteristics are given in Table 9. It is interesting to note that the hydrogen content and plateau pressures of the alloy containing 5 atomic percent Sn (35L) are about the same as were obtained with $Mg_{0.7}Li_{0.1}Ni_{0.1}Sn_{0.1}$, which has the highest plateau pressure and one of the highest hydrogen contents attained to date on the quaternary systems (refer to Alloy 14L in Table 9 and Fig. 20).

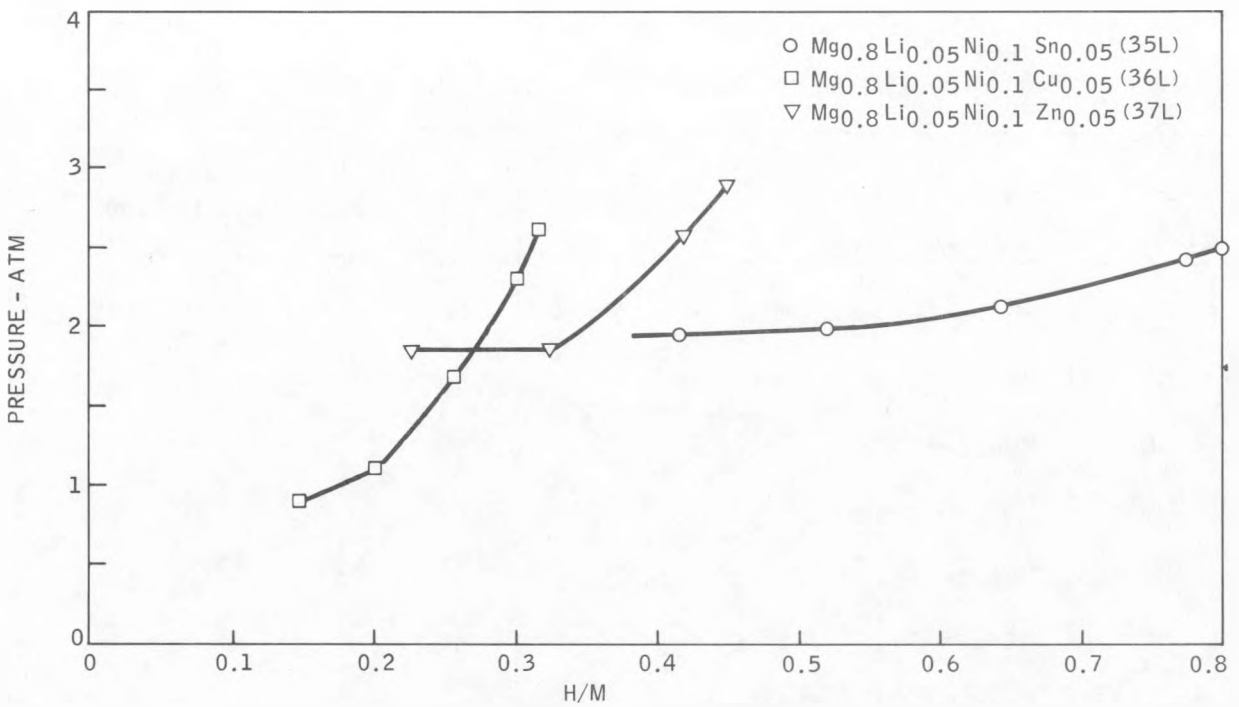

Figure 21. Pressure-Composition Isotherms of $Mg_{0.8}Li_{0.05}Ni_{0.1}X_{0.05}$ Systems at 310°C

3.2.5 Multicomponent Alloys (see Table 10)

This discussion considers all alloys of five or more components. Initially a study was conducted on multicomponent systems, using $Mg_{0.75}Li_{0.1}Ni_{0.1}Sn_{0.05}$ as a base. Additions of a fifth component were made to determine what, if any, synergistic effects may exist between the multiple addition elements. Figure 22 shows the mini-PC isotherms obtained with the addition of approximately 5 to 6 atomic percent of Si, Cu, and Zn. Additions of Cu and Zn appear to produce higher decomposition pressures at the higher H/M ratios, and also a somewhat flatter plateau region. Hydriding characteristics of these quinary alloys are listed in Table 10.

Other quinary alloys along with a six-component alloy (34L) were also included in this study to determine the effect of a number of small additions (2.5 atomic percent) of Sn, Zn, and Cu. The results of these hydriding studies are summarized in Figure 23. It was concluded that there were no particular advantages or synergistic effects with these multicomponent systems. Hydriding characteristics of these alloys are listed in Table 10.

In general, a comparison of the hydriding characteristics of the five- or six-component systems (Table 10) with the quaternary system (Table 9) shows higher decomposition pressures at higher H/M ratios and lower hydrogen contents than the quaternary alloys.

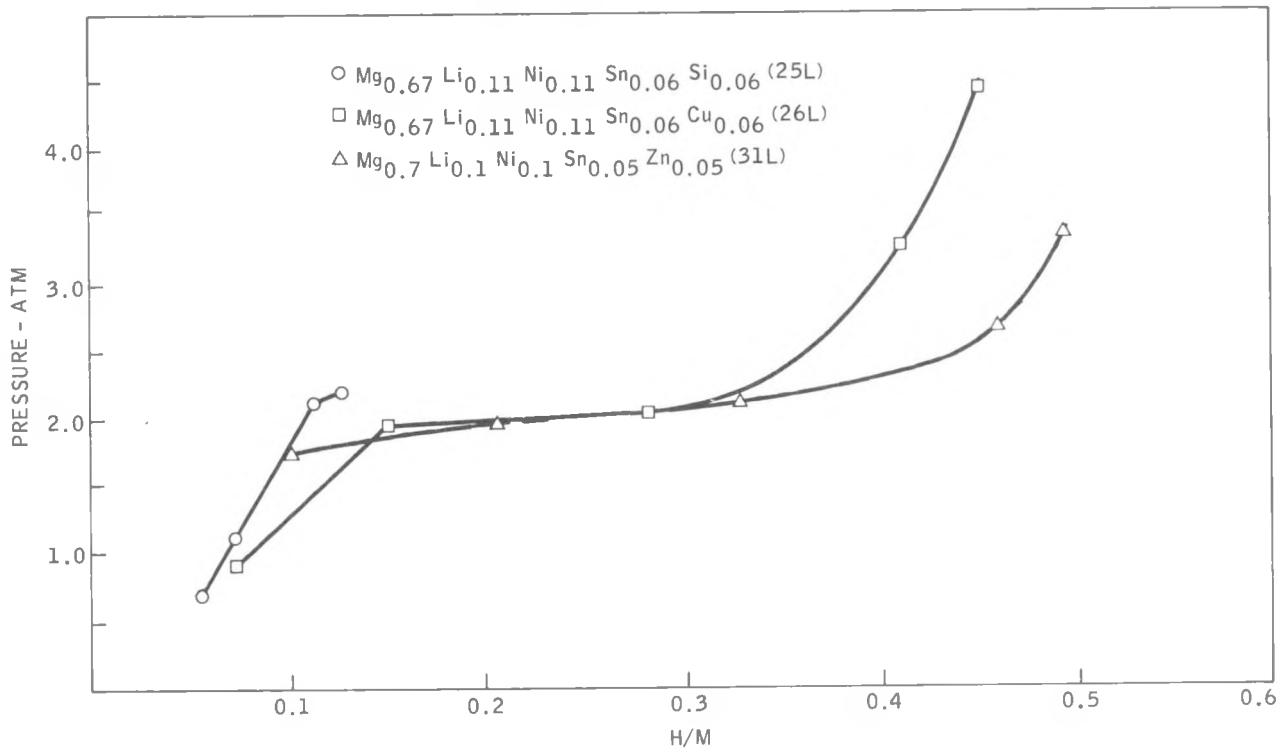

Figure 22. Pressure-Composition Isotherms of Mg-Li-Ni-Sn-X at 310°C

Table 10

Hydriding Characteristics of Mg-Li-Ni-Sn-X and Mg-Li-Ni-Sn-X-Y

Alloy	Composition	ΔT, °C	% H_2 Absorbed	Plateau Pressure at 310°C (atm)
25L	$Mg_{0.67}Li_{0.11}Ni_{0.11}Sn_{0.06}Si_{0.06}$	30	0.67	--
26L	$Mg_{0.67}Li_{0.11}Ni_{0.11}Sn_{0.06}Cu_{0.06}$	60	1.30	2.0
31L	$Mg_{0.7}Li_{0.1}Ni_{0.1}Sn_{0.05}Zn_{0.05}$	55	1.48	2.0
32L	$Mg_{0.725}Li_{0.1}Ni_{0.1}Sn_{0.05}Cu_{0.025}$	61	1.67	2.0
33L	$Mg_{0.75}Li_{0.1}Ni_{0.05}Sn_{0.05}Cu_{0.05}$	53	1.31	--
34L	$Mg_{0.725}Li_{0.1}Ni_{0.1}Sn_{0.025}Zn_{0.025}Cu_{0.025}$	42	1.36	--

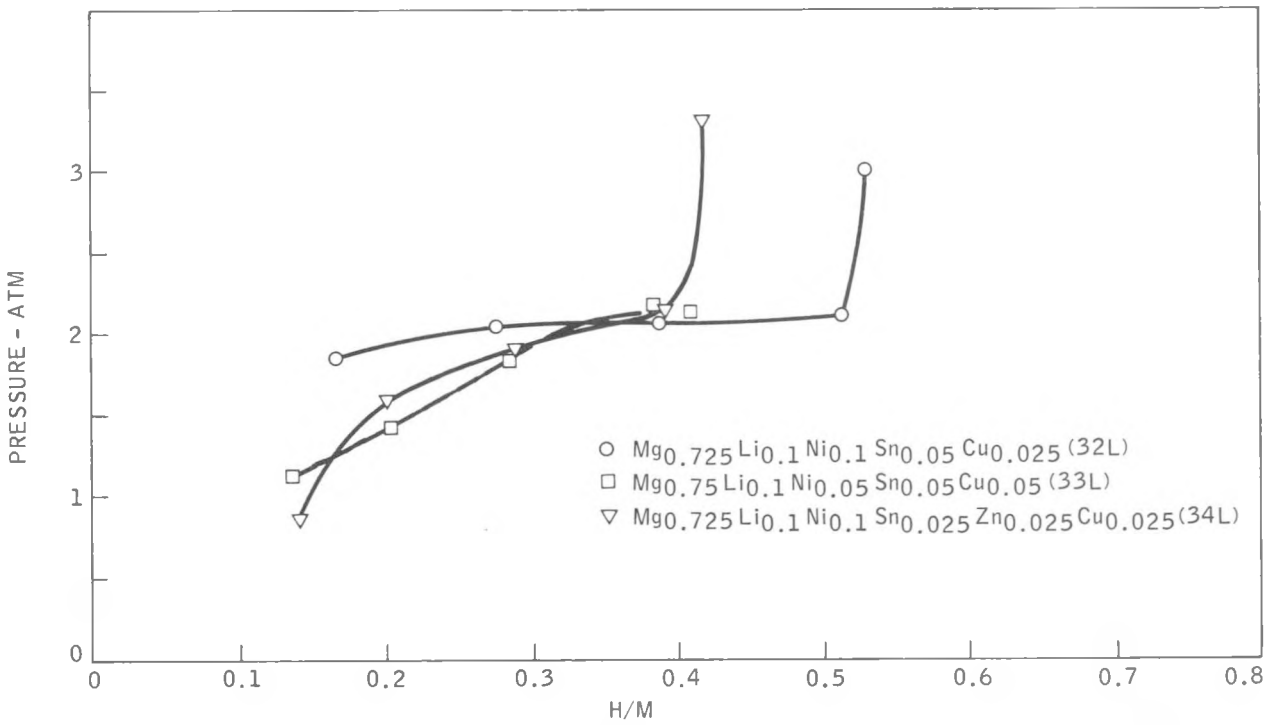

Figure 23. Pressure-Composition Isotherms of Multicomponent Systems at 310°C

It would appear from the results of this investigation that the thermodynamic stability of LiH is not easily overcome by decreasing interstitial hole size. Similar conclusions were reached by Air Products and Chemicals, Inc. (Ref. 10) in their studies of the Mg-5Li alloy, in which the structural model predicts an opposite trend to chemical stability.

3.3 MAGNESIUM-ALUMINUM BASE ALLOY SYSTEMS

Research by a number of investigators (Refs. 6, 10, 11, 12, and 13) indicates the potential of this system for higher plateau pressures and resistance to comminution, especially the Mg-10Al alloys (Ref. 2). Data on hydriding of $Mg_{17}Al_{12}$ and other alloys of the Mg-Al system are summarized in Table 11. The very poor hydriding-dehydriding kinetics, however, render this system impractical for most applications. The authors undertook research on the effects of alloy additions to gamma ($Mg_{17}Al_{12}$), Mg-10Al, and more recently the beta (Mg_2Al_3, Mg_5Al_8) and epsilon (Mg_4Al_5) phases (Ref. 14). These studies are discussed in greater detail under the individual headings.

Table 11

Mg-Al Systems Summary*

Alloy Composition Atomic Ratio	Wt. Percent	Mesh Size	Maximum Hydrogen Wt. Percent	Results
$Mg_{0.91}Al_{0.09}$ (Ref. 6)	90Mg-10Al	-25 +32 -32 +42	7.0	Kinetics hyd./dehyd. poor
$Mg_{17}Al_{12}$ (γ phase)	56.1Mg-43.9Al	-20	0.60	
$Mg_{17}Al_{12}$ (γ phase)	56.1Mg-43.9Al	-20	1.7	
$Mg_{17}Al_{12}$ (γ phase)	56.1Mg-43.9Al	-100	2.25	Pt black catalyst
$Mg_{17}Al_{12}$ (γ phase)	56.1Mg-43.9Al	-200	3.31	
MgAl ($\beta + \gamma$)	52.0Al-48.0Mg	-20	0.38	
Mg_4Al_5 (ε phase)	58.0Al-42.0Mg	-20	0.64	
Mg_4Al_5 (ε phase)	58.0Al-42.0Mg	-20	1.4	
Mg_4Al_5 (ε phase)	58.0Al-42.0Mg	-200	2.20	
Mg_4Al_5 (ε phase)	58.0Al-42.0Mg	-200	2.77	
Mg_2Al_3 (β phase)	62.5Al-37.5Mg	-20	0.7	
Mg_2Al_3 (β phase)	62.5Al-37.5Mg	-200	2.34	
Mg_2Al_3 (β phase)	62.5Al-37.5Mg	-200	3.28	
Al_6CuMg_4	50.2Al-19.7Cu-30.1Mg	--	0.30	
Al_7CuMg_6	35.9Al-36.3Cu-27.8Mg	--	0.76	

*All data from Reference 11 except for 90Mg-10Al Alloy (wt. percent).

3.3.1 $Mg_{17}Al_{12}$ Base Alloys

Initial investigations were centered around the $Mg_{17}Al_{12}$ intermetallic compound, whose hydride was reported by Brookhaven National Laboratory to contain 3.31 percent hydrogen (Ref. 11). Interest in the Mg-Al system has been stimulated to a great extent by the existance of the complex hydride $[Mg(AlH_4)_2]$, containing 9.3 weight percent hydrogen. Preparation of this compound to date has been possible only through indirect synthesis by complicated organometallic reactions. Processes of this type are not suitable for vehicular use because of their irreversibility.

Hydriding and dehydriding of Mg-Al alloys is generally characterized by poor kinetics. This prompted Brookhaven to use hydriding pressures of 1000 to 5000 psi plus very fine powder (-200 mesh). The higher hydrogen content reported by Douglass on the 90-Mg-10Al alloy listed in Table 11 was also achieved by hydriding at 400 to 450°C under a pressure of 600 psi for periods of time up to 20 hours (Ref. 6).

As stated before, one of the objectives of this program was to attempt to decrease the thermodynamic stability of magnesium-base alloy hydrides by single or multiple additions of alloying elements consisting of Ni, Cu, Zn, Sn, Si, as well as Li and rare earths. These latter active elements, particularly the rare earths, may behave as scavengers to prevent oxidation of aluminum, which is believed to be responsible for the poor hydriding kinetics of the aluminum-containing alloys.

The first experiments were designed to investigate the effect of a change of lattice parameter upon hydriding characteristics of the gamma-phase ($Mg_{17}Al_{12}$), which is isotypic with the complex cubic structure of αMn. Lattice constants vary linearly from a = 10.469 A. at 51.6 at. percent Mg to a = 10.591 A. at 61.5 at. percent Mg (Ref. 9). Recent work (Ref. 7) indicates that a decrease in lattice parameter suggests a smaller interstitial hole size with a decrease in thermodynamic stability of the resulting hydride (lower decomposition temperature).

Preparation of Hydriding Alloys

The Mg-Al alloys were prepared around the ideal composition of $Mg_{17}Al_{12}$ ($Mg_{0.59}Al_{0.41}$), using the standard induction melting and radiographic inspection procedures described earlier. Alloying additions, consisting of Ni, Cu, Sn, Zn, Li, Y, and La, were made to the $Mg_{17}Al_{12}$ intermetallic with the basic composition of $Mg_{0.62}Al_{0.38}$ (4A). The ratio of Mg/Al of approximately 1.63 was kept constant in these alloys based upon the $Mg_{0.62}Al_{0.38}$ composition.

Previously, difficulty was encountered in the preparation of magnesium alloys containing both Ni and Al additions due to the formation of the refractory compound NiAl. By the use of a master alloy containing 74 percent Al-26 percent Ni (M.P. ~ 850°C) we have found it possible to prepare homogeneous

alloys. To keep the melting temperature of the master alloys at 850°C, and at the same time maintain the Mg/Al ratio at approximately 1.63, it was necessary to limit the Ni addition to five atomic percent.

Radiography indicated no macrosegregation or unmelted phases in any of the newly prepared alloys. Alloys containing added elements were given a homogenization anneal to minimize microsegregation prior to hydriding. All alloys, except the low-melting ones containing Zn, Li, and Cu, were homogenized at 400°C. The annealing temperature was lowered to 300°C for the latter.

Hydriding and Mini-PC Isotherms

The homogeneous Mg-Al alloys were subjected to the standard hydriding procedure at a pressure of 600 psi. Because of the relatively poor hydriding kinetics of these alloys, the alloy was crushed to -100 mesh powder. Normally such fine powders are avoided because of the greater chance of losing part of the sample during evacuation of the reaction chamber.

After hydriding, mini-PC isotherms were determined on each alloy at 310°C. As in a previous section, the discussion is facilitated by organizing the results according to alloy category, i.e., binary, ternary, etc.

Binary Variations of $Mg_{17}Al_{12}$

Hydriding studies were conducted on the gamma-phase alloys containing two extremes in composition; 51.6 atomic percent Mg (a = 10.469A), and 61.5 atomic percent Mg (a = 10.591A).

Because Douglass' work (Ref. 6) indicated that up to 20 hours were necessary to fully hydride the 90Mg-10Al alloy, Alloy 4A was hydrided for approximately 12 hours overnight at 400°C under a pressure of 600 psi. The PC relationships are plotted in Figure 24. Hydriding characteristics are tabulated in Table 12.

Hydrogen absorption by Alloys 2A and 3A was about 30 percent of that reported by Brookhaven. This can probably be attributed to much higher pressures employed by the Brookhaven investigators (1000 to 5000 psi), as well as to the much finer powder (-200 mesh) used in their studies.

Some improvement in hydrogen absorption was obtained by sample preparation in the dry box in an argon atmosphere. Compare Alloy 2A with and without dry box preparation in Table 12. The greatest amount of hydrogen absorption was obtained with Alloy 4A, which was prepared in the dry box and held at 400°C for approximately 12 hours under a hydrogen pressure of 600 psi. Total hydrogen absorbed for the 12 hour period was two and one-half times that of the standard hydriding procedure. The highest plateau pressure of about 1.5 atmospheres at 310°C was also observed with Alloy 4A which has the largest lattice parameter of the gamma phase (see Fig. 24). This result appears to run counter to van Mal's rule of "reversed stability" (Ref. 15). However, in

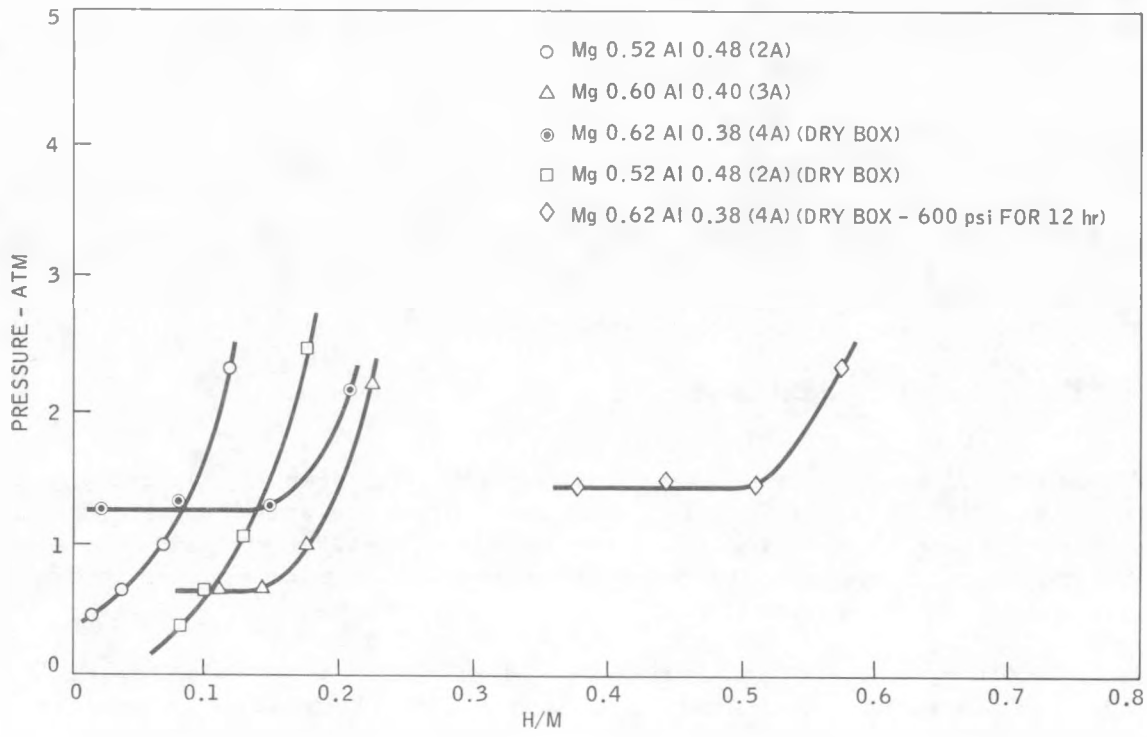

Figure 24. Pressure-Composition Isotherms of Mg_xAl_y at 310°C

order to predict the thermodynamic stability of hydrides, one should know the exact crystal structure and lattice parameter to determine interstitial hole size (Ref. 16).

Ternary Additions to the Gamma-Phase $Mg_{17}Al_{12}$

Studies described in this section were carried out on ternary additions of Ni, Sn, Si, Li, Cu, Y, an La to the basic $Mg_{0.62}Al_{0.38}$ composition, keeping the Mg/Al ratio constant at 1.63. In these studies the kinetics of hydriding were greatly improved by the addition of five atomic percent Ni (Alloy 5A). Hydrogen content and hydriding characteristics were nearly identical to Alloy 4A, which required 12 hours of hydriding under 600 psi as described in the previous sections. Compare the PC isotherms in Figure 25 and hydriding characteristics in Table 12. On the other hand, addition of five atomic percent Sn to the basic alloy 5A causes a deterioration of the dissociation pressure and hydrogen content. See Table 12 and Figure 26.

The highest plateau pressure observed for the five atomic percent level of additions was 2.3 atmospheres at 310°C, achieved with Alloy 13A, which contains five atomic percent of yttrium. Kinetics of hydriding were also greatly improved by the yttrium addition. Compare the PC isotherms in Figure 26 and hydriding characteristics in Table 12. The improved kinetics can perhaps be attributed to the very stable oxide that yttrium forms, in effect scavenging the oxygen and preventing the formation of the impervious and stable Al_2O_3, which is believed to act as a barrier responsible for the poor hydriding

Table 12

Hydriding Characteristics of $Mg_{17}Al_{12}$ Alloys

Alloy	Composition	ΔT, °C	% H_2 Absorbed	Plateau Pressure at 310°C (atm)	Remarks
2A	$Mg_{0.52}Al_{0.48}Ni_{0.05}$	15	0.55	--	-100 mesh
3A	$Mg_{0.6}Al_{0.4}$	7	0.95	0.7	-100 mesh
4A	$Mg_{0.62}Al_{0.38}$	19	0.88	1.3	-100 mesh (dry box)
2A	$Mg_{0.52}Al_{0.48}$	12	0.77	--	-100 mesh (dry box)
4A	$Mg_{0.62}Al_{0.38}$	20	2.30	1.4	-100 mesh (dry box plus 12 hours at 400°C plus 600 psi)
5A	$Mg_{0.59}Al_{0.36}Ni_{0.05}$	28	2.16	1.3	-100 mesh (dry box)
8A	$Mg_{0.59}Al_{0.36}Sn_{0.05}$	8	0.45	0.5	-100 mesh (dry box)
6A	$Mg_{0.56}Al_{0.34}Cu_{0.10}$	27	0.81	--	-100 mesh (dry box)
5A	$Mg_{0.59}Al_{0.36}Ni_{0.05}$	--	3.36	1.8	-40 plus -100 mesh (dry box) plus 12 hours 600 psi at 400°C
10A	$Mg_{0.59}Al_{0.36}Li_{0.05}$	26	1.78	0.7	-40 plus -100 mesh (dry box)
13A	$Mg_{0.59}Al_{0.36}Y_{0.05}$	30	2.01	2.2	-40 plus -100 mesh (dry box)
9A	$Mg_{0.59}Al_{0.36}Si_{0.05}$	10	0.63	0.4	-40 plus -100 mesh (dry box)
14A	$Mg_{0.56}Al_{0.34}Y_{0.1}$	40	2.51	1.9 - 2.4	-40 plus -100 mesh (dry box)
14A	$Mg_{0.56}Al_{0.34}Y_{0.1}$	40	3.29	2.1 - 2.6	Same as above plus 12 hours 600 psi at 400°C
12A	$Mg_{0.59}Al_{0.36}La_{0.05}$	31	2.68	1.9	-40 plus -100 mesh (dry box)
12A	$Mg_{0.59}Al_{0.36}La_{0.05}$	31	3.04	1.9	Same as above plus 12 hours 600 psi at 400°C
12A-1	$Mg_{0.56}Al_{0.34}La_{0.1}$	94	1.68	~1.8	-20 plus -40 mesh
12A-1	$Mg_{0.56}Al_{0.34}La_{0.1}$	--	2.12	~1.7	Same as above plus 12 hours 600 psi at 400°C
16A	$Mg_{0.56}Al_{0.34}Ni_{0.05}Y_{0.05}$	35	2.05	1.3	-40 plus -100 mesh
16A	$Mg_{0.56}Al_{0.34}Ni_{0.05}Y_{0.05}$	--	2.58	1.5	Same as above plus 12 hour 600 psi at 400°C
17A	$Mg_{0.56}Al_{0.34}La_{0.05}Y_{0.05}$	106	2.10	2.0	-20 mesh (dry box)
17A	$Mg_{0.56}Al_{0.34}La_{0.05}Y_{0.05}$	--	3.06	2.0	Same as above plus 12 hour 600 psi at 400°C
18A	$Mg_{0.56}Al_{0.34}MM_{0.10}$	107	1.85	1.3 - 1.9	-40 plus -100 mesh
18A	$Mg_{0.56}Al_{0.34}MM_{0.10}$	--	2.15	1.8 (sloping)	Same as above plus 12 hours 600 psi at 400°C
19A	$Mg_{0.56}Al_{0.34}YM_{0.1}$	80	2.38	1.9	+20 plus -20 mesh
19A	$Mg_{0.56}Al_{0.34}YM_{0.1}$	--	2.88	1.9	Same as above plus 12 hours 600 psi at 400°C
20A	$Mg_{0.56}Al_{0.34}YM_{0.05}MM_{0.05}$	79	1.13	1.5	-20 plus -120 mesh
20A	$Mg_{0.56}Al_{0.34}YM_{0.05}MM_{0.05}$	--	1.78	1.9	Same as above plus 12 hour 600 psi at 400°C

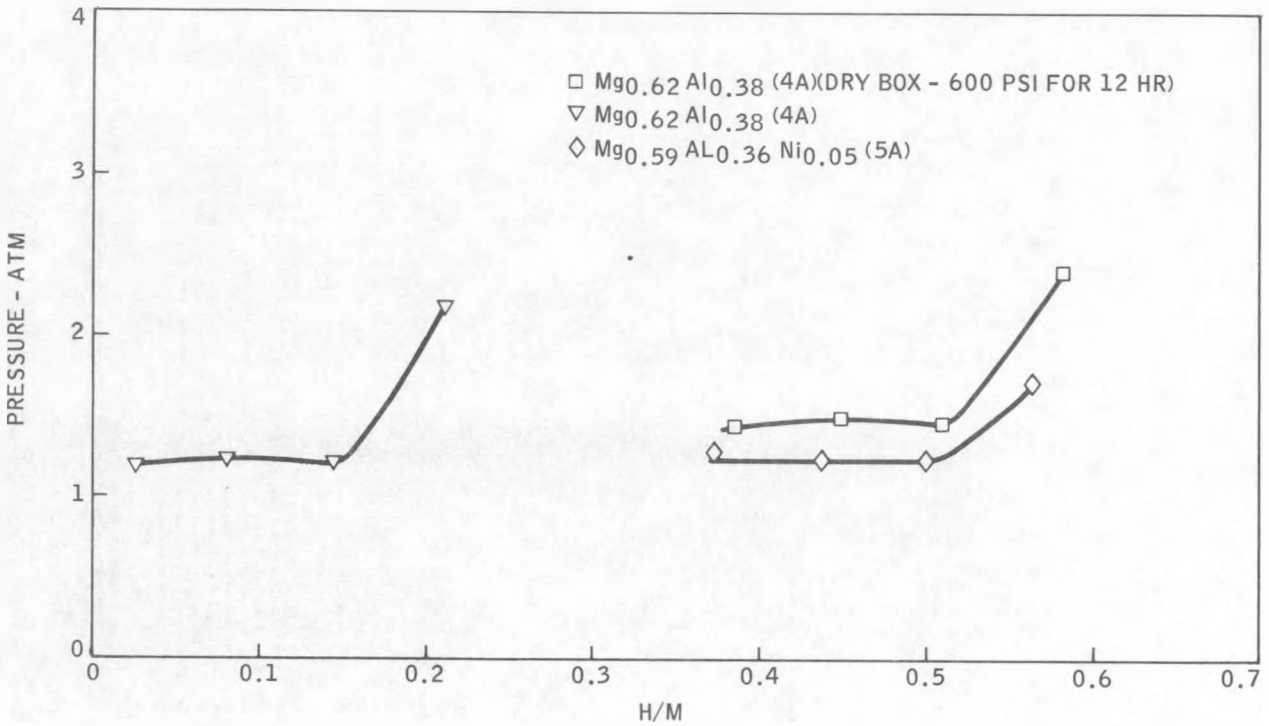

Figure 25. Pressure-Composition Isotherms for Mg-Al-X System

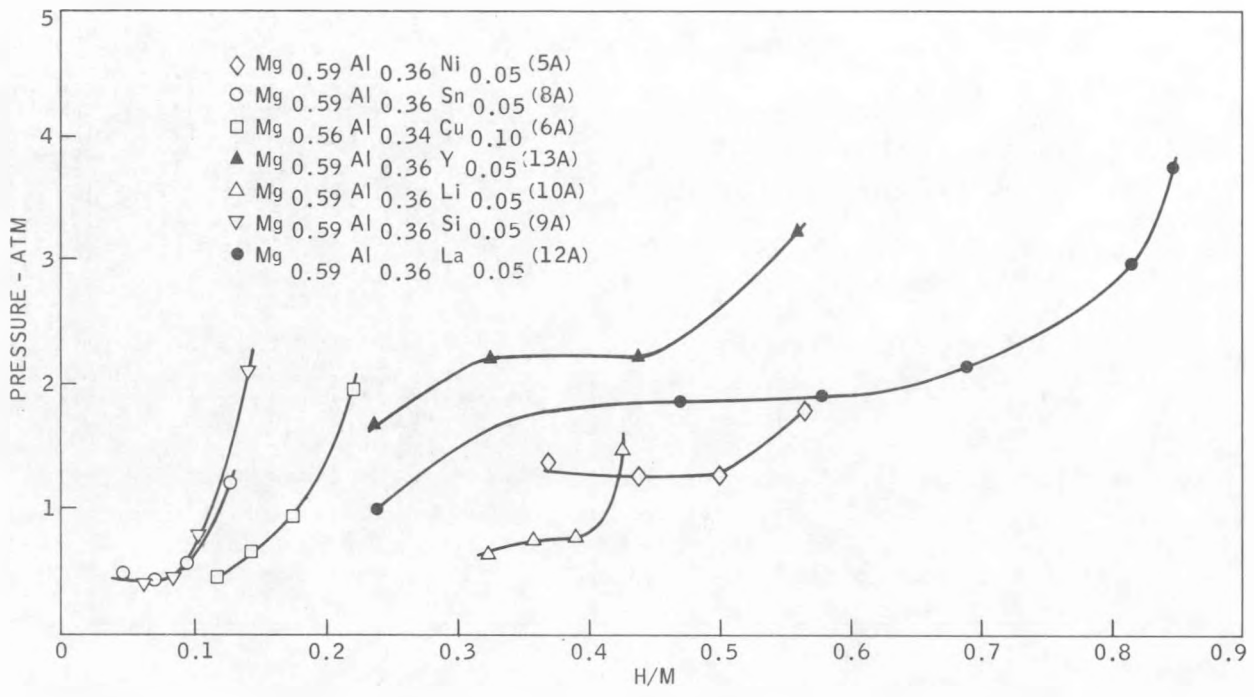

Figure 26. Pressure-Composition Isotherms for Mg-Al-X Systems at 310°C (Standard Hydriding Procedure)

kinetics of Al-containing alloys. See Table 13 for a comparison of the thermodynamic stabilities of various oxides. The relatively poor hydriding kinetics of Mg can also be attributed to the very stable oxide it forms. However, MgO is somewhat less impervious and protective than Al_2O_3. It is possible that the Y addition is also beneficial in this case, as Y_2O_3 is slightly more stable than MgO at elevated temperatures (Table 13).

Table 13

Free Energies of Formation of Selected Oxides (Ref. 17)

Oxide	Temperature °C (°K)	ΔG_{o_f}, kcal/gm-atom 0
Al_2O_3	400 (673)	-117
	1027 (1300)	-98
MgO	400 (673)	-126
	1027 (1300)	-106
La_2O_3	400 (673)	-129
	1027 (1300)	-115
Y_2O_3	400 (673)	-125
	1027 (1300)	-111
Li_2O	400 (673)	-121
	1027 (1300)	-97

The five atomic percent Li addition may also have some potential oxygen scavenging ability, as hydriding kinetics show some improvement and the hydrogen content (1.78%) after the standard hydriding procedure is considerably better than the Cu- and Sn-containing alloys. However, the dissociation pressure is too low (Fig. 26). The addition of five atomic percent of Si appears to provide no benefits to the hydriding behavior of the basic $Mg_{17}Al_{12}$ intermetallic compound (see Fig. 26 and Table 12).

Using the standard hydriding procedure, the highest H/M ratio of 0.85 was attained with Alloy 12A, which contains five atomic percent La (Fig. 26). La has a slightly higher free energy of formation of its oxide than Y (see Table 13), so that it would be expected to exhibit a similar hydriding behavior to Y. Figure 27 summarizes the results on alloys that have been subjected to a 12 hour hydriding procedure.

Hydriding studies were also conducted on alloys containing 10 atomic percent additions of Y, La, mischmetal, and yttrium mischmetal (contins 60% or more yttrium). The PC isotherms at 310°C are compared in Figure 28 and the hydriding characteristics are summarized in Table 12. Alloy 14A, containing 10

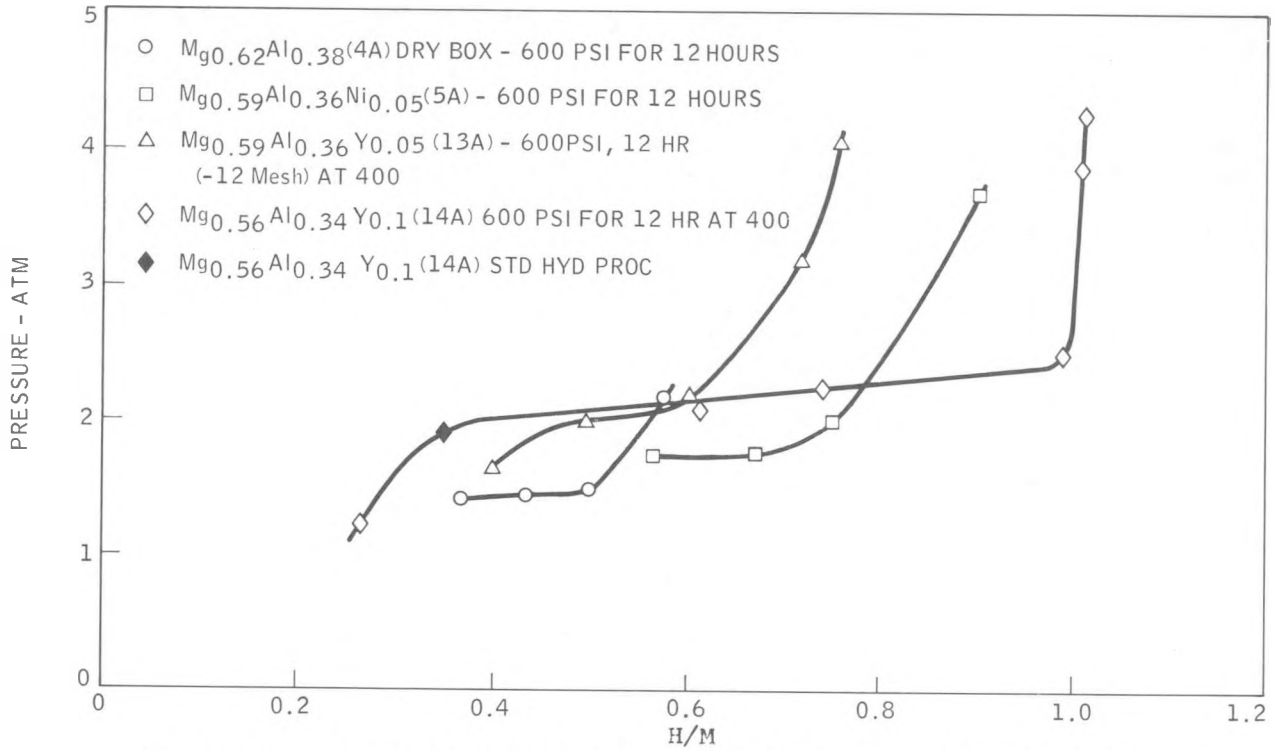

Figure 27. Pressure-Composition Isotherms (310°C) for Mg-Al-X Hydrided for Extended Times

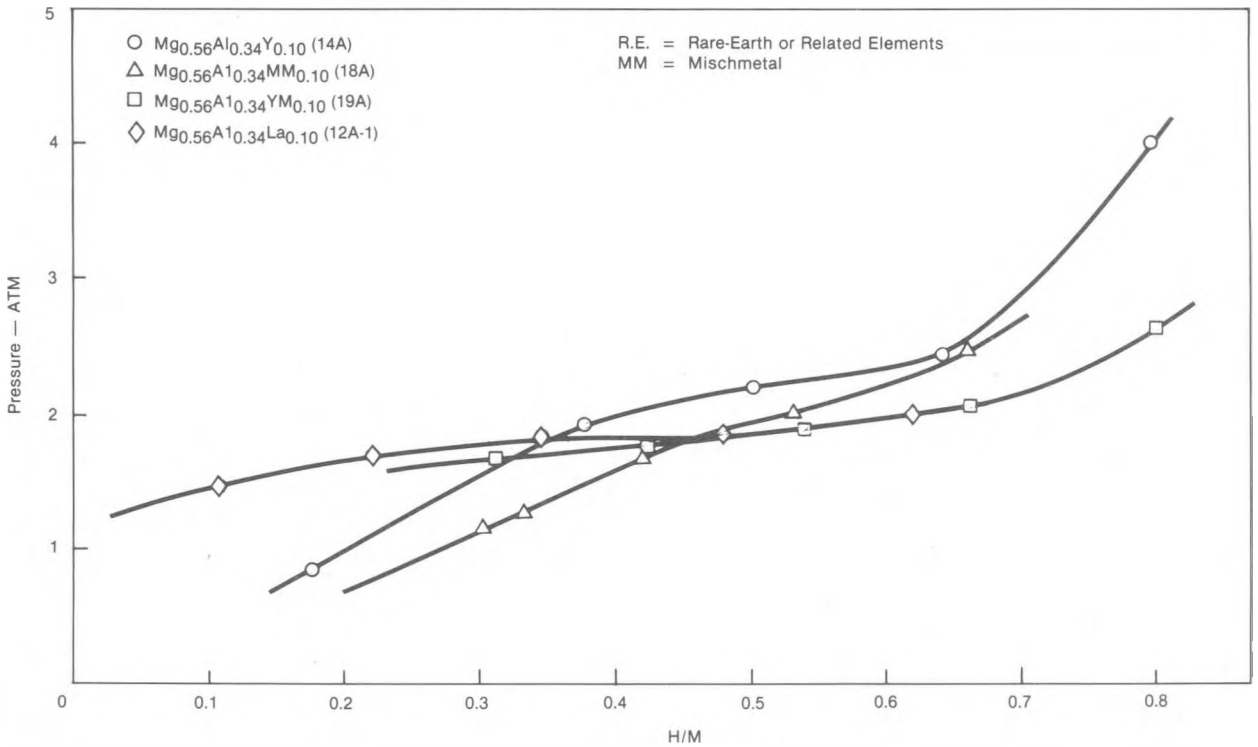

Figure 28. Pressure-Composition Isotherms for Mg-Al-RE Alloys

atomic percent yttrium, exhibits the higher dissociation pressure over the entire plateau region. Two of the alloys exhibit sloping plateau regions which may be a result of microsegregation. It is possible that this could be minimized by annealing for a longer period of time, or at a higher temperature.

In summary, alloying of the intermetallic phase $Mg_{17}Al_{12}$ has improved both the hydrogen capacities and plateau pressures. The best results for plateau pressures (2.4 atm) and hydrogen capacities (H/M = 1.1) were obtained with the alloy containing 10 atomic percent Y.

3.3.2 Mg-10Al Alloys

Douglass (Ref. 6) studied the formation of hydrides by the reaction of high-pressure hydrogen (300 to 800 psi) with Mg-10Al at 400 and 450°C. The emphasis of this research was on the kinetics and comminution resistance of the alloy. Curves for the reaction kinetics at 400°C and 450°C are shown in Figure 29. As mentioned in the section on Magnesium-Nickel Alloys, the reaction kinetics can be described by the Johnson-Mehl relationship, which is based upon a nucleation and growth process. The hydrides were observed to approximate a spherical shape and nucleated throughout the alloy independent of grain boundries or other irregularities.

After 20 hours at 450°C, the Mg-10Al absorbed 7 percent hydrogen. This corresponds to 92 percent of the material being hydrided. The hydrided alloy is remarkably free of fragmentation, and is attributed to the remaining ductile metal holding the brittle hydride particles together (Ref. 6).

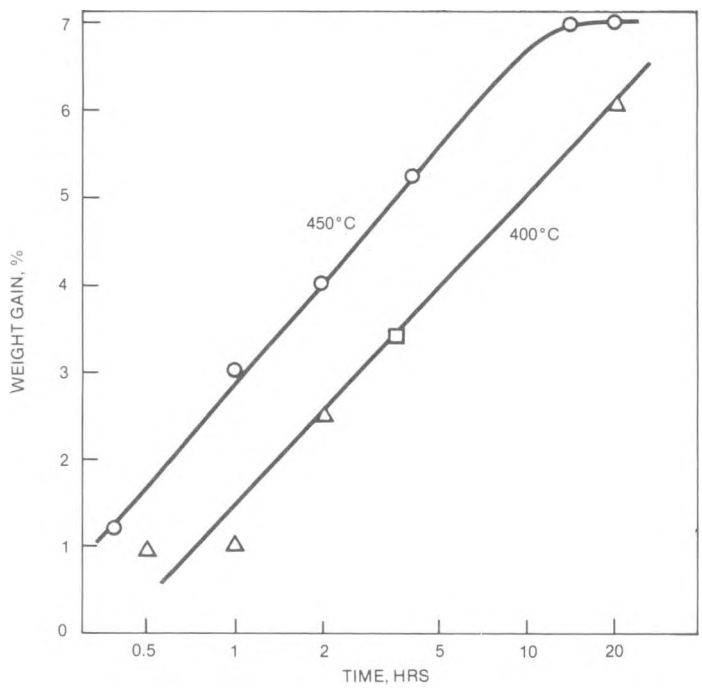

Figure 29.

Hydriding Kinetics of Mg-10Al (Ref. 6)

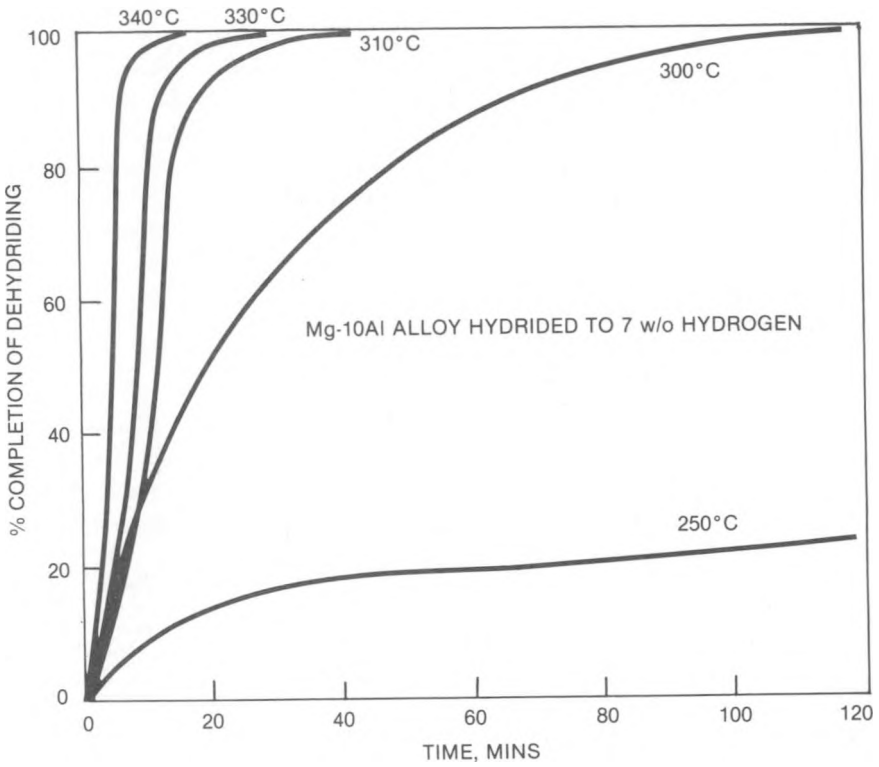

Figure 30.

Kinetics of Dehydriding MgH_2 into Vacuum (Ref. 6)

Figure 30 shows curves for the dehydriding process at different temperatures from 250 to 340°C. An Arrhenius plot of log time for 50 percent reaction versus reciprical temperature indicates an activation energy of 22.8 kcal/mol.

Because of the possibility of high hydrogen contents in the Mg-10Al alloys, the authors undertook the task of investigating the possibility of increasing the hydriding and dehydriding kinetics, without materially reducing the hydrogen capacity. Alloying studies with either single or multiple additions were conducted. Since the kinetics and hydrogen capacities of the $Mg_{17}Al_{12}$ alloys benefited substantially from the presence of rare-earths and yttrium, these additions were given emphasis.

Preparation of Hydriding Alloys

Alloys were prepared in accordance with procedures described earlier.

Hydriding and Mini-P-C Isotherms

The homogenized Mg-Al alloys were subjected to the standard hydriding procedure at a pressure of 600 psi. (See previous descriptions.) The Mg-10Al alloys containing rare earths and yttrium were more difficult to pulverize into fine mesh powder; however, this has little effect on the final results since these alloys hydrided readily with a relatively coarse powder size.

After hydriding, mini-PC isotherms were determined on each alloy at 310°C. The PC relationships are plotted in Figures 31 and 32. Hydriding characteristics are tabulated in Table 14.

Figure 31 compares the partial isotherms of alloys containing 10 atomic percent La and Y, respectively. Alloy 23A ($Mg_{0.8}Al_{0.1}La_{0.1}$) exhibits a much higher hydrogen content (3.18%) and a flatter and slightly higher plateau pressure after the standard hydriding procedure. The high T (123°C) of the 10 a/o La alloy also indicates relatively rapid hydriding kinetics. It has been noted that the hydriding characteristics of $Mg_{0.8}Al_{0.1}Y_{0.1}$ (22A) are not as good as Alloy 14A, which contains 34 atomic percent Al (see section 3.3.1 on $Mg_{17}Al_{12}$). SEM and EDX analysis suggests that all of the Al is tied up as YAl_3. This is discussed further under the Metallographic Analysis section below. It is also quite obvious that the P-C relationships of the Cu-containing Alloy 13A are inferior to the alloys containing La and Y. The kinetics of dehydriding of Alloy 12A are also extremely slow; up to four hours were required to equilibrate the pressure for each increment of gas withdrawn. The hydrogen content of 1.46 percent for $Mg_{0.8}Al_{0.1}Cu_{0.1}$ (Alloy 12A) is also substantially lower than the three to four percent levels of the La- and Y-containing alloys.

Figure 32 summarizes the results obtained with Alloys 22A and 23A hydrided for 12 hours at 400°C. Both alloys absorbed substantial quantities of hydro-

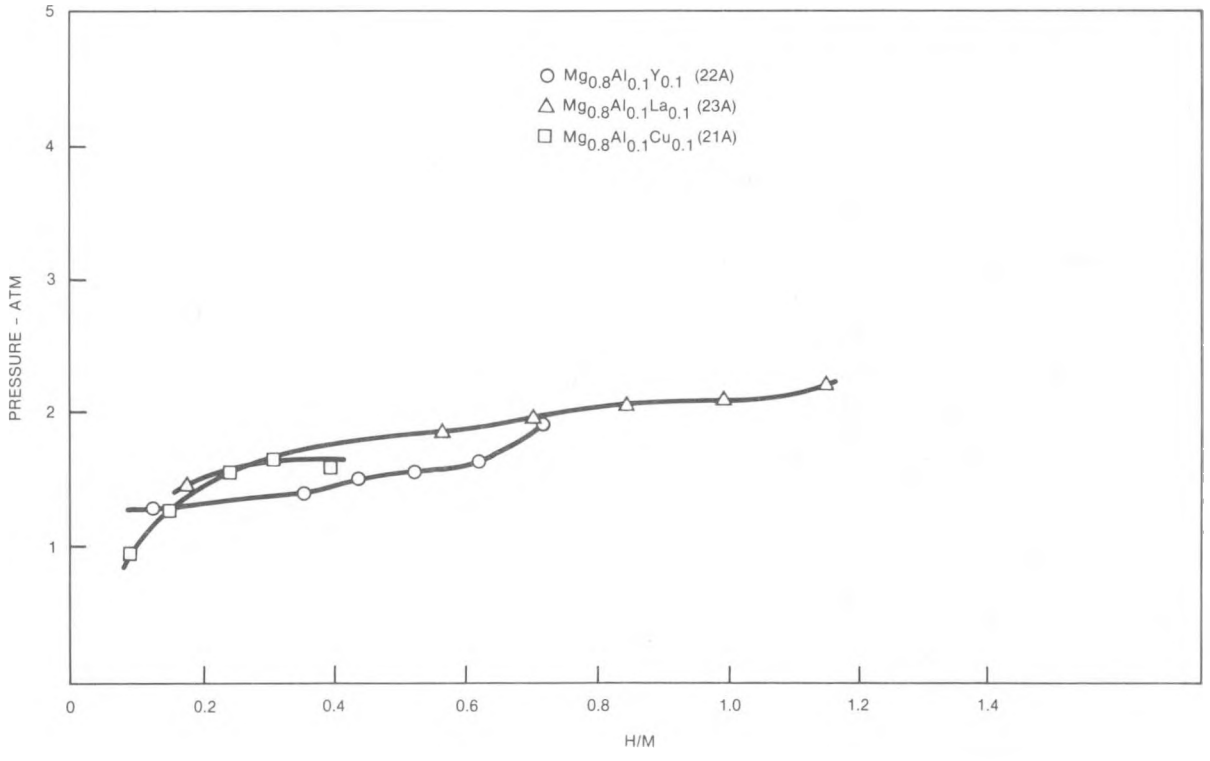

Figure 31. Pressure-Composition Isotherms for $Mg_{0.8}Al_{0.1}X_{0.1}$ at 301°C

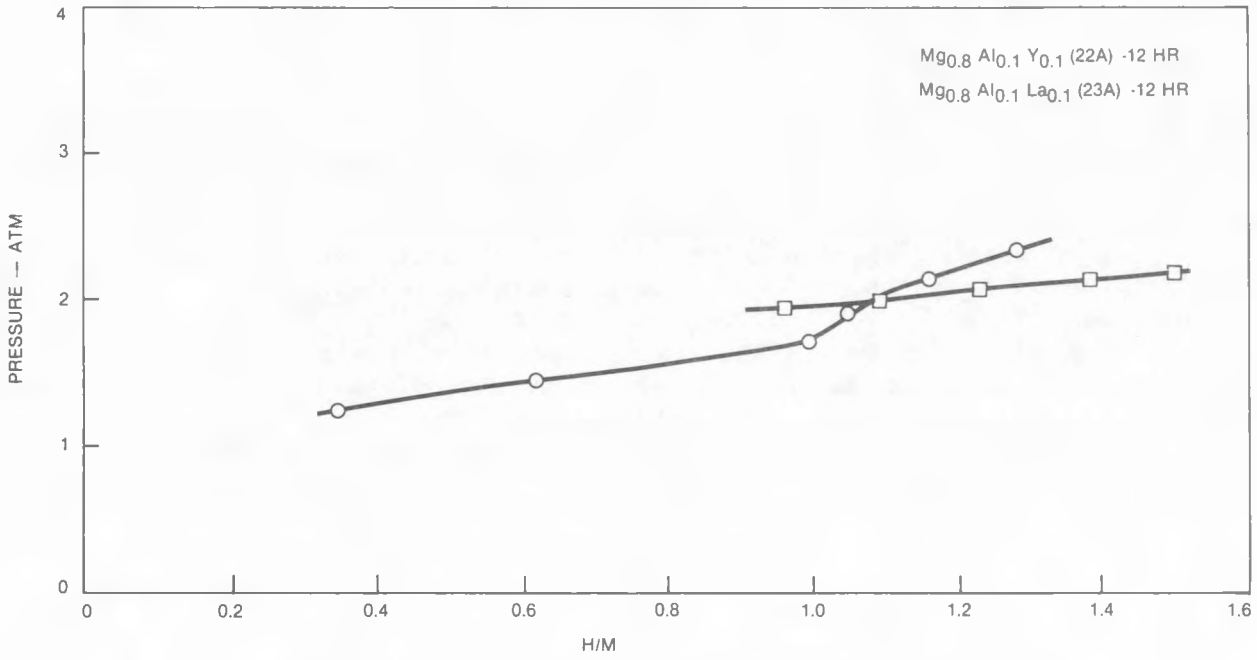

Figure 32. Pressure-Composition Isotherms for $Mg_{0.8}Al_{0.1}X_{0.1}$ Hydrided for Extended Times

Table 14

Hydriding Characteristics of Modified Mg-10Al Alloys

Alloy	Composition	ΔT, °C	H_2 Absorbed, %	Plateau Pressure at 310°C (atm)	Remarks
22A	$Mg_{0.8}Al_{0.1}Y_{0.1}$	65	2.35	1.5	-12 mesh. Standard hydriding
22A	$Mg_{0.8}Al_{0}{}_{0.1}Y_{0.1}$	--	4.08	1.6	-20 mesh. 12 Hours 600 psi at 400°C
23A	$Mg_{0.8}Al_{0.1}La_{0.1}$	123	3.18	2	-20 mesh. Standard hydriding
23A	$Mg_{0.8}Al_{0.1}La_{0.1}$	--	4.22	2.1	-20 mesh. 12 Hours 600 psi at 400°C
21A	$Mg_{0.8}Al_{0.1}Cu_{0.1}$	--	1.46	∿1.6	-10 mesh. Standard hydriding

gen after the 12 hour period; 4.22 wt. percent for $Mg_{0.8}Al_{0.1}La_{0.1}$ and 4.08 wt. percent for $Mg_{0.8}Al_{0.1}Y_{0.1}$. These represent the highest hydrogen capacities of the entire Mg-Al base hydride alloy series achieved by the authors to date.

Metallographic Analysis of Unhydrided Alloys

Microstructural analysis was undertaken in an attempt to develop a better understanding of the role that the various alloy phases play during the hydriding reaction. Center slices cut from alloy ingots of 22A and 23A, which had been homogenized for 106 hours at 425°C, were polished, and examined. SEM and optical micrographs were prepared and EDX was used for phase identification.

Alloy 22A is represented in the photomicrographs in Figure 33. The single phase regions are marked by A and B and the two-phase region, C. A tentative identification of these phases has been made with the aid of SEM/EDX techniques. Although exact ratios of the elements are difficult to establish with the EDX without correcting for mutual absorption, the ratios obtained are at least semi-quantitative. Based upon the elemental ratios established by EDX, Phase A most likely consists of the refractory intermetallic compound, YAl_3. Since all of the Al appears to be tied up in this refractory aluminide, the remaining portion of the alloy is essentially a binary system between the unreacted Y and Mg. Elemental ratios and X-ray dot patterns indicate that Phase B is almost all Mg and, as such, is undoubtedly the terminal solid solution of Y in Mg. Phase C appears to be a eutectic and is presumably composed of the intermetallic $Mg_{24}Y_5$ and the terminal solid solution of Y in Mg (see Fig. 34) (Ref. 18).

Photomicrographs of Alloy 23A and SEM micrographs are shown in Figures 35 and 37. Single phase regions are again denoted by A and B, and the two-phase region by C. Tentative phase identification was carried out with SEM/EDX.

As in Alloy 22A, Phase A in Figure 35 is identified as a refractory aluminide, probably a non-stoichiometric variant of $LaAl_2$. Again, essentially most of the Al is tied up in the highly stable and refractory aluminide form. The balance of the La and Mg substantially interact as a binary system of Mg and La. EDX indicates the Mg-rich, Phase B to be Mg_9Al with a small amount of Al present. Apparently some partitioning of Al takes place between the $LaAl_2$ and the $LaMg_9$ phases. The eutectic region C appears to be made up of Mg and $LaMg_9$, with the $LaMg_9$ presumably containing a small amount of Al in solid solution (refer to Fig. 36).

Figure 37a represents a SEM micrograph of Alloy 23A, showing constituents A, B, and C. Figure 37b is a MgK_α dot pattern of the same area as Figure 37a showing the Mg distribution in the microstructure of $Mg_{0.8}Al_{0.1}La_{0.1}$.

Metallographic Analysis of Partially Hydrided Alloys

The unhydrided specimens of Alloys 22A and 23A were partially hydrided, and examined with SEM/EDX. The phases present in the micrographs are designated in the same manner as they were in the previous section, e.g., A, B and C.

Alloy 22A is presented in the SEM micrographs in Figures 38 and 39. In Figure 38, Alloy 22A is shown as it appears prior to partial hydriding. Phase

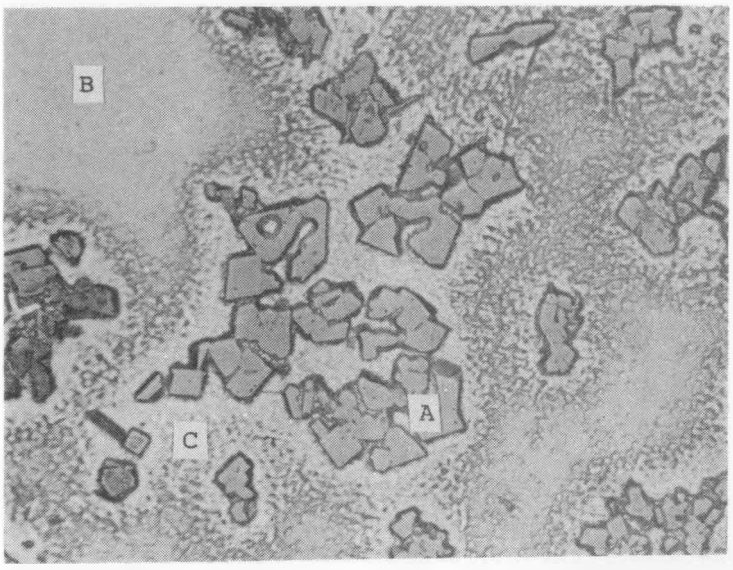

Figure 33a.

Photomicrograph (optical) of $Mg_{0.8}Al_{0.1}Y_{0.1}$ (Alloy 22A) Homogenized at425°C for 106 Hours. Unetched

Magnification: 500X

Note: A,B are single-phase regions;
C is the two-phase region

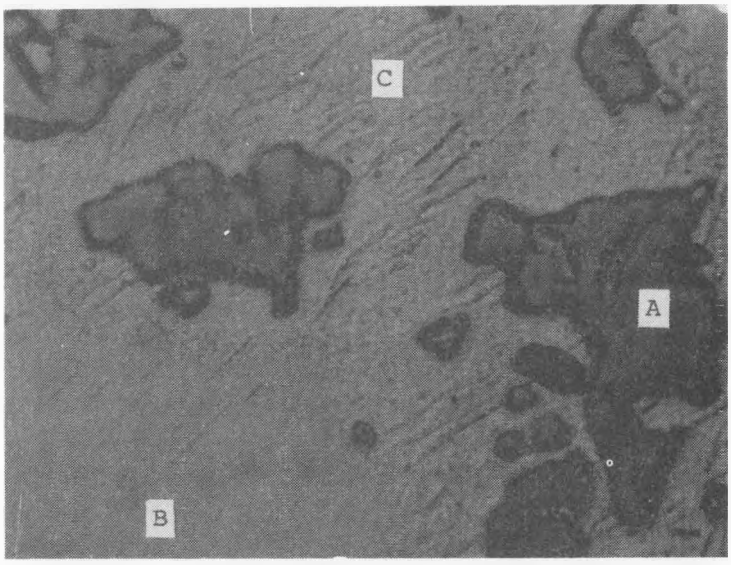

Figure 33b.

Photomicrograph (optical) of $Mg_{0.8}Al_{0.1}Y_{0.1}$ (Alloy 22A) Homogenized at 425°C for 106 Hours. Unetched.

Magnification: 1000X

A represents the refractory aluminides (probably YAl_3); B, the dark single phase, is the terminal solid solution of Y in Mg; and C represents the two-phase region presumably the eutectic composed of $Mg_{24}Y_5$ and the terminal solid solution of Y in Mg.

The SEM micrographs in Figure 39 illustrate the appearance of $Mg_{0.8}Al_{0.1}Y_{0.1}$ after partial hydriding. In Figure 39a, the acicular hydride phase appears to emanate from the aluminide particles and spreads out into the matrix. This would suggest that the YAl_3 is acting as a catalyst, thereby increasing the hydriding kinetics substantially. Figure 39b shows the formation of the hydride in the grain boundaries, which are areas of high energy and provide paths of higher diffusion rates. Since the grain boundary hydrides appear to be connected with the acicular hydride particles, it is possible that the

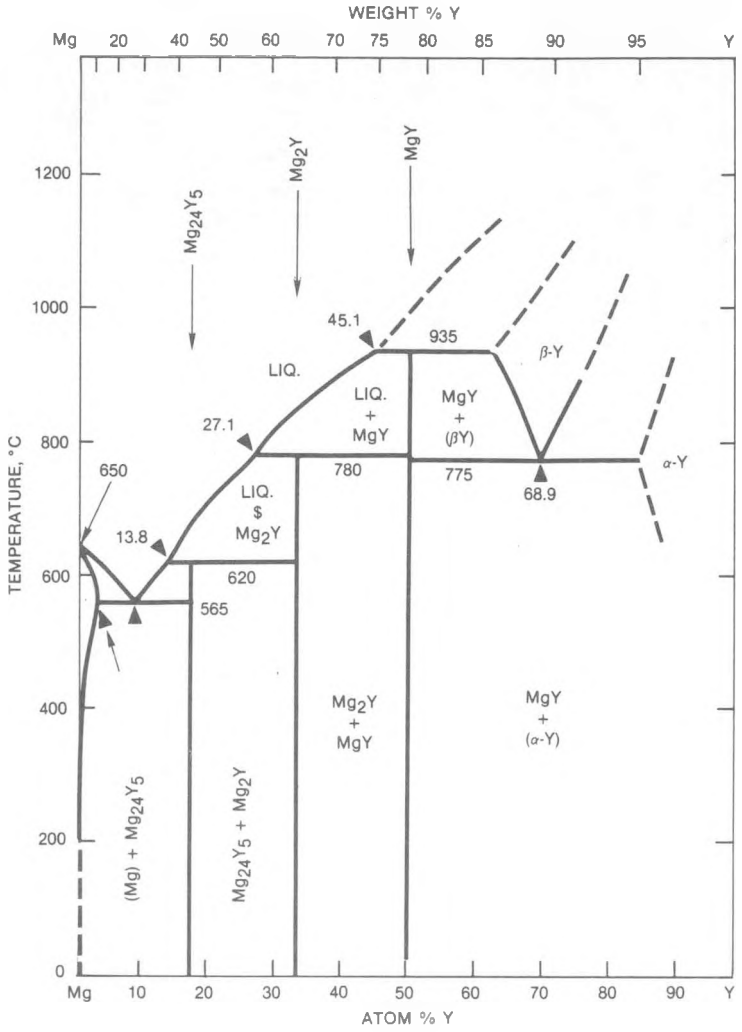

Figure 34.

Magnesium-Yttrium Phase Diagram (Ref. 18)

aluminide phase is also responsible for initiation of the hydriding reaction in the grain boundaries.

SEM micrographs of Alloy 23A ($Mg_{0.8}Al_{0.1}La_{0.1}$) are shown in Figures 40 and 41. Figure 40 is a SEM micrograph of the unhydrided alloy. The single phase regions are denoted by A and B, and the two phase region by C as in the previous section. As mentioned previously, phase A is a refractory aluminide, and is probably a non-stoichiometric variant of $LaAl_2$. The Mg-rich phase appears to be Mg_9La with some Al present. The eutectic region C appears to consist of Mg and Mg_9La.

Figure 41 represents the appearance of Alloy 23A after partial hydriding. It should be noted that the hydriding behavior of alloy 23A is quite different from Alloy 22A (see Fig. 39). The most obvious difference between the unhydrided and partially hydrided specimens is the considerable darkening in color of the aluminide (A) and the Mg_9La (B) phases. The partially hydrided and polished specimen in Fig. 41B shows cracking of these two phases due to the large volume expansion during hydriding.

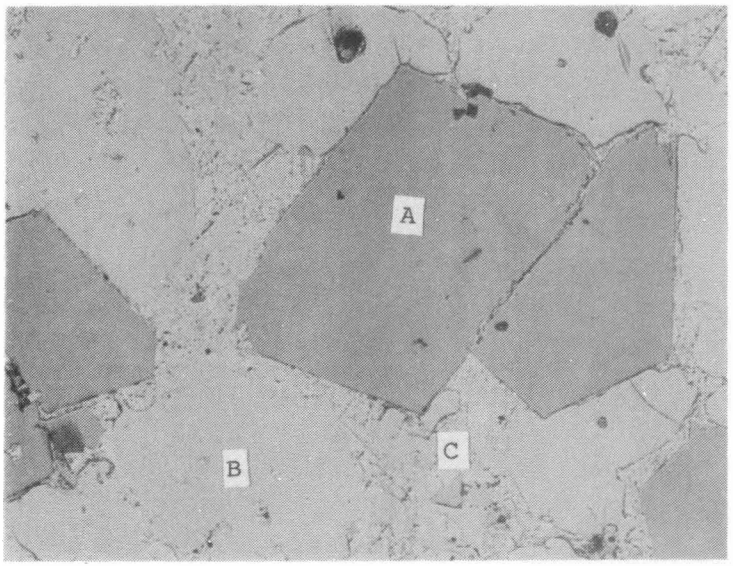

Figure 35a.

Photomicrograph of $Mg_{0.8}Al_{0.1}La_{0.1}$ (Alloy 23A) Homogenized at 425°C for 106 Hours. Unetched.

Magnification: 500X

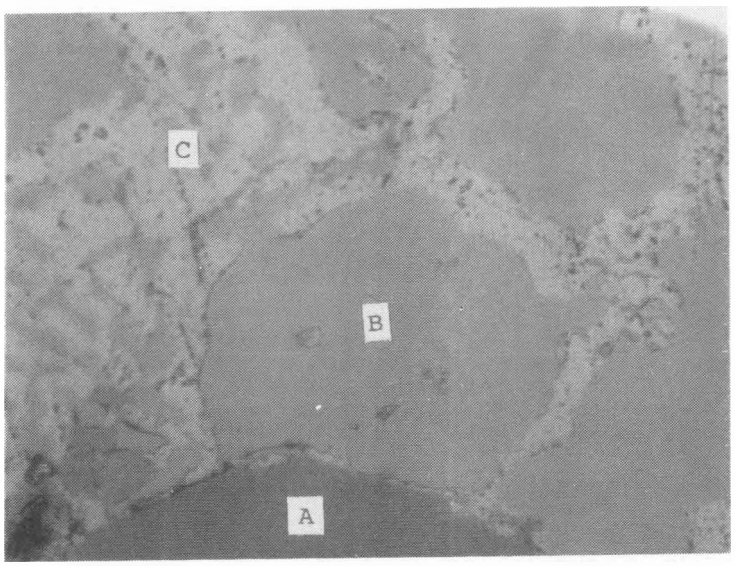

Figure 35b.

Photomicrograph of $Mg_{0.8}Al_{0.1}La_{0.1}$ (Alloy 23A) Homogenized at 425°C for 106 hours. Unetched

Magnification: 1000X

Apparently these phases hydride preferentially and then spread to the matrix material, until hydriding is complete. It is interesting to note, also, that the hydriding reaction for Alloy 23A appears to be more vigorous than Alloy 22A, as indicated by the ΔT of 123°C for 23A and 65°C for 22A.

3.3.3 Beta and Epsilon Phases

During their program of identification, synthesis, and evaluation of hydrides with a potential for automotive use, Reilly, et al. (Ref. 11) made a preliminary survey of a number of intermetallic compounds, including the beta and espilon phases. In their search for new hydrides, hydriding pressures ranged

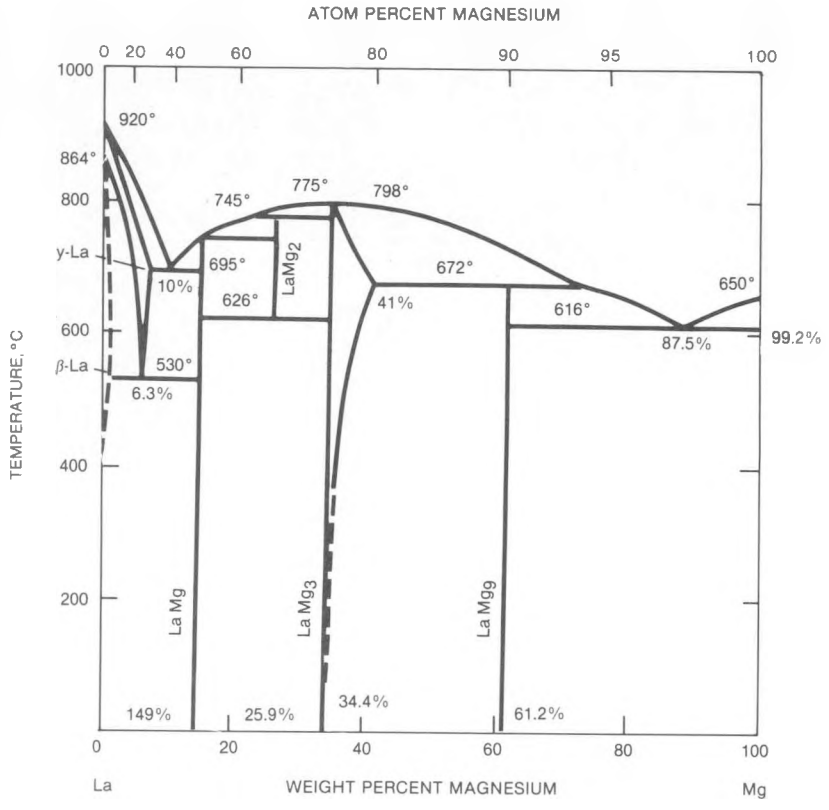

Figure 36. Magnesium-Lanthanum Phase Diagram (Ref. 19)

from 1000-5000 psia at temperatures of 275-325°C. Preliminary results appeared encouraging and are summarized in Table 11 and Figure 42.

Tests (Table 11) indicate that relatively coarse particle sizes (-20 mesh) yielded hydrogen contents as low as 0.7 weight percent. Decreasing the particle size to -200 mesh increased the hydrogen concentration significantly to 3.28 percent.

Figure 42 shows the equilibrium dissociation pressure during absorption at 302 and 326°C. More extensive investigations of the Mg_2Al_3 beta-phase were subsequently carried out by Air Products and Chemicals, Inc. (Refs. 10 and 12) and Mintz, et al. (Ref. 13).

Through X-ray diffraction analysis, Mintz, et al. (Ref. 13) concluded that the hydriding reaction occurs by disproportionation and takes place in a reversible manner as follows:

$$1/2\ Mg_2Al_3 + H_2 \rightleftarrows MgH_2 + 3/2\ Al \qquad (2)$$

Other investigators have also reported this reaction to proceed by disproportionation (Refs. 10 and 12).

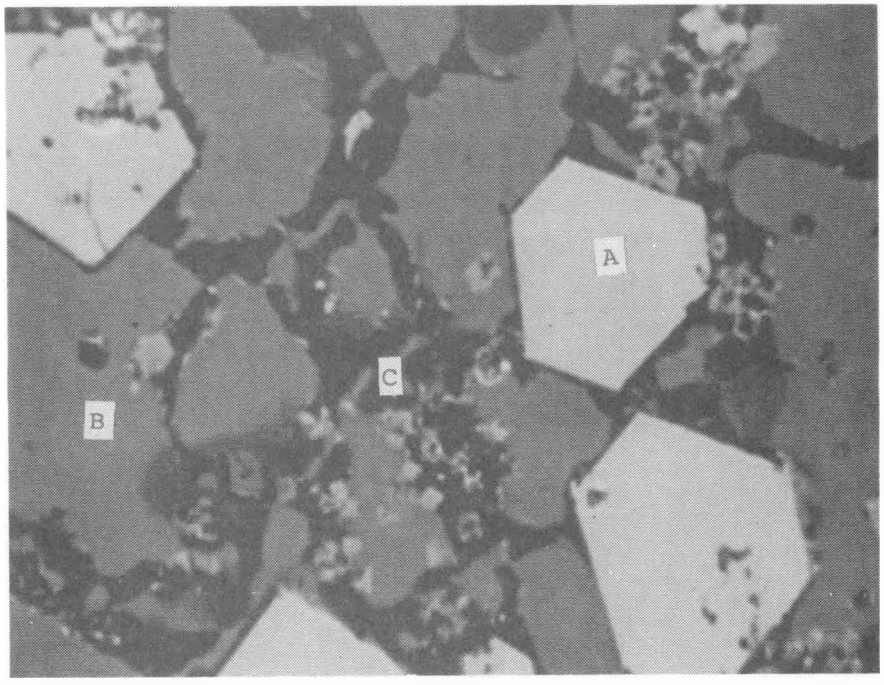

Figure 37a. SEM Micrograph of $Mg_{0.8}Al_{0.1}La_{0.1}$ (Alloy 23A) Unetched. Magnification: 850X

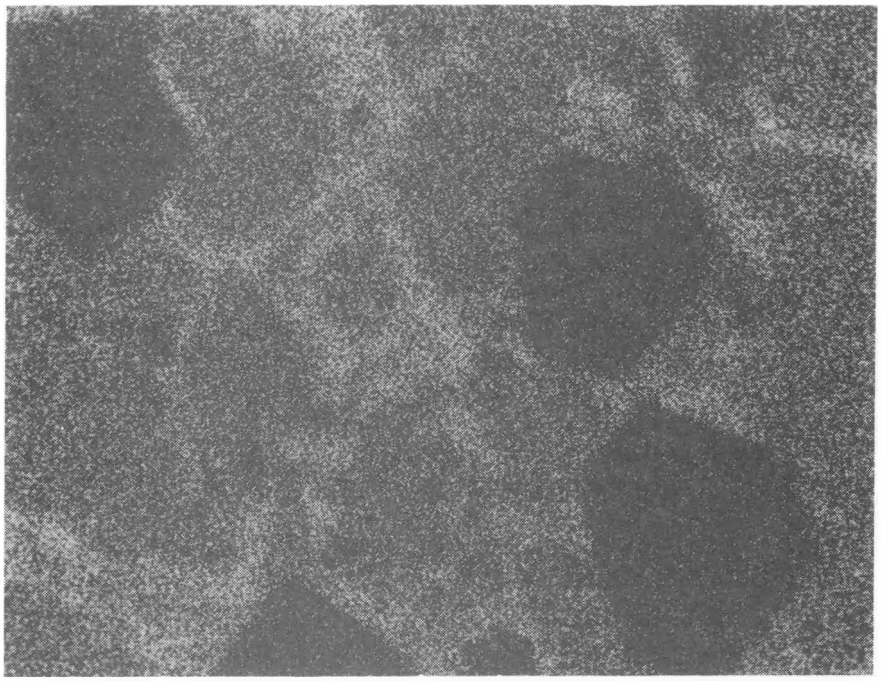

Figure 37b. MgKα Dot Pattern Same Area as Above. Magnification: 850X

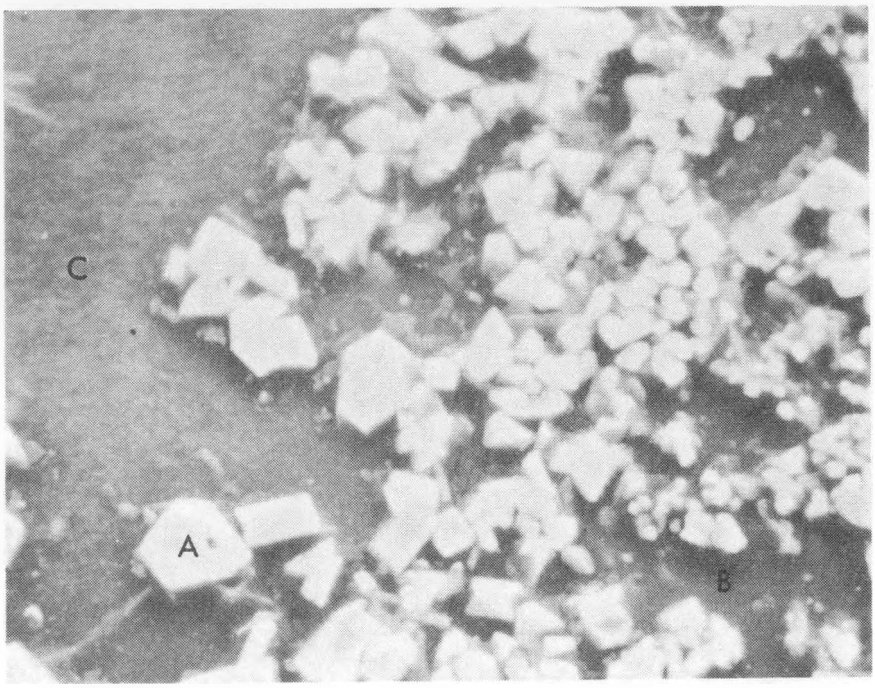

Figure 38. SEM Micrograph of $Mg_{0.8}Al_{0.1}Y_{0.1}$ (Alloy 22A) Prior to Partial Hydriding. Unetched. Magnification: 950X

The beta-phase Mg_2Al_3 appears to have potential for higher plateau pressures at relatively low temperatures, and has been reported to have one atmosphere plateau pressure at 323°C (Ref. 10). The difficulty is that below 250°C this alloy exhibits exceedingly slow absorption/desorption kinetics, which render it impractical for vehicle fuel system use. The dissociation temperature reported has been obtained by extrapolation of the Van't Hoff Plot. Mintz, et al. (Ref. 13) also point out the sluggish nature of reaction (2). Even activated alloys require several hours to reach equilibrium. Figure 43 presents the PC isotherms obtained by Mintz and coworkers (Ref. 13) for the Mg_2Al_3-hydrogen system. It can be seen that the plateau pressures are considerably higher than pure MgH_2. Dependence of the equilibrium dissociation pressure on temperature is given by the following relationship:

$$\log P_{atm} = -3306/T + 6.47 \qquad (3)$$

From these data the heat of formation of reaction (3) was calculated to be 15.1 kcal/mole.

Note also in Figure 43 that below 350°C two plateau regions appear in the PC isotherm of Mg_2Al_3. Mintz, et al., (Ref. 12) attribute this to partial rearrangement of Mg and Al during the buildup of Mg_2Al_3, due to the low mobility of these elements at the lower temperatures.

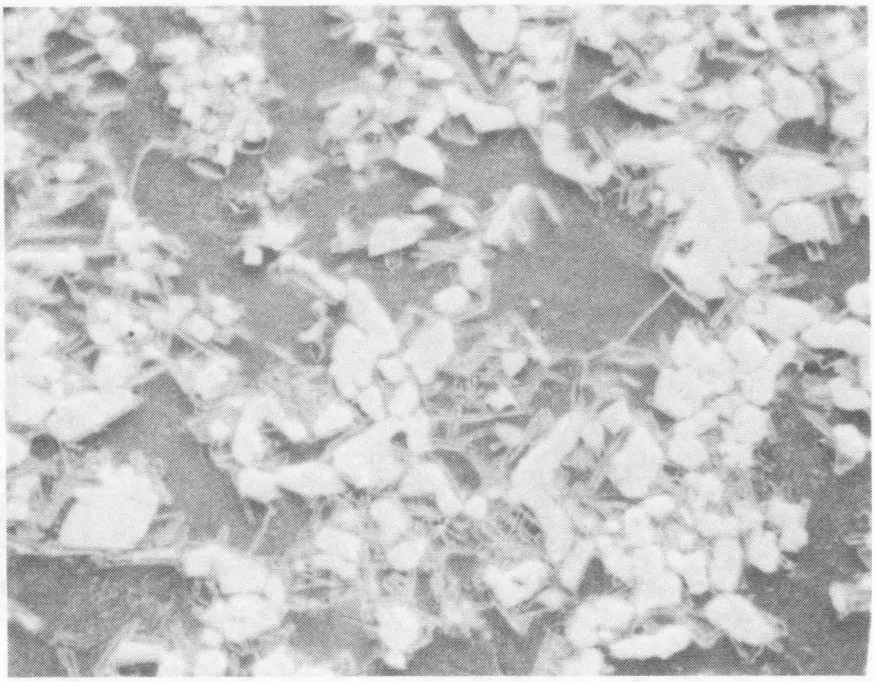

(a)

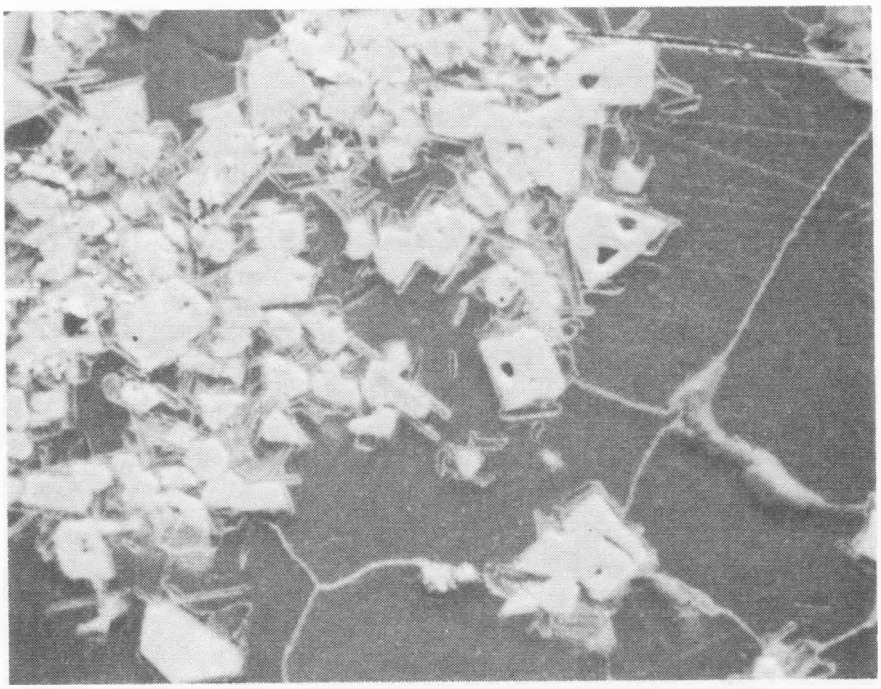

(b)

Figure 39. SEM Backscatter Micrograph of $Mg_{0.8}Al_{0.1}Y_{0.1}$ (Alloy 22A) After Partial Hydriding. Unetched. Magnification: 950X

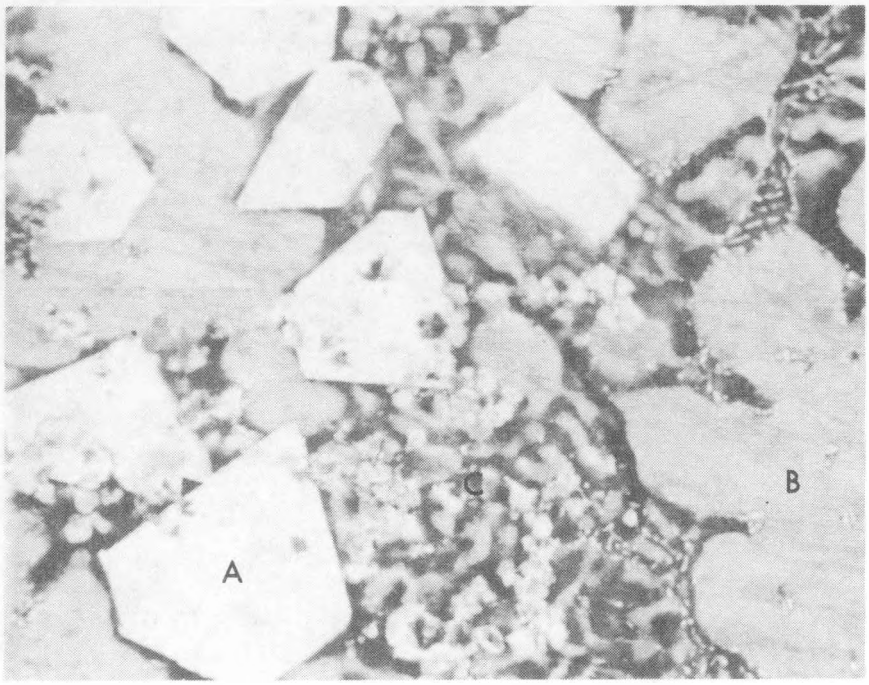

Figure 40. SEM Micrograph of $Mg_{0.8}Al_{0.1}La_{0.1}$ (Alloy 23A) Prior to Partial Hydriding. Unetched. Magnification: 950X

Effects of Alloying Mg_2Al_3 (Ni, In) Gavra, et al. (Ref. 20) and Air Products and Chemicals (Ref. 10) studied the effects of small alloying additions on kinetics of hydriding/dehydriding Mg_2Al_3. Gavra observed that 2 to 3 weight percent of Ni or In accelerates the activation process. However, the most pronounced effect of these additives is the rapid increase in hydriding rates during repeated cycling. Figure 44 compares the kinetics of the binary alloy and those containing Ni and In additions. Reaction rates for the binary alloy is on the order of hours, whereas the Ni- and In-containing alloys is on the order of minutes.

Apparently these observations do not agree with those of Eisenberg, et al. (Ref. 21) who reported that Ni additions do not affect the hydriding kinetics of Mg_2Al_3. Gavra, et al. (Ref. 20) attribute this difference to slow reaction rates at the low temperatures of 200-275°C employed by Eisenberg, et al. (Ref. 21), with a good possibility of overlooking the effect of the ternary additions.

Effects of Alloying Beta-Phase Alloys (Rare Earths)

Because of the potential advantages of the beta-phase alloys (Mg_2Al_3), the authors investigated the addition of rare-earth elements for the possible improvement of the kinetics and hydrogen capacity of these alloys. The addition of rare-earth elements or the related element yttrium indicated

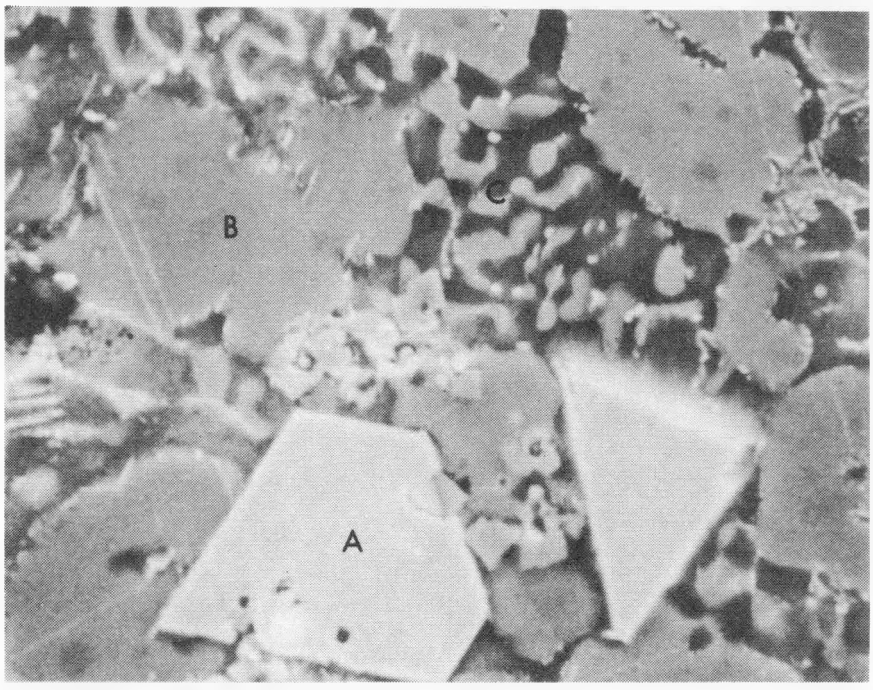

(a) Magnification: 950X

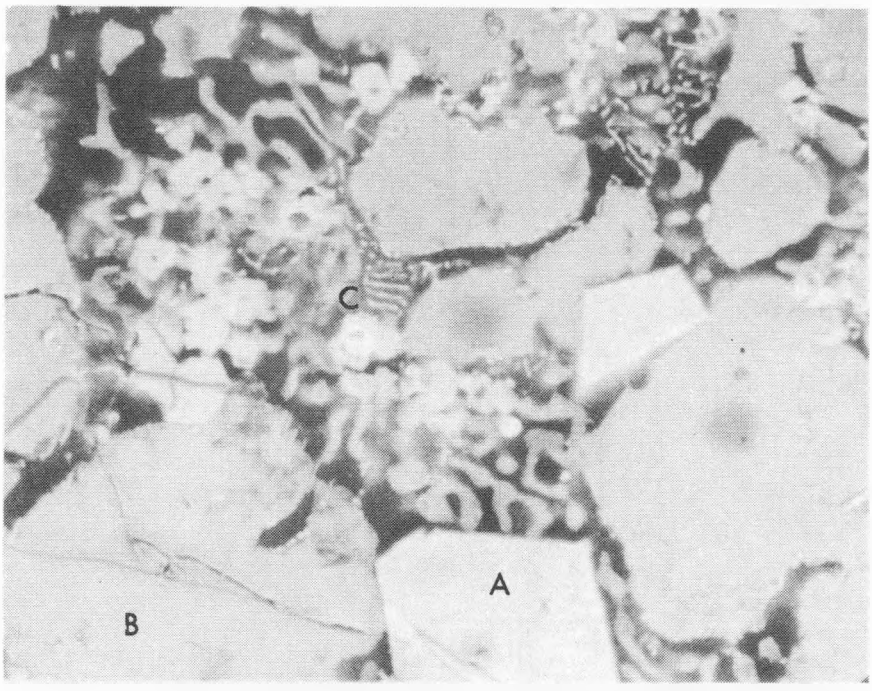

(b) Lightly Polished After Partial Hydriding
Magnification: 900X

Figure 41. SEM Micrographs of Partially Hydrided $Mg_{0.8}Al_{0.1}La_{0.1}$ (Alloy 23A)

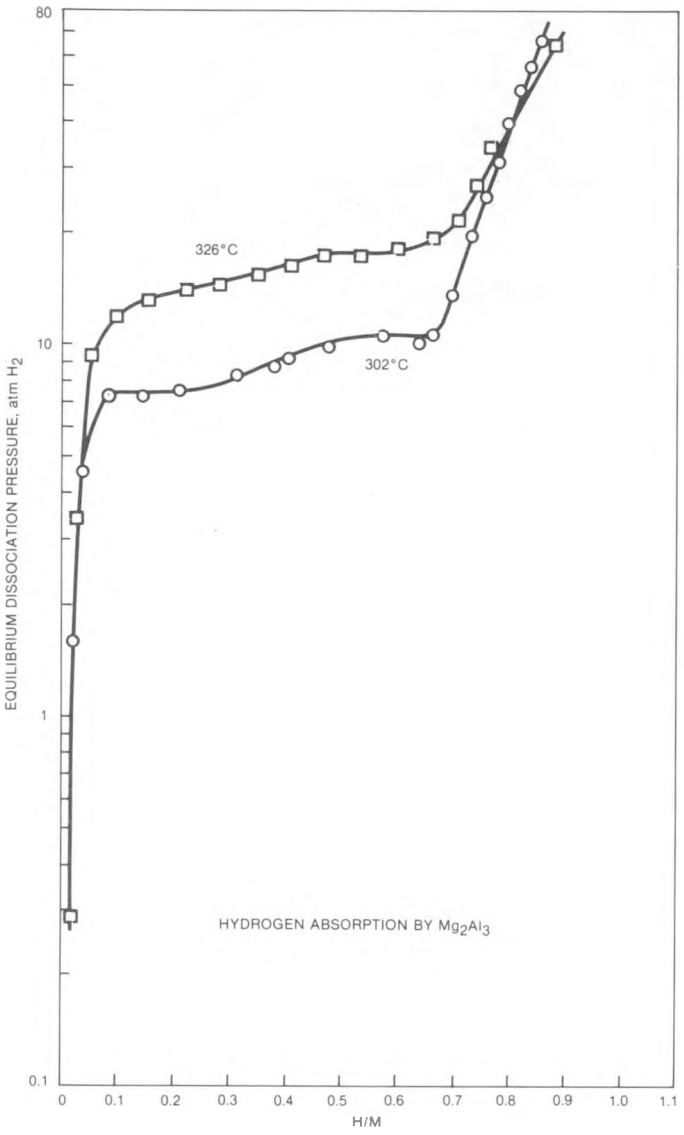

Figure 42.

Pressure-Composition Isotherms of the Mg_2Al_3-H System

that kinetics of hydriding/dehydriding and hydrogen capacities of $Mg_{17}Al_{12}$ alloys could be greatly improved, as described in an earlier section.

Baseline data were established with Mg_2Al_3. The alloy was crushed to -200 mesh and placed ($\sim$15 grams) into the reactor. Activation was accomplished by heating the reactor to 400°C and cycling the hydrogen pressure from 0 to 1000 psi several times. A ΔT of 23°C was obtained at this point. The reactor was pressurized to 1000 psi and maintained at a temperature of 400°C for 17 hours. After two additional pressurization-evacuation cycles, the ΔT increased to 38°C. The ΔT remained constant after a total of 15 cycles, indicating essentially complete activation. The reactor was pressurized to 1000 psi and maintained at 400°C for 60 hours for maximum hydrogen absorption.

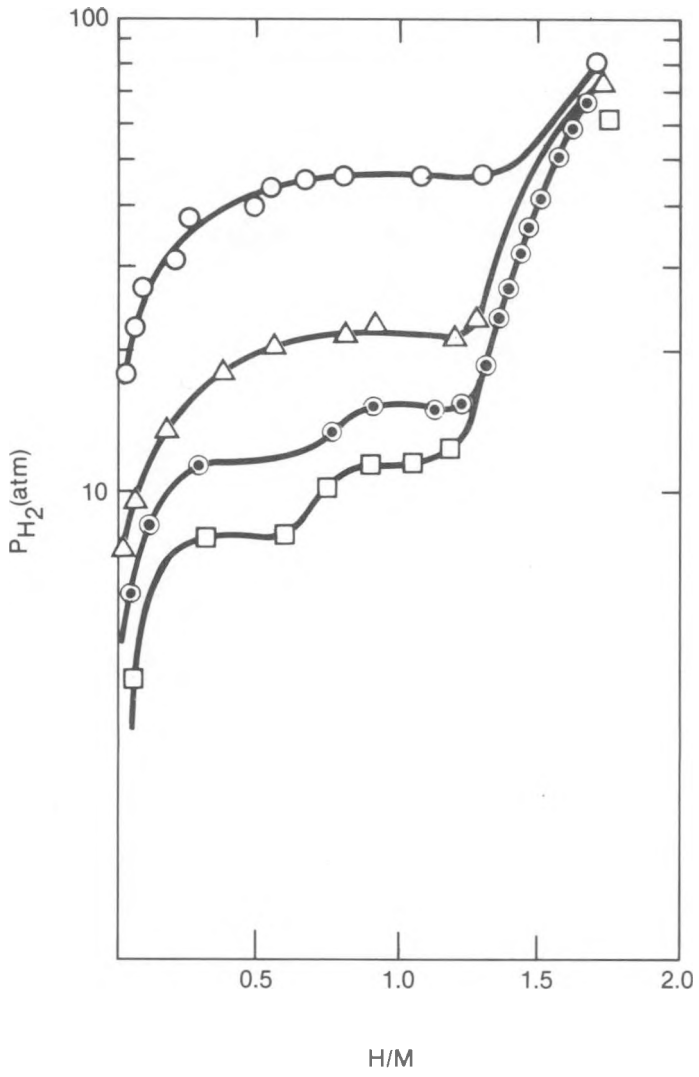

Figure 43.

Pressure-Composition Isotherms of the Mg_2Al_3-H System at 335°C (□), 350°C (◉), 375°C (△), and 410°C (○). (Ref. 13).

An isotherm was determined at a temperature of 350°C to eliminate the double plateau, which is reported to appear at temperatures below 350°C (Ref. 20). Because of the slow kinetics, each point was equilibrated for at least four hours. The isotherm is shown in Figure 45. Points from the data of Reference 11 are included and indicate good agreement with the authors' results.

Preparation of Alloys

Of the rare earths, lanthanum additions were studied initially. Compositions were selected on the assumption that a portion of the Al would be tied up as LaAl or $LaAl_2$. Fifty gram ingots of Alloy 34A, $Mg_{0.364}Al_{0.591}La_{0.046}$ (LaAl) and Alloy 35A, $Mg_{0.345}Al_{0.009}La_{0.044}$ ($LaAl_2$) were prepared by induction melting and homogenized at 425°C for 64 hours. The alloys were crushed to -200 mesh and hydrided in the reactor at 1000 psi and 400°C for 60 hours.

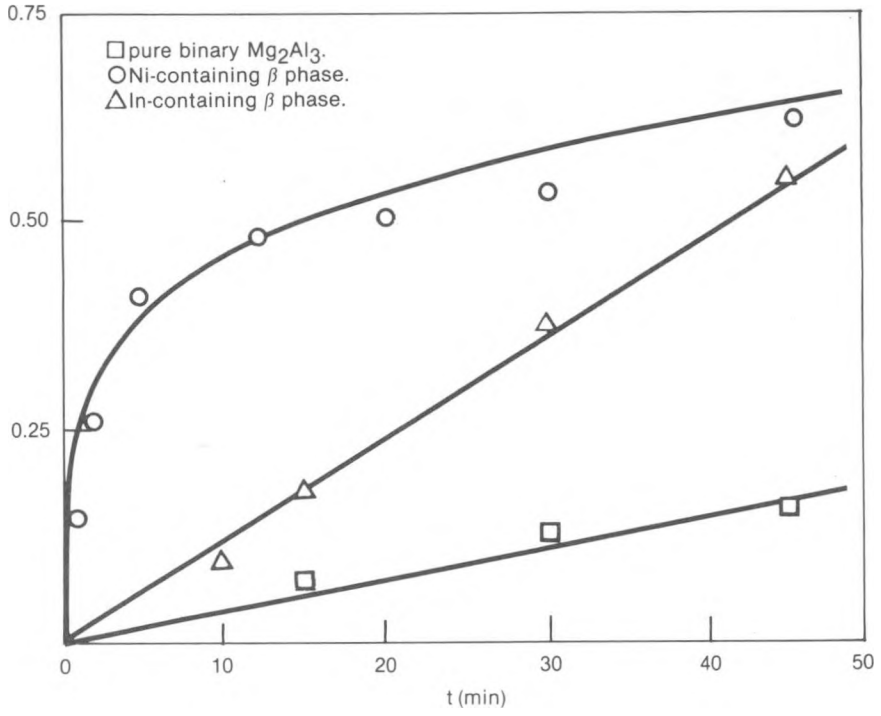

Figure 44. Hydriding Kinetics at 400°C of Cycled Beta-Phase Mg-Al Alloys (Ref. 20)

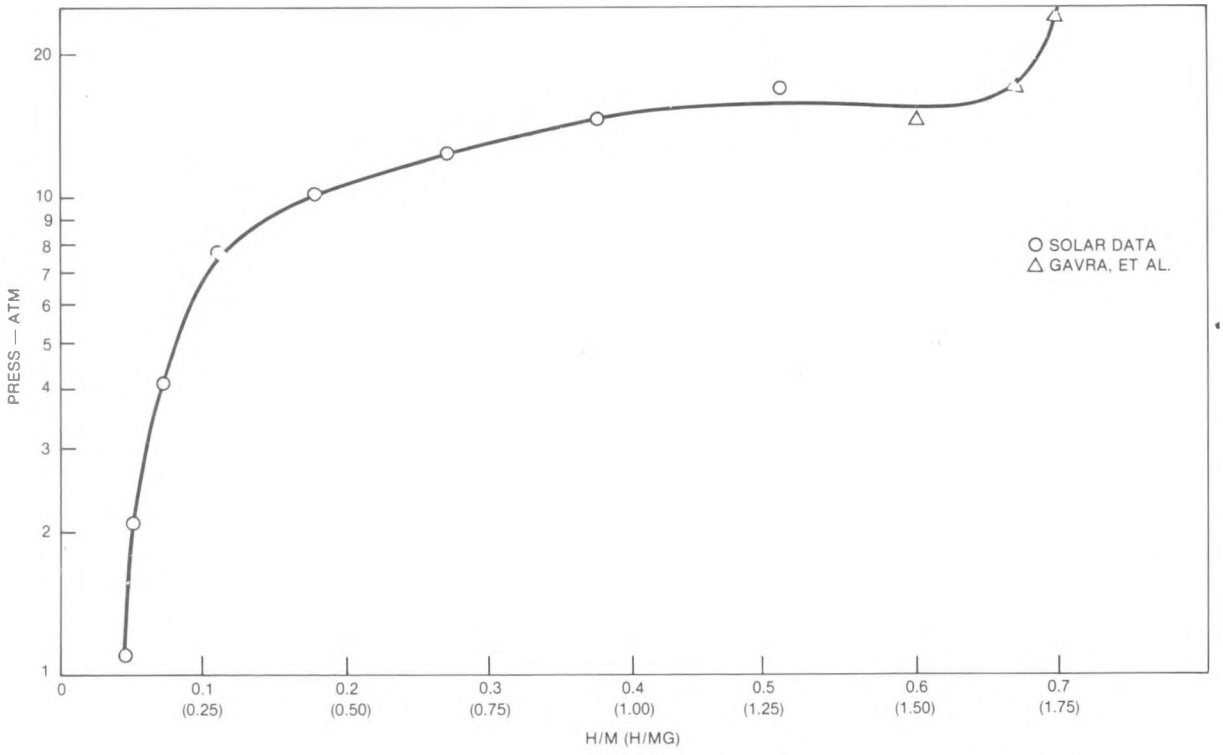

Figure 45. Pressure-Composition-Temperature of Mg_2Al_3 at 350°C

PC Isotherms

Isotherms were determined at 350°C and are compared to Mg_2Al_3 in Figure 46. In Alloy 34A the La is assumed to form LaAl. With Alloy 35A the assumption is the formation of $LaAl_2$. In both cases the H/M ratio has been increased as a result of the La additions, but the decompositon pressure in comparison to Mg_2Al_3 falls off at the lower H/M ratios. Alloy 35A with the assumed formation of $LaAl_2$ appears to produce the better results.

The time required for activation of Mg_2Al_3 appears to be substantially reduced by the addition of La. Reactivity of the alloys containing La, as measured by the ΔT, has also been enhanced (Table 15).

Investigations were also conducted on La additions to the Mg_5Al_8 composition, considered by some investigators to be closer to the actual composition of the beta-phase than Mg_2Al_3. Procedures for alloy preparation and determination of isotherms were identical to those used for Mg_2Al_3. Isotherms determined at 350°C are presented in Figure 47. In Figure 47, the highest dissociation pressure is exhibited by Alloy 37A with an assumed formation of $LaAl_2$. Note also that after 30 hours Alloy 36A had absorbed more hydrogen than the unalloyed Mg_5Al_8 after 60 hours of hydriding. This again indicates that the absorption kinetics are considerably improved by the La additions.

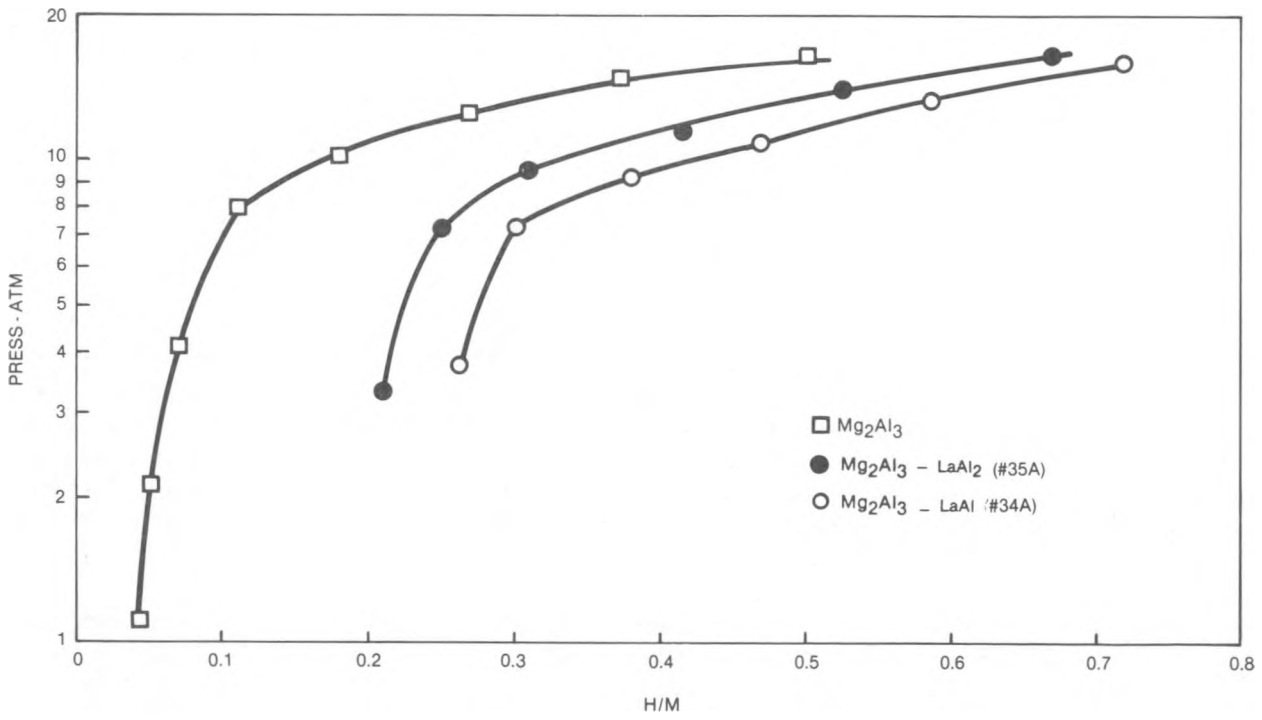

Figure 46. Comparative Pressure-Composition Isotherms at 350°C

Table 15

Effect of La Additions on Hydriding Characteristics of Mg_2Al_3, Mg_5Al_8, and Mg_4Al_5 Phases

Alloy	ΔT, °C	H_2 Absorbed, %	Mid-Plateau Pressure at 350°C (atm)
Mg_2Al_3 (32A) - Beta	38	1.93	14
$Mg_{0.364}Al_{0.591}La_{0.046}$ (34A)	55	2.28	12
$Mg_{0.345}Al_{0.609}La_{0.044}$ (35A)	58	2.13	13.5
Mg_5Al_8 (41A) - Beta	37	1.71	13.5
$Mg_{0.350}Al_{0.605}La_{0.046}$ (36A)	48	1.60 (30 hr)	13.5
$Mg_{0.335}Al_{0.622}La_{0.044}$ (37A)	49	1.73	14.5
Mg_4Al_5 (33A) - Epsilon	38	2.04	14
$Mg_{0.400}Al_{0.554}La_{0.046}$ (38A)	60	2.08	12
$Mg_{0.382}Al_{0.574}La_{0.044}$ (40A)	52	1.91	12
$Mg_{0.370}Al_{0.588}La_{0.042}$ (42A)	48	1.83	12.5

Effects of Alloying Epsilon-Phase Alloys

Standard procedures described above for the preparation of beta-phase alloys and their isotherms were also used for the epsilon (ϵ) phase alloys. Figure 48 compares isotherms of Mg_4Al_5 (epsilon phase) with aluminum contents adjusted for various assumed La-aluminide compositions. The best composition, or the one whose isotherm more nearly approximates that of the binary alloy, appears to be 40A with an assumed $LaAl_2$ formation. Alloy 42A (assumed $LaAl_3$ formation) indicates decreased plateau pressures at H/M ratios of 0.2 or below.

The hydriding characteristics of the beta- and epsilon-phase alloys with La additions are summarized and compared in Table 15. Dehydriding kinetics were also noted to be improved by the La additions, but not to the extent anticipated. Whereas the binary alloy requires about five hours for equilibration, the La-containing alloys, e.g., 37A will attain 99 percent of the equilibrium pressure in approximately 2.5 hours.

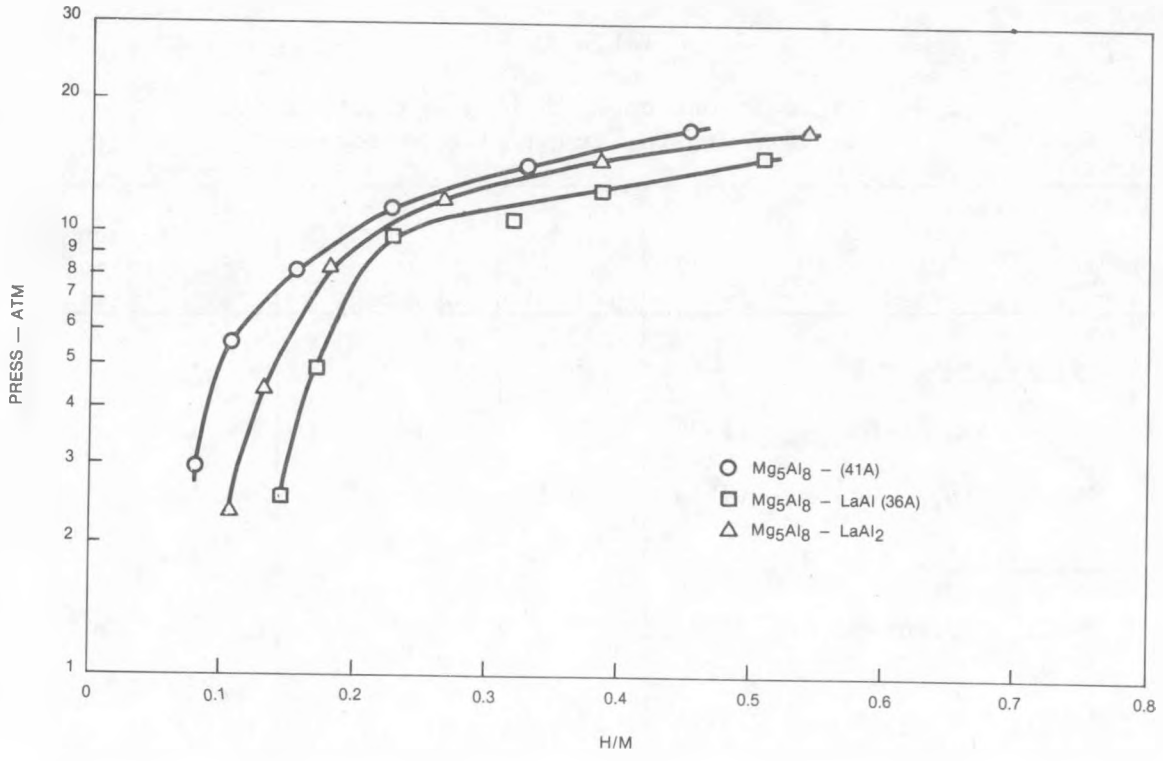

Figure 47. Comparative Isotherms for Mg_5Al_8 With Different Aluminides at 350°C

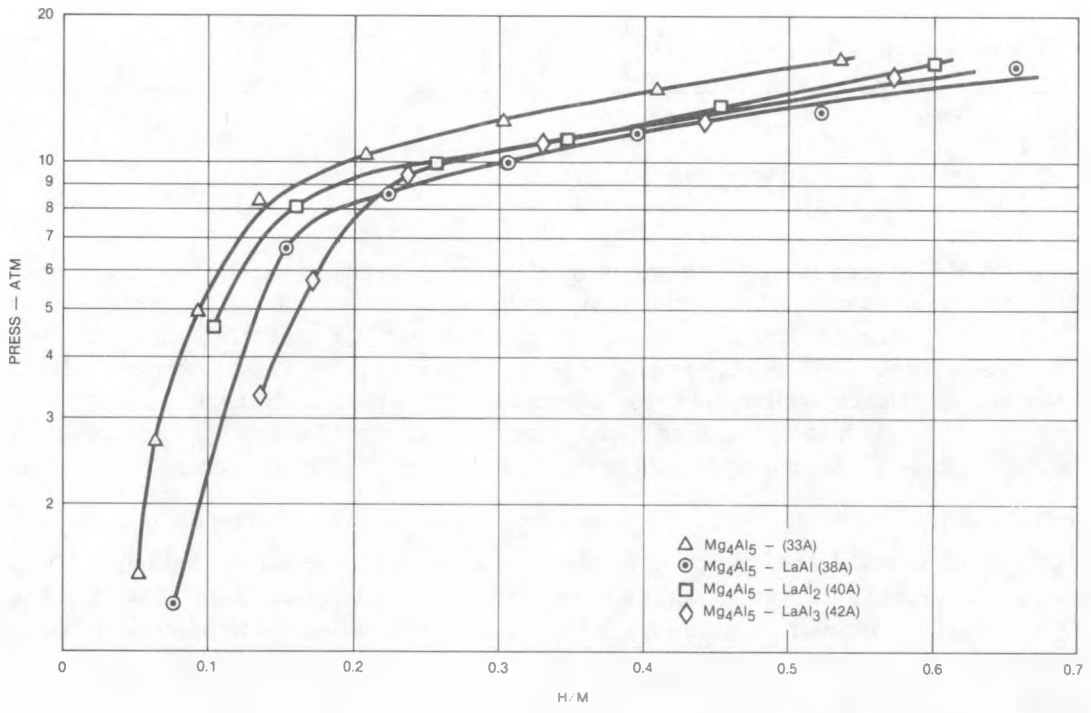

Figure 48. Comparative Isotherms for Mg_5Al_8 With Different Aluminides at 350°C

Another series of Mg_4Al_5 alloys were studied with a 5 atomic percent addition of Y, with aluminum contents adjusted for various assumed aluminide compositions. Isotherms were determined for these alloys containing various aluminides at 350°C and are presented in Figure 49. The highest overall plateau pressures are attained with the YAl_2 and YAl_3 assumed aluminide compositions, e.g., 43A, 43A-1, and 44A.

As with the La series, the best compositions, one whose isotherms more nearly approximate that of the binary alloy, appears to be 43A and 43A-1 with an assumed YAl_2 formation. Alloy 43A with a slight excess of Mg maintains a slightly higher plateau pressure at the very low H/M ratios. Plateau pressures decrease substantially with the yttrium-rich aluminides, especially Alloy 46A (assumed Y_3Al_2 formation).

Hydriding characteristics of the yttrium-containing alloys are summarized in Table 16.

Because of the relatively low cost of mischmetal (MM), an alloy of Mg_4Al_5 with an assumed mischmetal dialuminide formation was prepared, followed by the determination of the 350°C isotherm. Figure 50 and Table 17 compare the effects of the various rare-earth dialuminides on the isotherms and hydriding

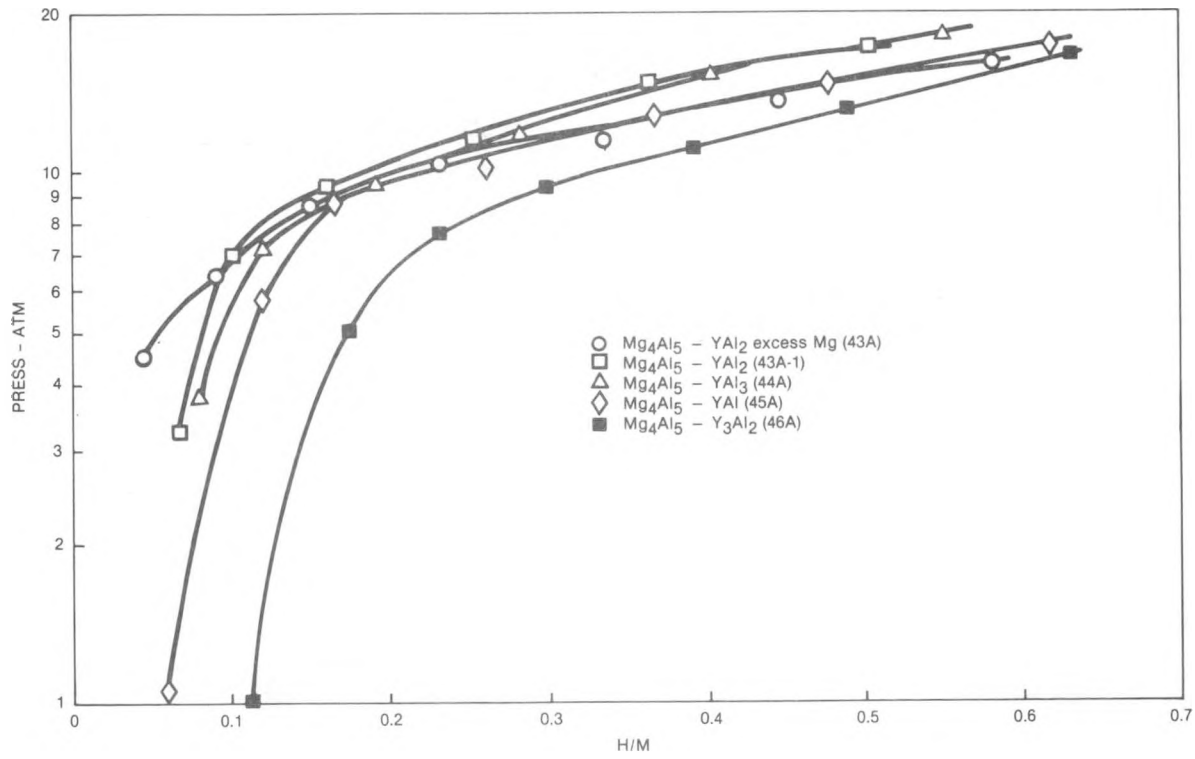

Figure 49. Comparative Isotherms for Mg_4Al_5 With Different Y-Aluminides at 350°C

Table 16

Effect of Y Additions on Hydriding Characteristics of Mg_4Al_5 (Epsilon-Phase)

Alloy No.	Alloy Composition	ΔT, °C	H_2 Absorbed, %	Mid-Plateau Pressure at 350°C (atm)
43A	$Mg_{0.420}Al_{0.539}Y_{0.042}$ (YAl_2) Hi Mg	54	2.00	12.3
43A-1	$Mg_{0.386}Al_{0.570}Y_{0.044}$ (YAl_2)	50	1.74	13.3
44A	$Mg_{0.370}Al_{0.588}Y_{0.042}$ (YAl_3)	50	1.89	13.5
45A	$Mg_{0.404}Al_{0.550}Y_{0.046}$ (YAl)	56	2.11	13.3
46A	$Mg_{0.410}Al_{0.544}Y_{0.046}$ (Y_3Al_2)	64	2.15	12

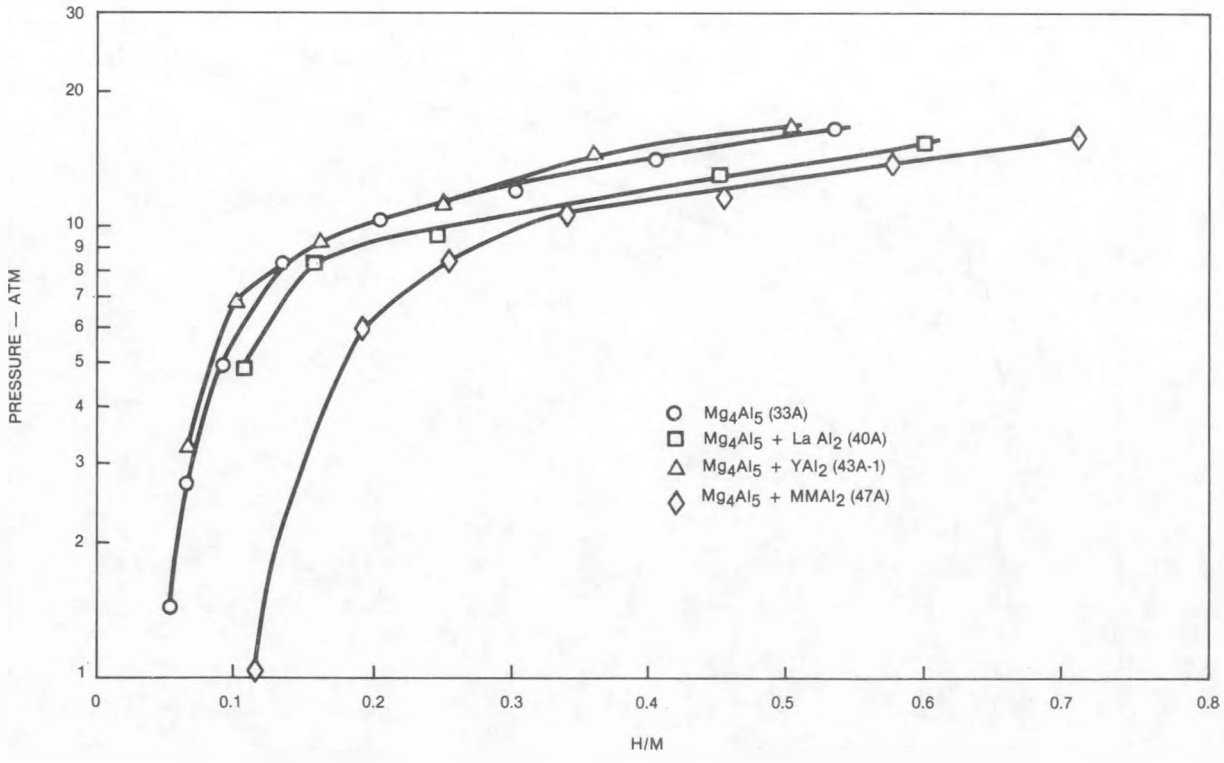

Figure 50. Effect of Different Rare-Earth Dialuminides on Isotherms of Mg_4Al_5 at 350°C

Table 17

Effect of Rare-Earth Dialuminides on Hydriding Characteristics of Mg_4Al_5 (Epsilon-Phase)

Alloy No.	Alloy Composition	ΔT, °C	H_2 Absorbed, %	Mid-Plateau Pressure at 350°C (atm)
33A	Mg_4Al_5-$Mg_{0.444}Al_{0.556}$	38	2.04	14.5
40A	$Mg_{0.383}Al_{0.574}La_{0.044}$ ($LaAl_2$)	52	1.91	12
43A-1	$Mg_{0.386}Al_{0.570}Y_{0.044}$ (YAl_2)	50	1.89	14
47A	$Mg_{0.386}Al_{0.570}MM_{0.044}$ ($MMAl_2$)	51	2.30	12.5

characteristics of Mg_4Al_5. The best behavior, based again upon plateau pressures and close approximation of the isotherm to the binary alloy isotherm, appears to be exhibited by Alloy 43A-1 (YAl_2), followed closely by Alloy 40A ($LaAl_2$). Although 47A ($MMAl_2$) contains the highest hydrogen content, its decomposition pressures at low H/M ratios are considerably lower than those of the other alloys.

As shown in Table 17, the reactivities (ΔT) of the rare-earth containing alloys are superior to the binary Mg_4Al_5, indicating improved hydriding kinetics over the binary alloy.

3.4 COMBINED ALLOY HYDRIDES

The purpose of this study was to determine hydriding characteristics of mixtures of low-temperature hydrides (Fe-Mn-Ti and V-Nb) and the higher temperature hydrides of the Mg-base alloys. Mixing given proportions of these hydride alloys could result in composite P-C isotherms that exhibit superior hydriding and dehydriding characteristics over the relatively stable Mg-base alloys.

Initial experiments were centered about mixtures of Fe-Mn-Ti and Alloy 149 ($Mg_{0.845}Cu_{0.1}Ni_{0.05}Y_{0.005}$), which was one of the better alloys developed previously. Hydriding characteristics and composite P-C-T curves were determined on the 20 percent Fe-Mn-Ti/80 percent Mg alloy mixtures. Stability of the Fe-Mn-Ti alloys was altered by varying the Mn and Ti contents.

A limited number of investigations were also conducted with mixtures of V-Nb and Alloy 149 hydrides.

3.4.1 Preparation of Hydriding Alloys

The Mg-base alloys were prepared by the standard induction melting techniques described earlier in this report. Button ingots of V-Nb and Fe-Mn-Ti were prepared by arc melting in an inert argon atmosphere. The ingots were inverted and remelted at least five times to assure homogeneity.

3.4.2 Hydriding and Mini-PC Isotherms (20% Fe-Mn-Ti/80% Mg Alloy Mixtures)

The alloys were crushed with a steel mortar and pestle to -12 mesh. Proper proportions of each alloy were weighed up to make a charge of approximately 15 grams, which was placed into the reactor.

The mixture began to hydride at room temperature under a pressure of 600 psi. Temperatures were finally increased to 400°C and the pressure reduced to 300 psi for the hydriding procedure.

During the determination of the P-C isotherm at 270°C, it was noted that the pressure began to decrease after building up to approximately 105 psia. Apparently the Mg alloy was hydriding preferentially under this higher pressure. To minimize this phenomenon, the hydriding was carried out at 300 psi and 400°C over a 12 hour period to saturate both hydride alloys.

The composite isotherms for the various mixtures at 270°C and 285°C are presented in Figures 51 through 56. Hydriding characteristics are summarized in Table 18.

The plateau pressures of about 0.6 atmosphere at 270°C are essentially those of Alloy 149, which agree with the P-C isotherm previously determined at this temperature.

The highest hydrogen capacity of 3.99 percent (H/M = 1.42) is exhibited by alloy mixture (10M) containing 20% $Fe_{0.05}Mn_{0.40}Ti_{0.55}$/80% Alloy 149 (see Figs. 53 and 54). Best overall composite curve shape exhibiting a small plateau region, however, is achieved with the 20% $Fe_{0.05}Mn_{0.45}Ti_{0.5}$/80% Alloy 149 mixture (8M). Alloy mixture 8M appears in several figures for comparative purposes.

Included in Figure 55 are isotherms for alloy mixtures containing 20% $Fe_{0.05}Mn_{0.45}Ti_{0.5}$/80% $Mg_{0.976}La_{0.024}$ (eutectic composition) and 20% $Fe_{0.05}Mn_{0.45}Ti_{0.5}$/80% Alloy 149 (homogenized). The eutectic composition was investigated for possible synergistic effects between $Fe_{0.05}Mn_{0.45}Ti_{0.5}$ and the lean La alloy. Results for the lean La alloy were not too encouraging from the standpoint of hydrogen capacity and curve shape. In an attempt to improve the plateau characteristics of $Fe_{0.05}Mn_{0.45}Ti_{0.5}$ (8M), the alloy was homogenized at 1000°C for a period of 72 hours. The results were not as good as those obtained with the unhomogenized alloy (compare 8M to 8M-2 in Figure 55). Perhaps the difference between these two alloy mixtures can be attributed to a substantial loss of Mn in the vacuum environment during the high-temperature, long-time anneal.

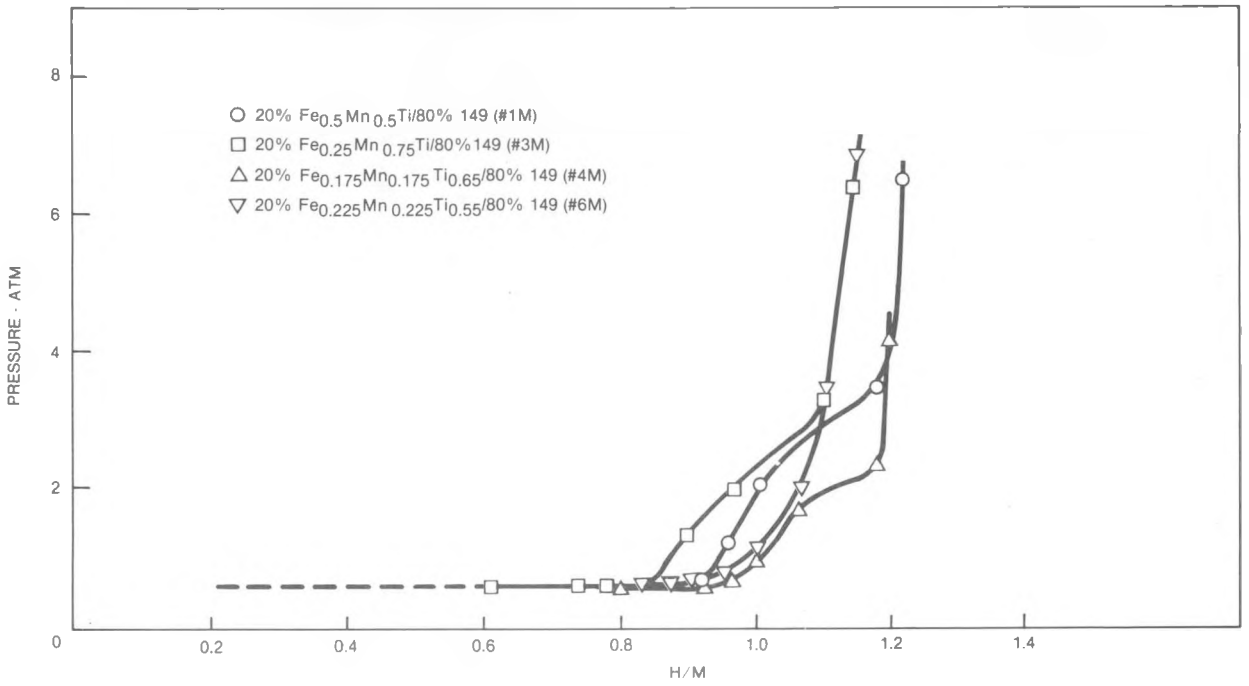

Figure 51. P-C Isotherms of 20% Fe-Mn-Ti/80% Alloy 149 at 270°C

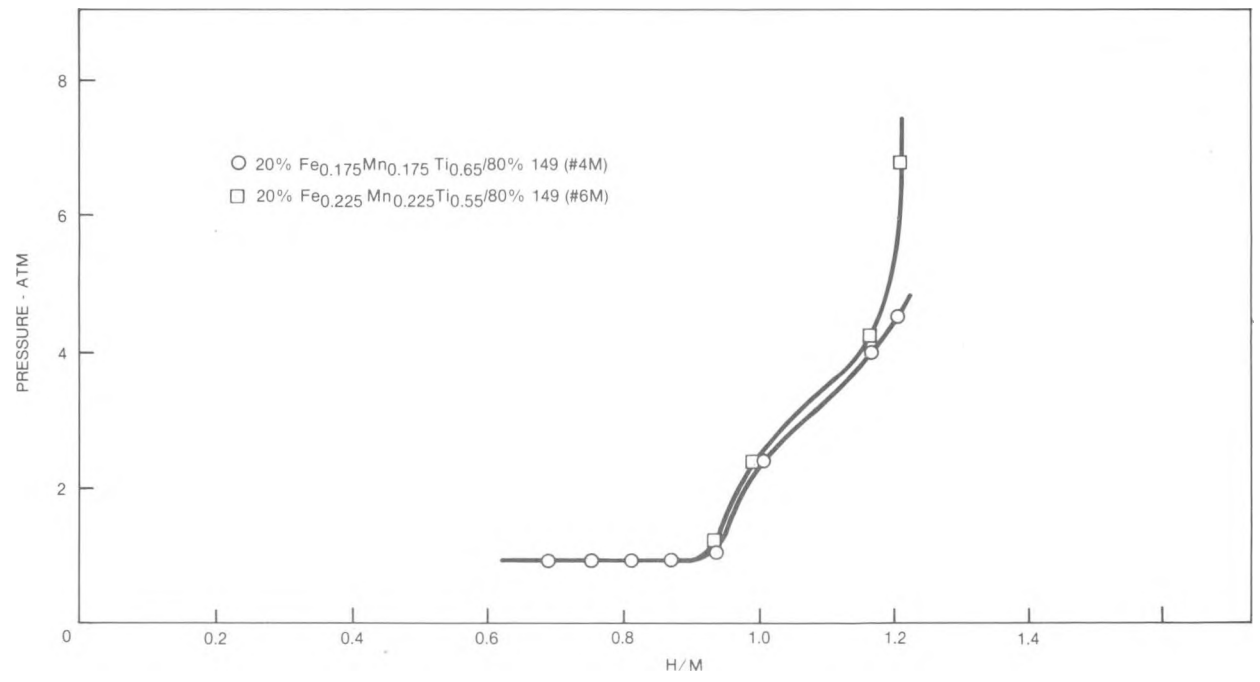

Figure 52. Composite P-C Isotherms at 285°C

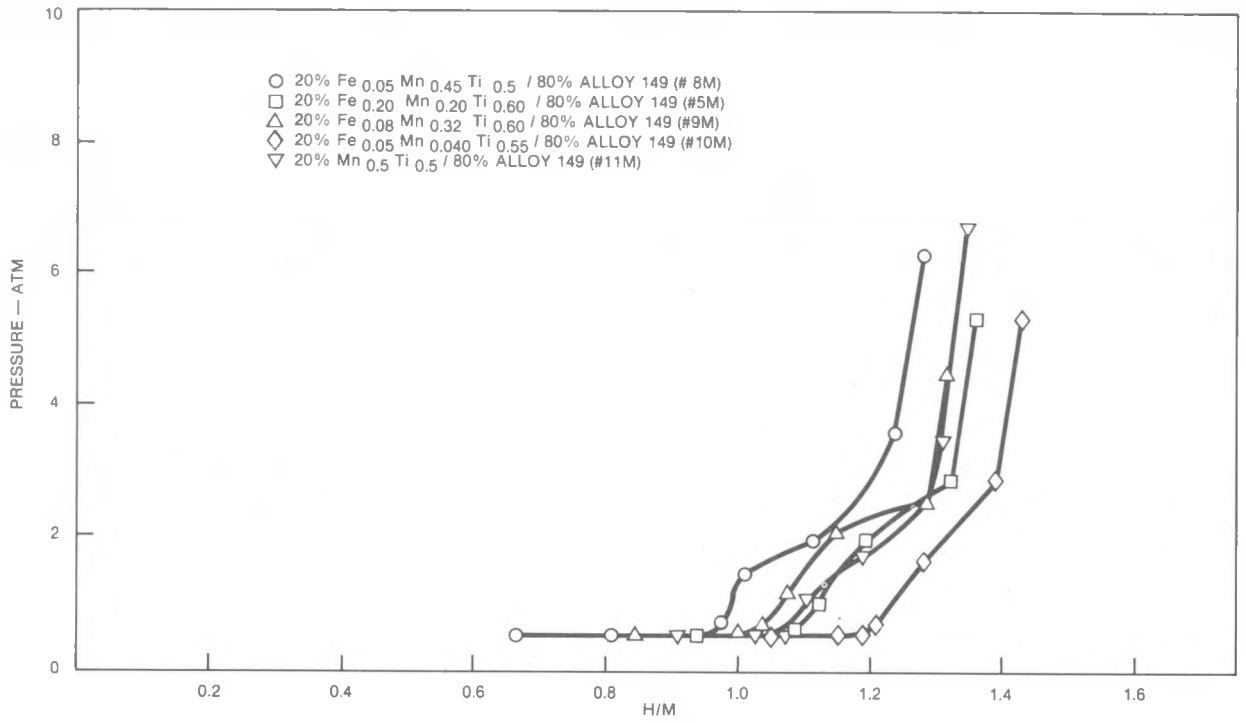

Figure 53. Composite P-C Isotherms at 270°C

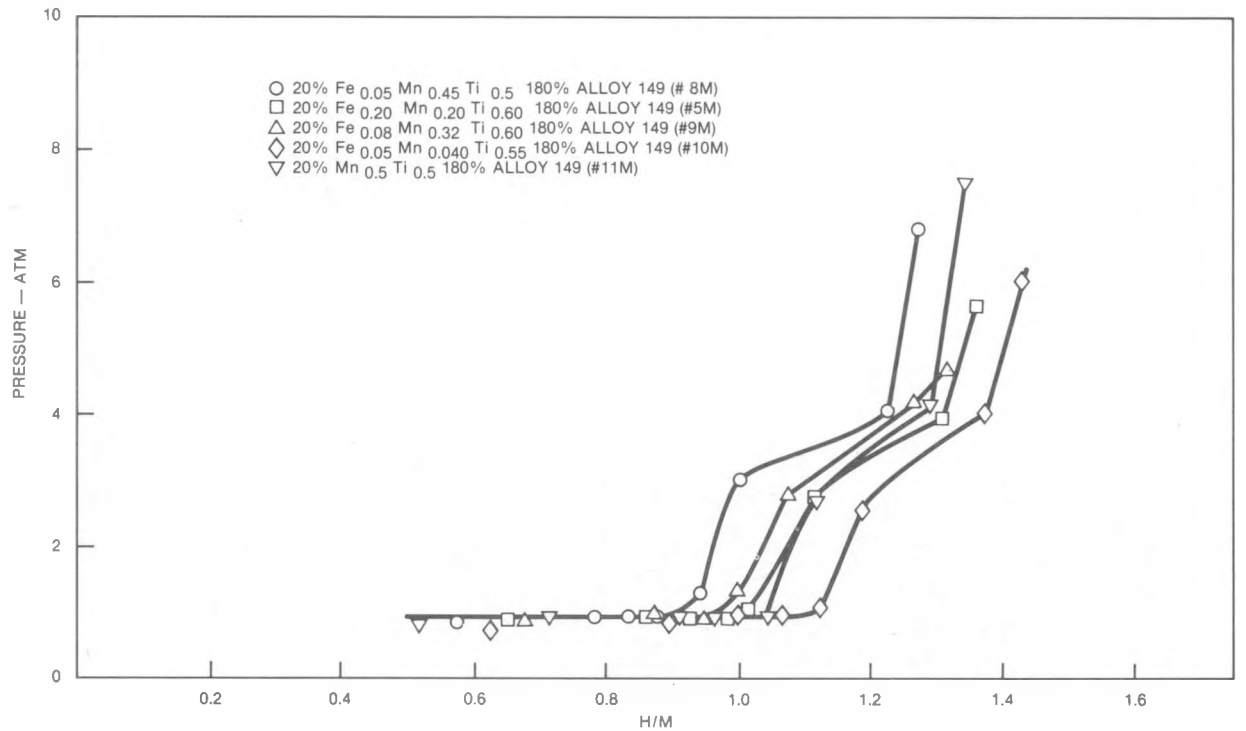

Figure 54. Composite P-C Isotherms at 285°C

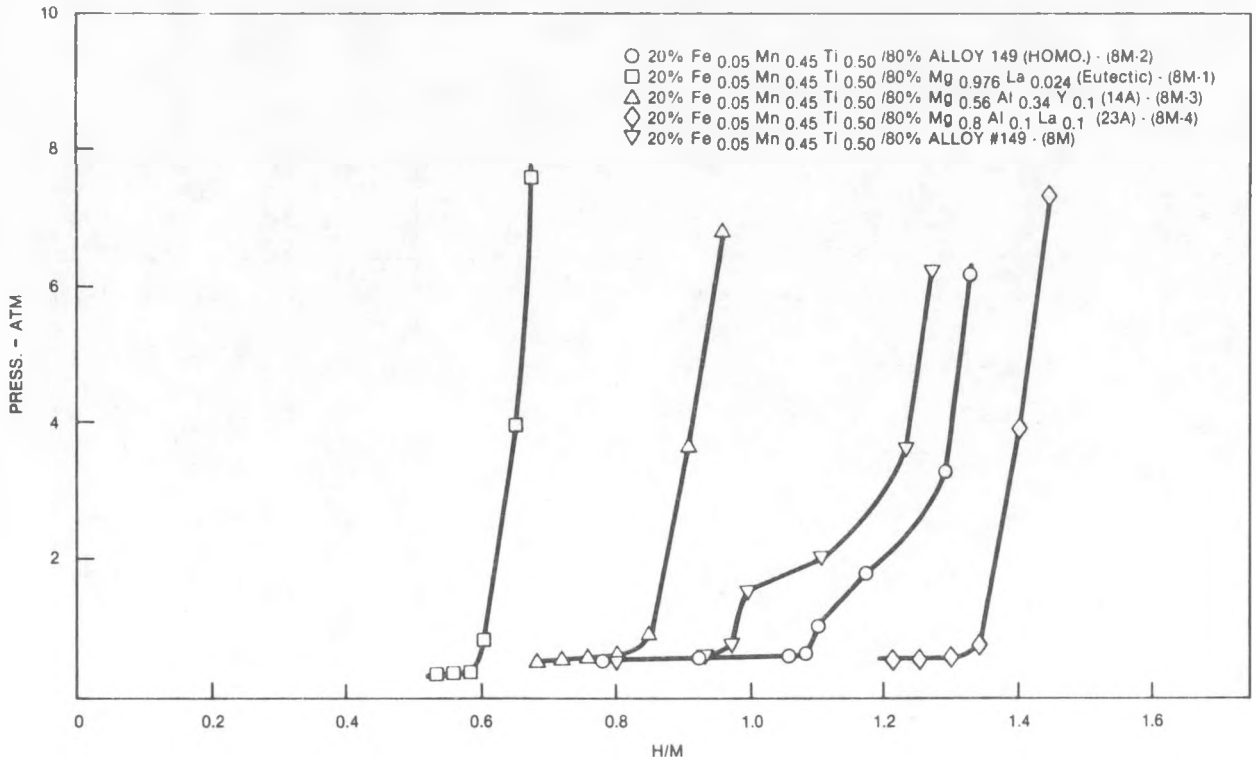

Figure 55. Composite P-C Isotherms of Selected Alloy Mixtures at 270°C

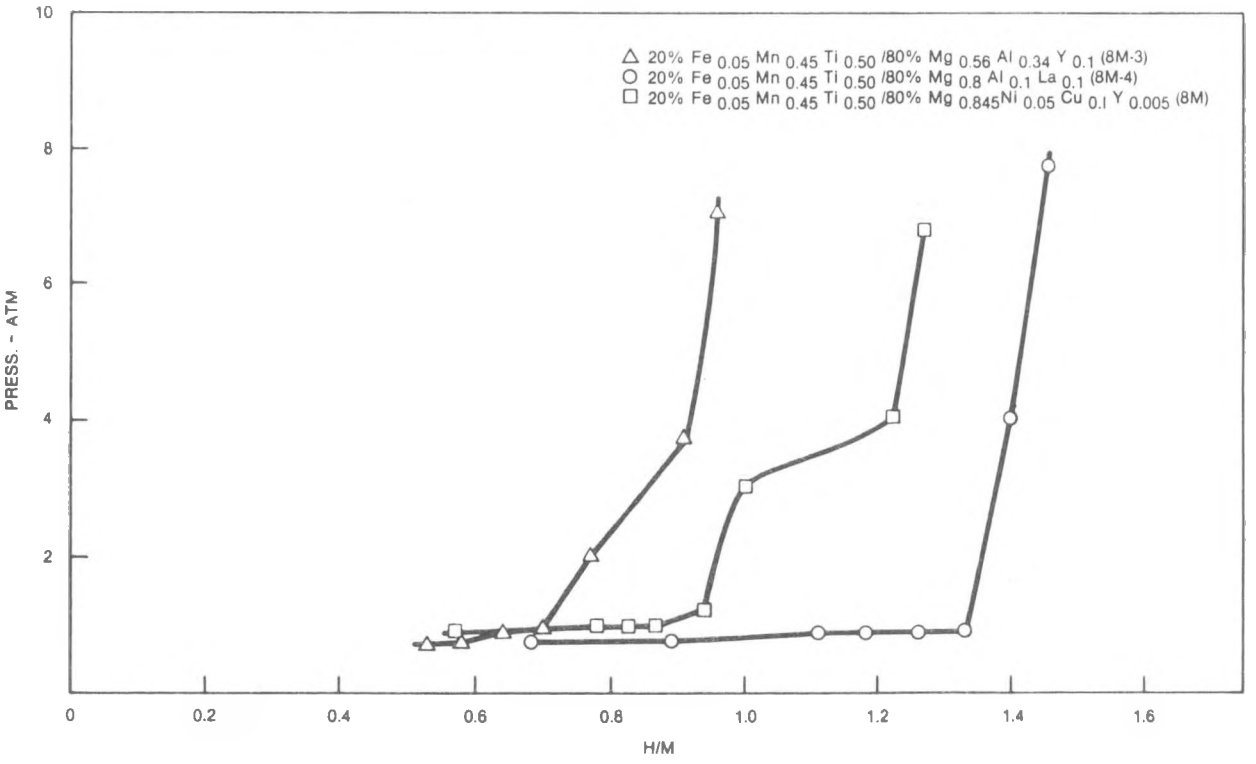

Figure 56. Composite P-C Isotherms of Selected Alloy Mixtures at 285°C

Table 18

Hydriding Characteristics of Fe-Mn-Ti/Alloy 149 Composites

Alloy	Composition	T, °C	Percent H_2 Absorbed	H/M Ratio
1M	20% $Fe_{0.5}Mn_{0.5}Ti$/80% #149	77	3.44	1.20
3M	20% $Fe_{0.25}Mn_{0.75}Ti$/80% #149	84	3.23	1.14
4M	20% $Fe_{0.175}Mn_{0.175}Ti_{0.65}$/80% #149	64	3.41	1.20
6M	20% $Fe_{0.225}Mn_{0.225}Ti_{0.55}$/80% #149	80	3.25	1.15
5M	20% $Fe_{0.20}Mn_{0.20}Ti_{0.60}$/80% #149	85	3.80	1.35
8M	20% $Fe_{0.05}Mn_{0.45}Ti_{0.5}$/80% #149	90	3.58	1.27
9M	20% $Fe_{0.08}Mn_{0.32}Ti_{0.60}$/80% #149	105	3.70	1.31
10M	20% $Fe_{0.05}Mn_{0.40}Ti_{0.55}$/80% #149	90	3.99	1.42
11M	20% $Fe_{0.5}Ti_{0.5}$/80% #149	95	3.77	1.34
8M-1	20% $Fe_{0.05}Mn_{0.45}Ti_{0.5}$/80% $M_{0.976}La_{0.024}$	69	2.14	0.69
8M-2	20% $Fe_{0.05}Mn_{0.45}Ti_{0.5}$/80% Alloy 149 (Homo.)	103	3.74	1.33
8M-3	20% $Fe_{0.05}Mn_{0.45}Ti_{0.5}$/80% $Mg_{0.56}Al_{0.34}Y_{0.1}$ (14A)	64	2.56	0.96
8M-4	20% $Fe_{0.05}Mn_{0.45}Ti_{0.5}$/80% $Mg_{0.8}Al_{0.1}La_{0.1}$ (23A)	111	3.60	1.45

3.4.2 Hydriding and Mini-PC Isotherms (20% V-Nb/80% Alloy 149)

The V-Nb/#149 alloys were crushed with a steel mortar and pestle to -12 mesh. Proper proportions for each alloy mixture were weighed up to form approximate 15 gram samples which were placed in the reactor.

In separate runs, each mixture, 20% $V_{0.75}Nb_{0.25}$/80% Alloy 149 and 20% $V_{0.50}Nb_{0.50}$/80% Alloy 149, began to hydride at room temperature under a pressure of 950 psi. The temperature was increased to 450°C for the hydriding procedure.

Composite P-C isotherms at 270°C and 285°C are shown in Figures 57 and 58. Hydriding characteristics are summarized in Table 19.

Although the isotherm shapes are inferior to those of mixture 8M (20% $Fe_{0.05}Mn_{0.45}Ti_{0.50}$/80% Alloy 149) in the foregoing series, a high hydrogen content of 4.18 percent (H/M = 1.58) was achieved with the 20% $V_{0.75}Nb_{0/25}$/80% Alloy 149 mixture.

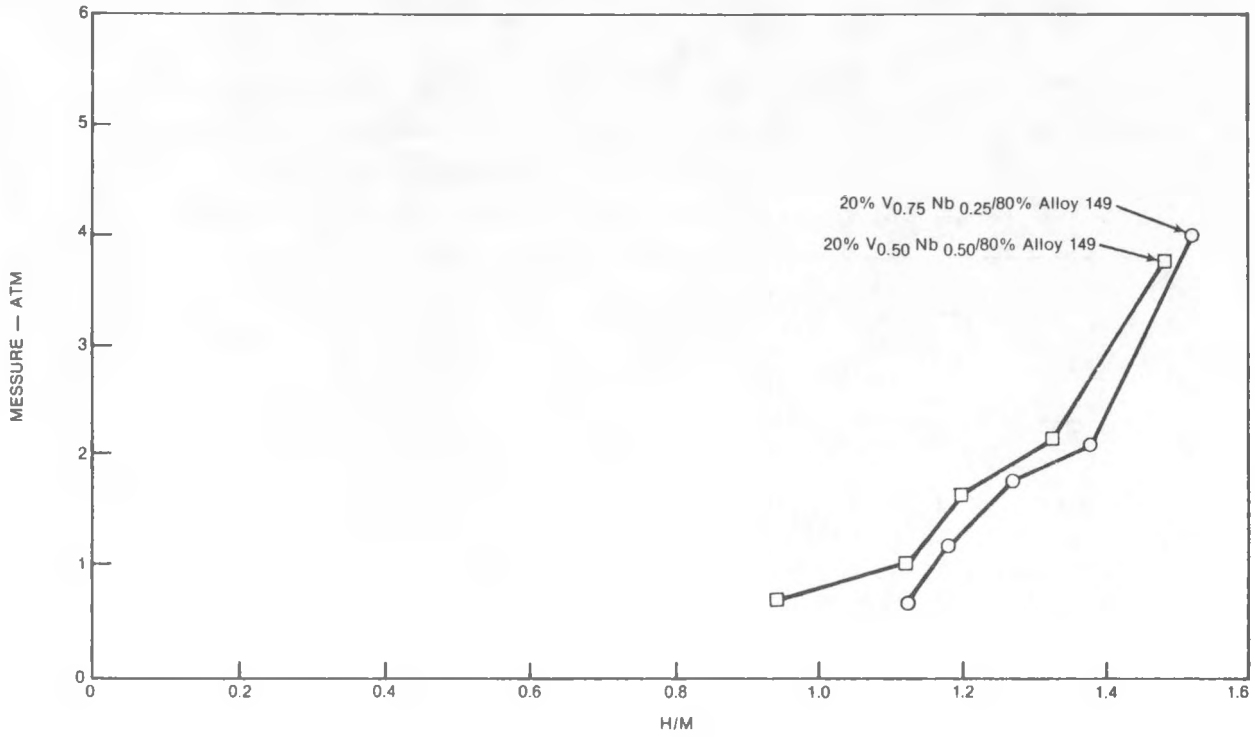

Figure 57. Composite P-C Isotherms of Selected Alloys at 270°F

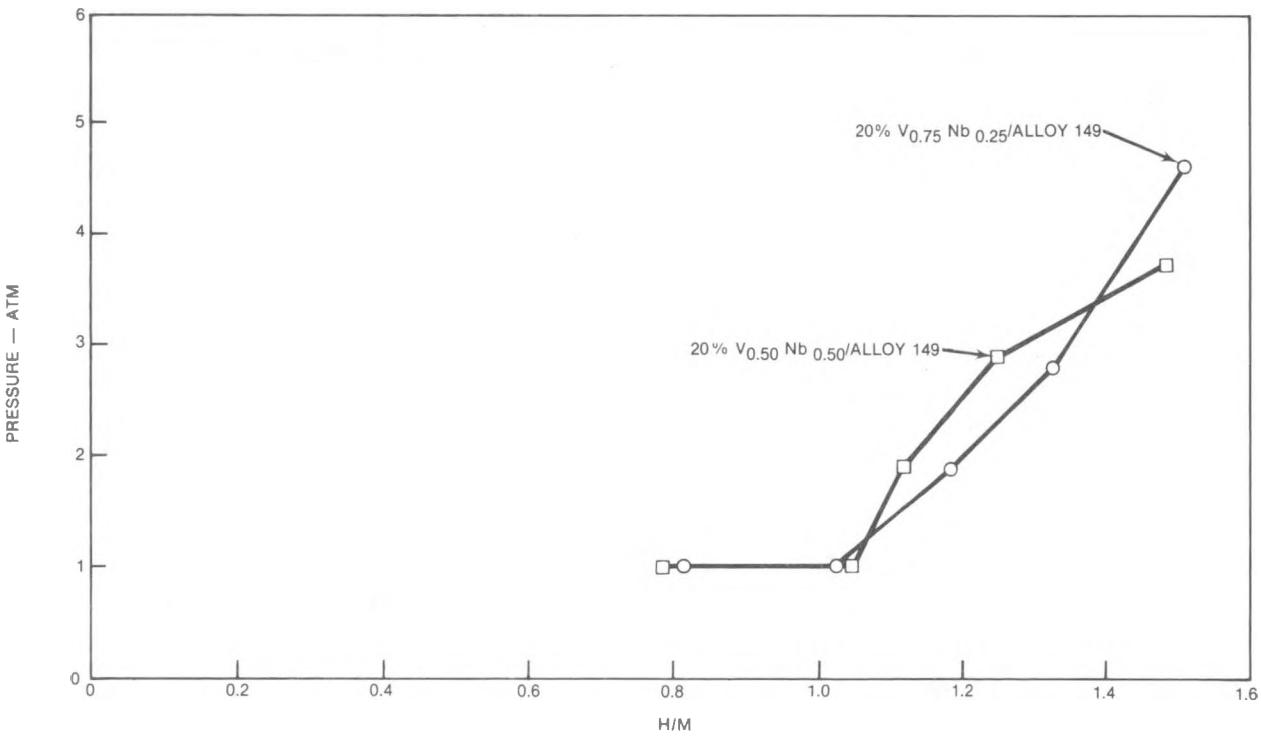

Figure 58. Composite P-C Isotherms of Selected Alloys at 285°C

Table 19

Hydriding Characteristics of V-Nb/Alloy 149 Composites

Composition	ΔT, °C	Percent H_2 Absorbed	H/M Ratio
20% $V_{0.75}Nb_{0.25}$/80% #149	143	4.18	1.58
20% $V_{0.50}Nb_{0.50}$/80% #149	76	3.85	1.53

It can be concluded from these studies that isotherms can be tailored by mixing high-temperature hydrides with low-temperature hydrides, but that no great improvements in the lower temperature operation of magnesium hydrides was observed with the particular mixtures under investigation.

3.5 IMPURITY SENSITIVITY STUDIES

There are times during the life of automotive hydride fuel tanks that contamination of the hydride fuel can occur. This is particularly true when the hydride alloy is being recharged and some contact with air is inevitable. The purpose of this study was to determine the extent of deterioration of hydriding properties after contamination with measured amounts of oxygen and nitrogen.

Alloy 14A ($Mg_{0.56}Al_{0.34}Y_{0.1}$) was selected for these studies involving oxygen and nitrogen contamination. The alloy was prepared according to standard procedures developed during the course of this program, and which have been described in earlier sections of this report.

3.5.1 Oxygen Contamination

Alloy 14A was crushed to -50 +100 mesh and hydrided at 400°C and 600 psi, followed by the determination of the isotherm for the uncontaminated alloy at 310°C.

Pure oxygen in increments of 0.1, 0.2, and 0.7 weight/percent was introduced to the reactor containing the dehydrided alloy at ambient temperatures. An immediate reaction was indicated by a rise in temperature (10 to 14°C) and a drop in pressure within the reactor chamber with the addition of the first two increments of oxygen. To ensure complete reaction of the oxygen with the alloy, the reactor was heated to 200°C for 12 hours before the hydriding procedure was repeated. The effect of oxygen contamination upon the hydriding characteristics after addition of each increment is summarized in Table 20 and Figure 59.

Table 20

Effect of Oxygen Contamination Upon Hydriding Characteristics of Alloy 14A

O_2 Increments, (w/o)	Total Added O_2 (w/o)	ΔT, °C Hydriding	H_2 Content (w/o)	H/M Ratio
0	0	90	2.89	0.973
0.1	0.1	42	2.70	0.907
0.2	0.3	58	2.72	0.915
0.7	1.0	80	2.63	0.882

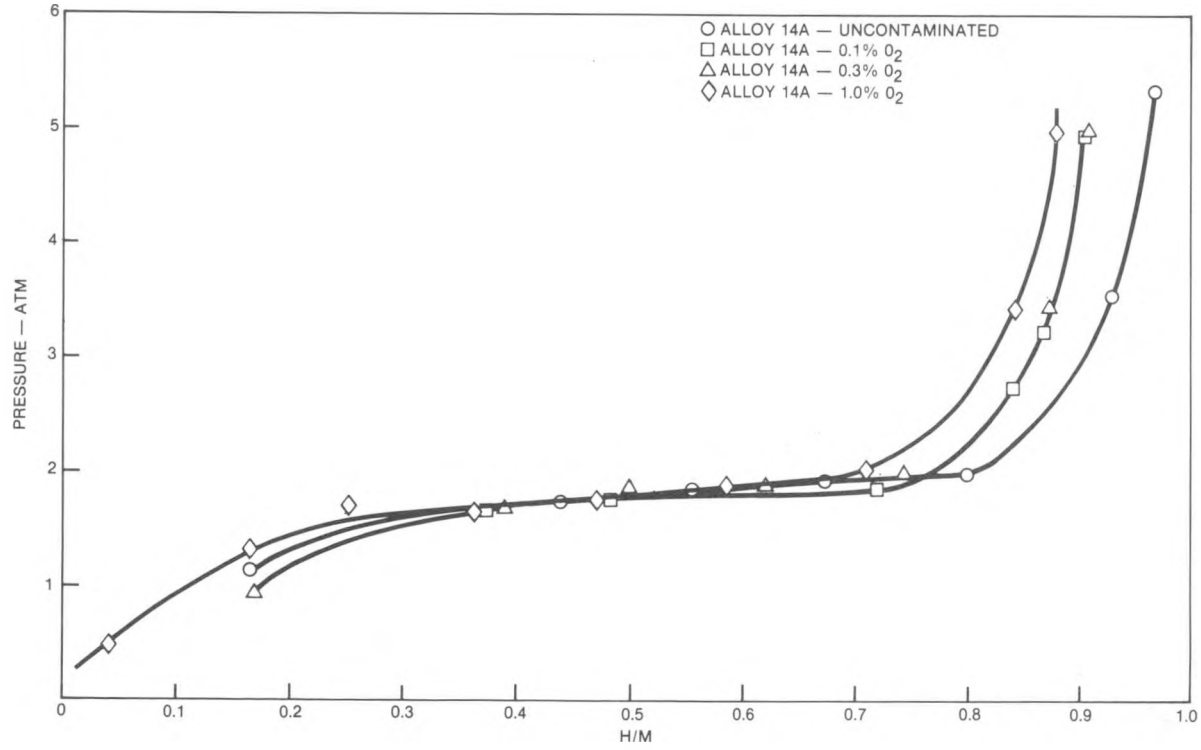

Figure 59. Effect of Oxygen Upon Isotherms of Alloy 14A ($Mg_{0.56}Al_{0.34}Y_{0.1}$) at 310°C

Figure 59 shows isotherms for Alloy 14A in the uncontaminated condition and with oxygen contents of 0.1, 0.3 and 1.0 percent. There is an initial decrease in the H/M ratio, or hydrogen content, from 0.97 to 0.91 upon the introduction of 0.1 percent oxygen. An additional 0.2 percent oxygen (total of 0.3 percent) appears to make no difference in the H/M ratio. However, with the total oxygen content at 1.0 percent additional deterioration of the H/M ratio takes place.

This phenomenon can perhaps be explained on the basis of the protective nature of a thin oxide layer. When the oxide becomes sufficiently thick it will crack, allowing the metal in the interior of the particles to oxidize further. With less metallic magnesium available for hydriding, the H/M ratio progressively decreases. This is similar to the results of the work of Vigeholm, et al., who found that hydriding of unalloyed magnesium proceeded more rapidly with thick oxide layers, due to the cracking of this thick crystalline oxide (Ref. 22).

Plateau pressures, on the other hand, appear to be affected very little by varying amounts of oxygen contamination.

Note in Table 20 that the ΔT is also mostly affected by the addition of the first 0.1 percent increment of oxygen. After the oxygen content reaches the 1.0 percent level, the reaction appears more vigorous and the ΔT increases to 80°C. This again is probably due to the cracking of the thicker oxide.

3.5.2 Nitrogen Contamination

Another sample of Alloy 14A was crushed to -50 +100 mesh and hydrided at 400°C and 600 psi, again followed by the determination of the isotherm for the uncontaminated alloy at 310°C.

Pure nitrogen in increments of 0.1 weight/percent was introduced to the evacuated reactor containing the dehydrided alloy at 400°C. To ensure complete reaction of the nitrogen with the alloy, the reactor was maintained at 400°C for 12 hours before the hyriding procedure was repeated. The effect of each nitrogen increment upon the hydriding characteristics is summarized in Table 21 and Figure 60.

Unlike the oxygen additions, the nitrogen contamination does not seem to materially affect the ΔT of the hydriding reaction (Table 21).

Figure 60 shows isotherms for Alloy 14A in the uncontaminated condition and with nitrogen contents of 0.1, 0.3 and 1.0 percent. Other than a small incremental decrease of hydrogen content (H/M ratio) with addition of nitrogen, the isotherms are affected very little. The slight variations in plateau pressures appears to be well within the experimental error.

Table 21

Effect of Nitrogen Contamination Upon Hydriding Characteristics of Alloy 14A

N_2 Increments (w/o)	Total Added N_2 (w/o)	ΔT, °C Hydriding	H_2 Content (w/o)	H/M Ratio
0	0	87	3.08	1.04
0.1	0.1	78	2.93	0.986
0.2	0.3	89	2.91	0.979
0.7	1.0	89	2.80	0.943

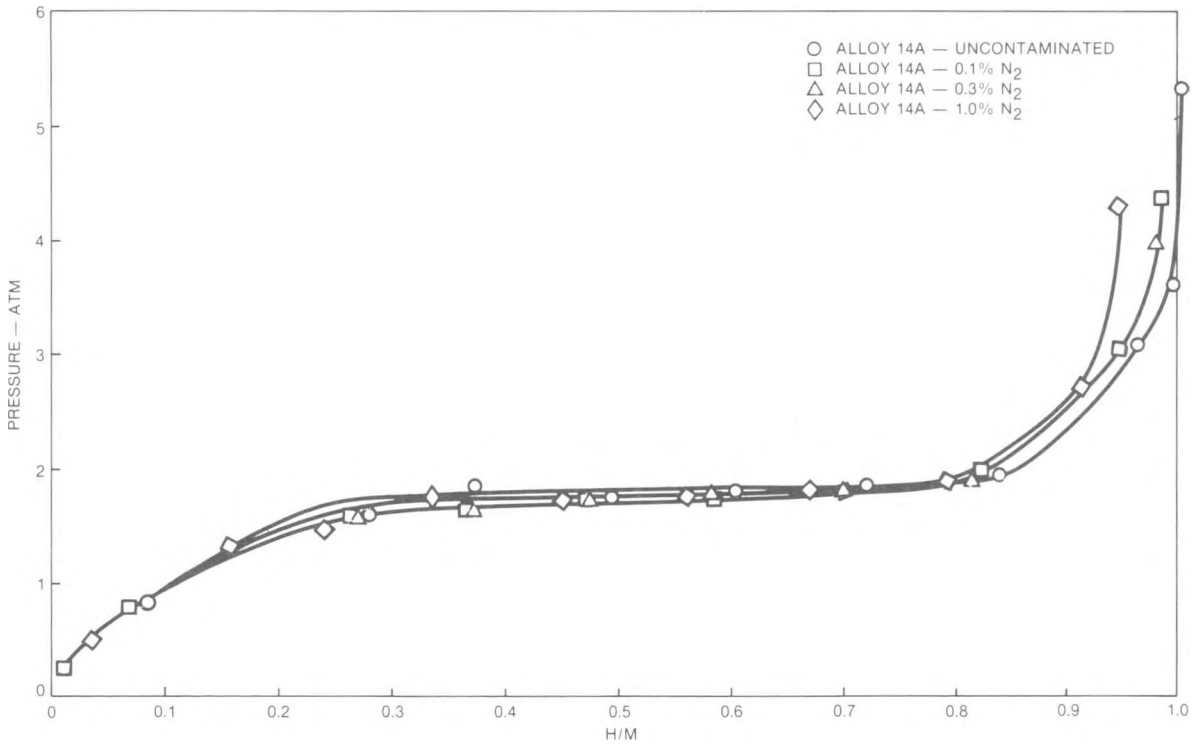

Figure 60. Effect of Nitrogen Upon Isotherms of Alloy 14A ($Mg_{0.56}Al_{0.34}Y_{0.1}$) at 310°C

3.6 ALLOY OPTIMIZATION

3.6.1 Mg-Al Alloys

Results of the investigations of the beta-and epsilon-phases of the Mg-Al system indicate that aluminum in the presence of rare-earth elements is tied up in the highly stable $REAl_2$ compounds. Since much of the aluminum in Mg-Al alloys is tied up in these intermetallic compounds, it was decided to compensate for the aluminum tied up in this manner in alloys 14A and 23A, containing yttrium and lanthanum, respectively. Assuming the formation of dialuminides, an excess amount of aluminum was added to bring the uncombined portion back to the original atom fraction in each respective alloy.

Preparation of Alloys

Alloys of modified 14A ($Mg_{0.477}Al_{0.446}Y_{0.077}$) and modified 23A ($Mg_{0.692}Al_{0.231}La_{0.077}$) compositions were prepared according to the standard procedures developed for the Mg-Al system.

Hydriding and PC Isotherms

Modified alloys 14A and 23A were crushed to -20 mesh and hydrided at 400°C and 600 psi for 12 hours.

Isotherms were determined at 310°C and are shown in Figures 61 and 62. In both cases, the modified alloys exhibited inferior properties in comparison to the original compositions. The hydrogen contents were considerably decreased, and in the case of modified 23A there was also a decrease in the plateau pressure. From these results, there appears to be no advantage in compensating for the aluminum tied up in the rare-earth dialuminide for these particular compositions.

3.6.2 Mg-Ni-Cu Alloys

In an attempt to limit the use of strategic metals still further, a modification of Alloy 149 ($Mg_{0.845}Ni_{0.05}Cu_{0.1}Y_{0.005}$) was investigated in which copper was substituted for nearly all of the nickel, except for one atomic percent. The rare-earth content was also increased for improved catalytic effects.

Hydriding and PC Isotherms

The homogenized ingot of $Mg_{0.84}Ni_{0.01}Cu_{0.14}Y_{0.01}$ (Alloy 149-Mod. A) was crushed to -10 mesh and hydrided at 400°C and 600 psi for a period of 12 hours.

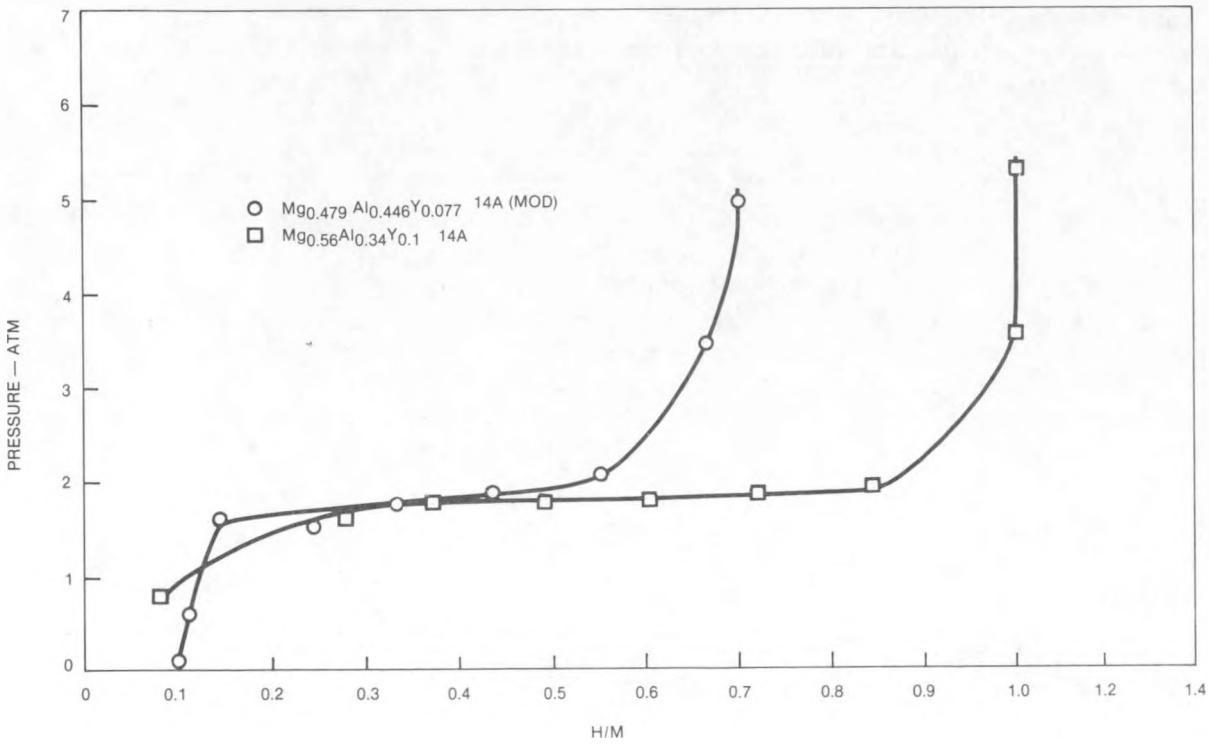

Figure 61. Comparative Isotherms for Alloy 14A and Modified 14A

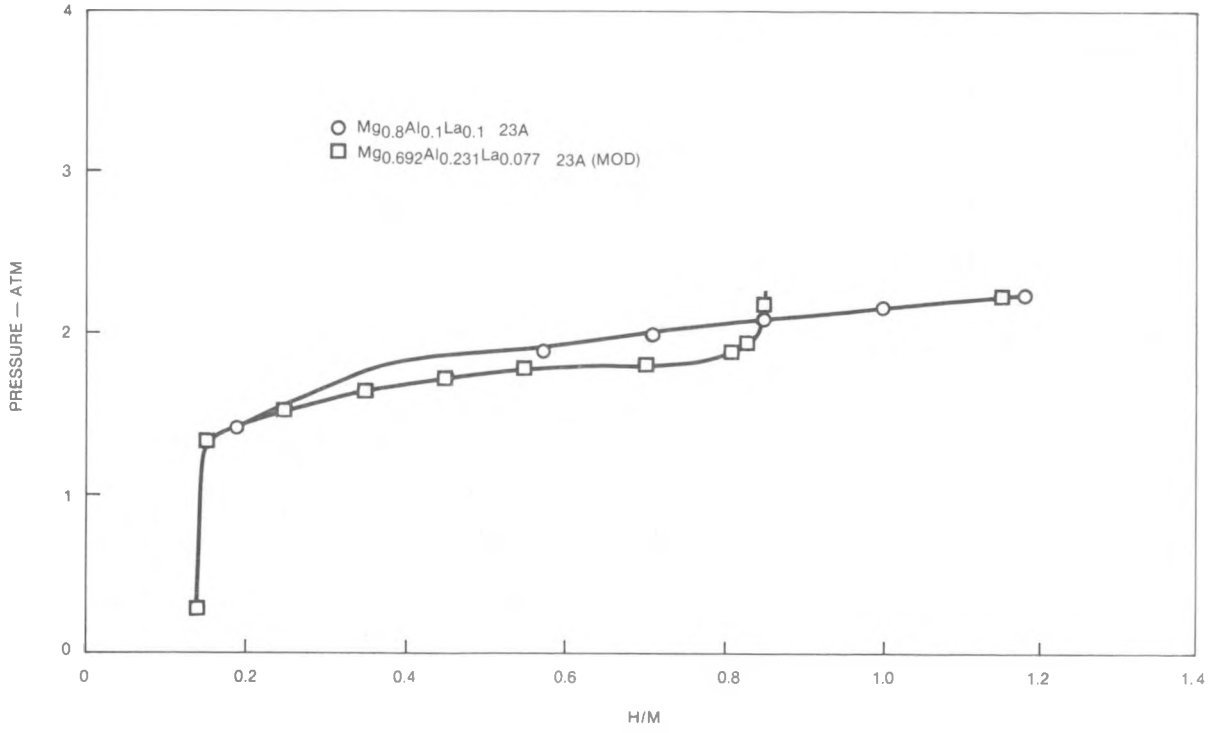

Figure 62. Comparative Isotherms for Alloy 23A and Modified 23A

An isotherm was determined at 310°C and is presented in Figure 63. The hydriding characteristics are summarized in Table 22, along with those of Alloy 149 for comparison.

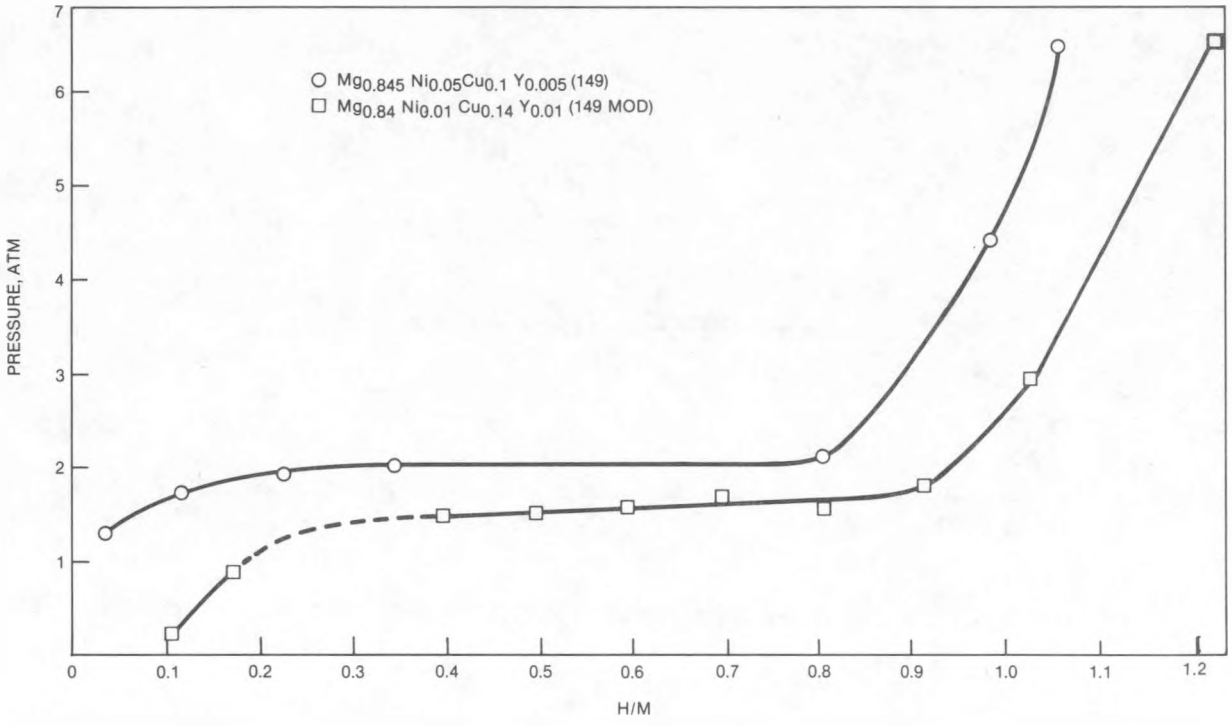

Figure 63. Comparative Isotherms of Alloy 149 and Modified Alloy 149 at 310°C

Table 22

Comparison of Hydriding Characteristics of Alloy 149 and Alloy 149 (Mod. A)

Alloy	Composition	ΔT, °C	H_2 Absorbed, %	Mid-Plateau Pressure at 310°C (atm)
149	$Mg_{0.845}Ni_{0.05}Cu_{0.1}Y_{0.005}$	94	3.72	2.2
149 (Mod. A)	$Mg_{0.84}Ni_{0.01}Cu_{0.14}Y_{0.01}$	120	4.03	1.6

Although the modified Alloy 149 exhibits a higher ΔT and contains more hydrogen, the mid-plateau pressure at 310°C is about 0.6 atmosphere lower than the original alloy. These results indicate that it is not possible to make

a direct substitution of Cu for Ni and maintain the hydriding characteristics of Alloy 149. The additional amounts of Y no doubt accounts for the increased activity (ΔT) and the higher hydrogen content of the modified alloy. An obvious conclusion is that Alloy 149 represents a nearly optimum composition for this family of nickel-lean alloys.

4

ALLOY CYCLING

4.1 INTRODUCTION AND DESCRIPTION OF APPROACH

In studying magnesium alloy hydrides, researches to date have generally measured most properties after approximately ten hydriding/dehydriding cycles. This number of cycles is sufficient to insure total saturation of the alloy with hydrogen, but may be inadequate in exposing the hydride alloy to actual conditions that would develop over the life cycle of an automotive fuel system. To realistically simulate multiple refueling cycles, an automatic hydride cycling test rig (see Figs. 64 through 66) was designed and fabricated that made it possible to study the effect of a large number of hydriding/dehydriding cycles upon the alloys, e.g., 1000-2000 cycles.

The process of hydrogen absorption and desorption (or hydriding and dehydriding) causes the metal crystal lattice to expand and contract leading to the breakdown of the original hydride alloy particles into finer powder. This process is referred to as comminution. After many cycles, the hydride particles reach the micron size range. This allows for a much larger, cleaner surface area exposed to the hydrogen enhancing kinetics. However, it also increases the possibility that the exposed surfaces will be contaminated. The hydride cycling test rig was used to study this matter. Parameters investigated as a function of cycling were comminution of the hydride particles, contamination of the hydride alloys by gaseous impurities present in the hydrogen supply and the effects of cycling upon kinetics and hydrogen capacity of the magnesium alloy hydrides.

4.2 TEST PROCEDURE

Approximately 0.5 kg (~1 lb) of magnesium alloy powder was loaded into the two liter pressure vessel (see Fig. 67). Activation of the hydride alloy was achieved by first evacuating and backfilling the vessel with high purity hydrogen at room temperature and 300 psig. Then, at that pressure the temperature was increased to approximately 315°C and held at these parameters for a few hours. This was done a few times until a drop in pressure occurred indicating hydrogen absorption.

With activation completed, automatic repetitive-condition cycling commenced. At the test temperature of 315°C commercial quality hydrogen was added to the vessel at 300 psig. At the fully hydrided condition, the hydride powder soaked for 15 minutes. The gas was then withdrawn and disposed of until the stored hydrogen was completely removed. This process was repeated with new commercial quality hydrogen. The established cycle time was 20 minutes.

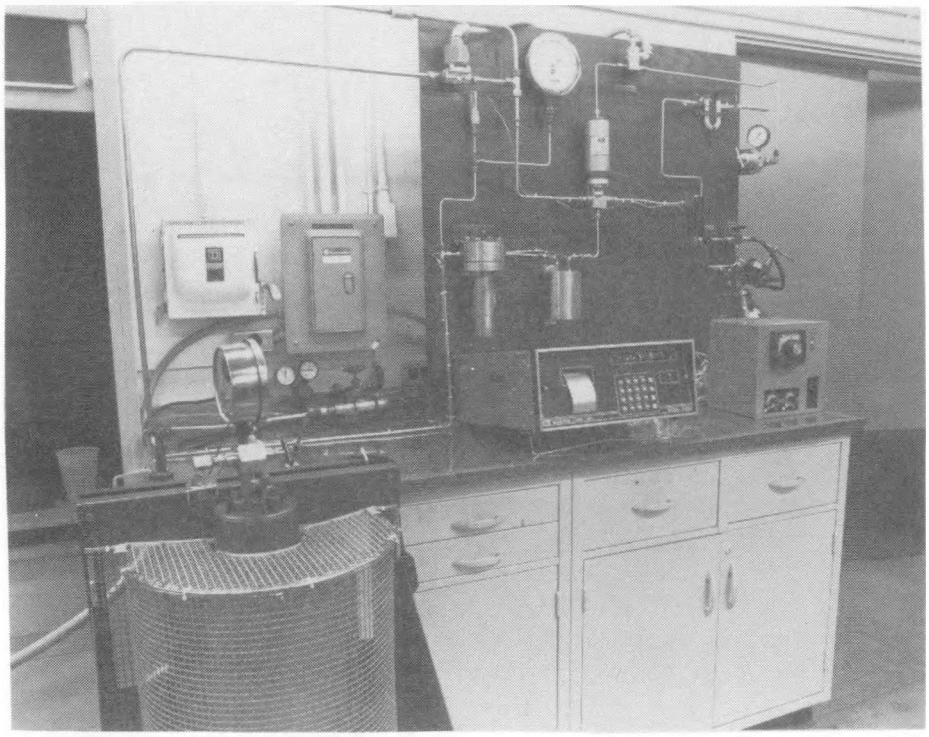

Figure 64. Hydride Cycling Rig

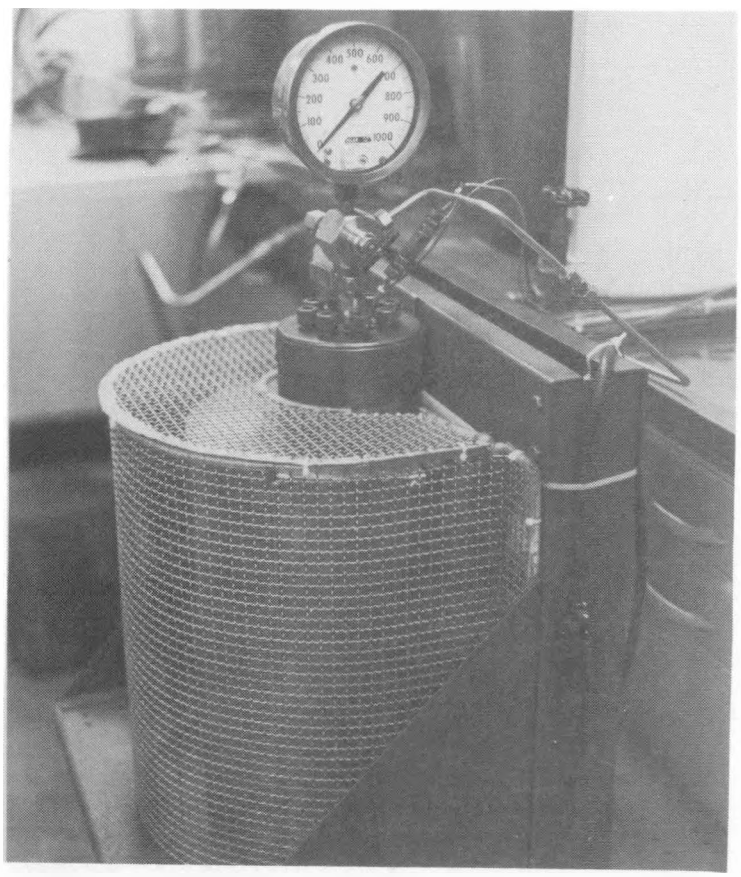

Figure 65.

Hydride Cycling Rig Pressure Vessel and Furnace Unit

Figure 66. Hydride Cycling Rig Control Box

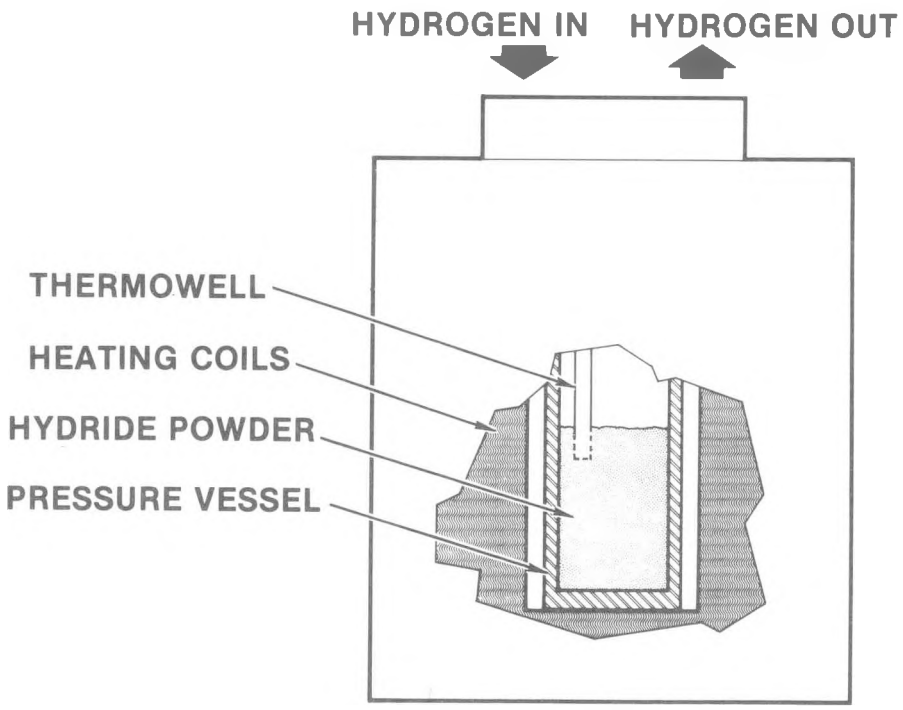

Figure 67. Hydride Cycling Rig Schematic

At regular intervals, a small powder sample was removed from the rig. The alloy was left in its fully hydrided state and cooled to room temperature at 300 psig to assure maximum hydrogen absorption. Argon was then used to purge the system as a necessary precaution to avoid oxygen contamination of the alloy. The sample was monitored for any deterioration brought about by change in particle size and impurity levels.

In the series of hydride cycling tests conducted, five test runs were made on four selected alloys with the initially tested material run twice to check the effect of moisture content of the commercial hydrides used.

4.3 Alloy 149 ($Mg_{0.845}Ni_{0.05}Cu_{0.1}Y_{0.005}$)

The initial hydride alloy chosen for characterization was Alloy 149 ($Mg_{0.845}Ni_{0.05}Cu_{0.1}Y_{0.005}$). The 0.5 kg (~1 lb) sample was crushed to -12 mesh (~1700 microns) before loading into the reactor. A goal of 2,000 cycles was set to achieve the maximum possible effects of long-term cycling. The sampling results are shown in Table 23. Figure 68 shows the effect of comminution on hydriding of the alloy sample. The "-1" designation refers to the first of two tests.

Table 23

Cyclic Effects Upon Alloy 149-1

Sample Number	Cycle Number	H/M	% H_2 Absorbed
1	48	0.98	3.16
2	1243	0.84	2.72
3	2015	0.44	1.46

Analysis of these results show that comminution had a major effect on the alloy causing a large amount of alloy surface area to be exposed. A majority of particles initially at -12 mesh (~1700 microns) were reduced to -100/+200 mesh (~112 micron average) after the large number of cycles. The amount of absorbed hydrogen was also greatly reduced. It was determined that this is due to the impurities such as O_2, N_2, CO and H_2O (32 ppm) in the commercial quality hydrogen.

A second sample of Alloy 149 (149-2) was prepared and tested. To ensure that water contamination would not occur, an in-line commercial water trap was used with the commercial grade hydrogen. The number of cycles recorded in this test was 1523. As expected, hydrogen capacity of the second test alloy with the water trap was higher than that of the first alloy. Table 24 shows

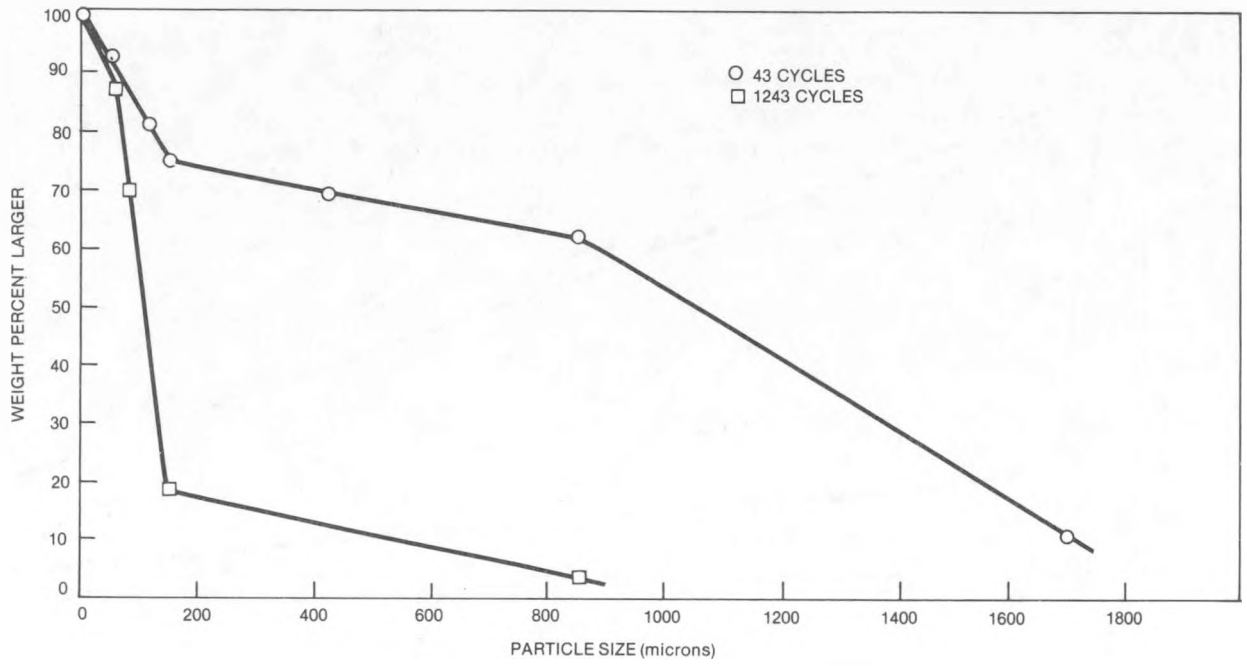

Figure 68. Comminution Effect Upon Alloy 149 - No. 1

Table 24

Cyclic Effects Upon Alloy 149-2

Sample Number	Cycle Number	H/M	% H_2 Absorbed
1	215	1.39	4.42
2	604	1.11	3.55
3	1523	0.79	2.54

the sampling results. Figure 69 is an illustration of the comminution effect on this test of Alloy 149. Comminution was not as severe as in the first test run. Figure 70 is a comparison of the H/M ratios of the two tests of Alloy 149. The noticeable difference between the two tests is due to the absence of water in the hydrogen.

4.4 Alloy 14A ($Mg_{0.56}Al_{0.34}Y_{0.1}$)

The subsequent hydride alloy to be tested was Alloy 14A ($Mg_{0.56}Al_{0.34}Y_{0.1}$). This alloy was crushed to -20/+40 mesh (~640 micron average) before loading

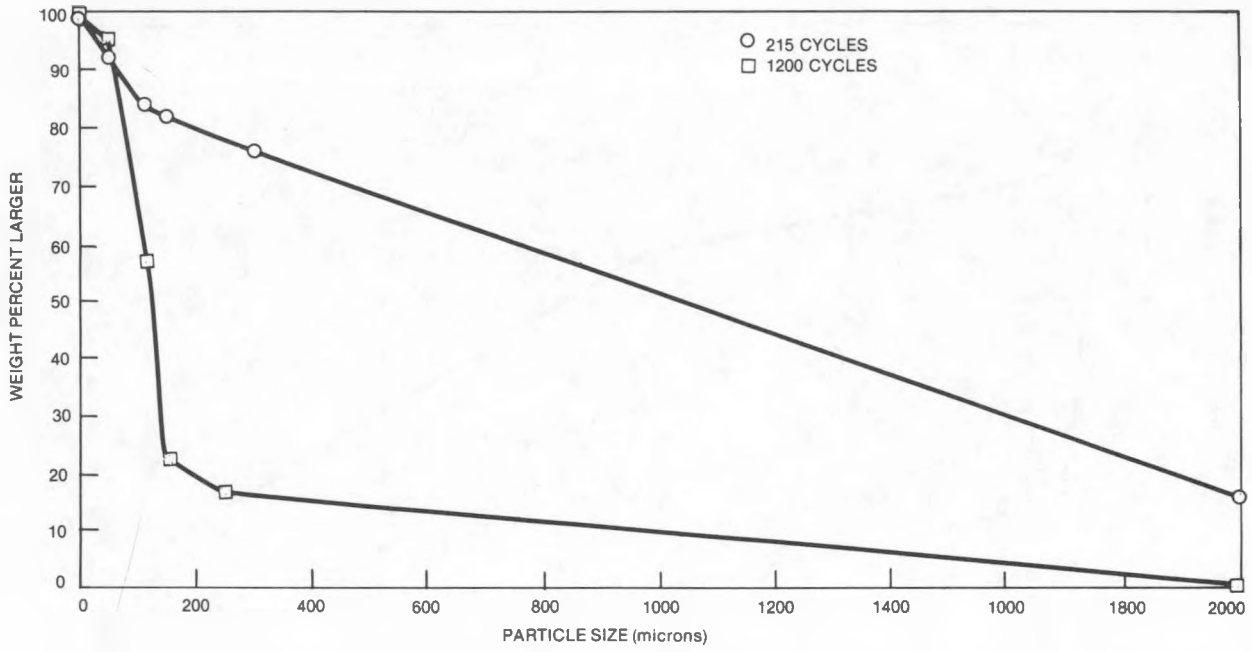

Figure 69. Communition Effect Upon Alloy 149 - Test Run #2

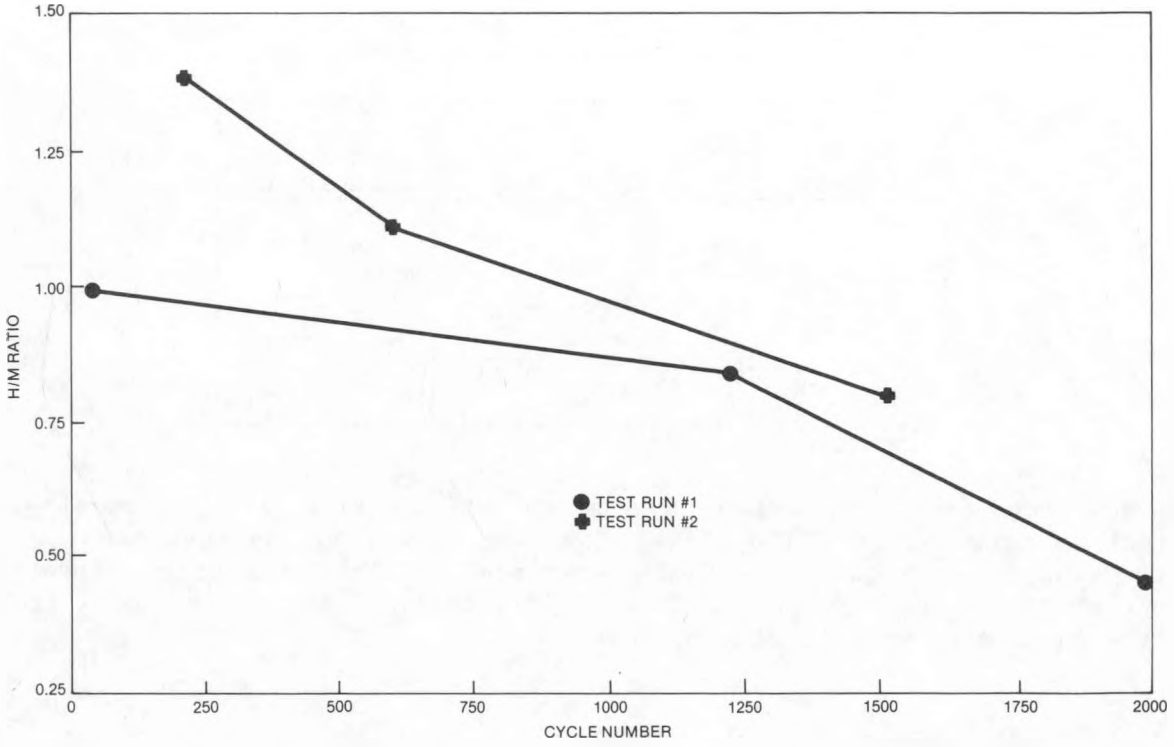

Figure 70. Comparison of the Two Test Runs of Alloy 149

Table 25

Cyclic Effects Upon Alloy 14A

Sample Number	Cycle Number	H/M	% H_2 Absorbed
1	198	0.89	2.64
2	487	0.87	2.59
3	1211	0.52	1.58
4	1478	0.45	1.36

into the pressure vessel. Activation took place and cycling commenced. Over 1400 cycles were recorded on this hydride alloy. Sampling results are shown in Table 25. It was interesting that this hydride alloy did not exhibit any particle comminution over the large number of hydriding/dehydriding cycles as is shown in Figure 71. This could be a very important factor in the life of a practical fuel alloy. However, the decreasing hydrogen uptake with number of cycles is seen to occur as with Alloy 149.

During the cyclic testing of this alloy, a gas sampling line was installed on the hydride cycling rig. Tests were made to indicate how effectively the in-line water trap removes water from the commercial quality hydrogen. Gas chromatography showed that the water content in the hydrogen was negligible.

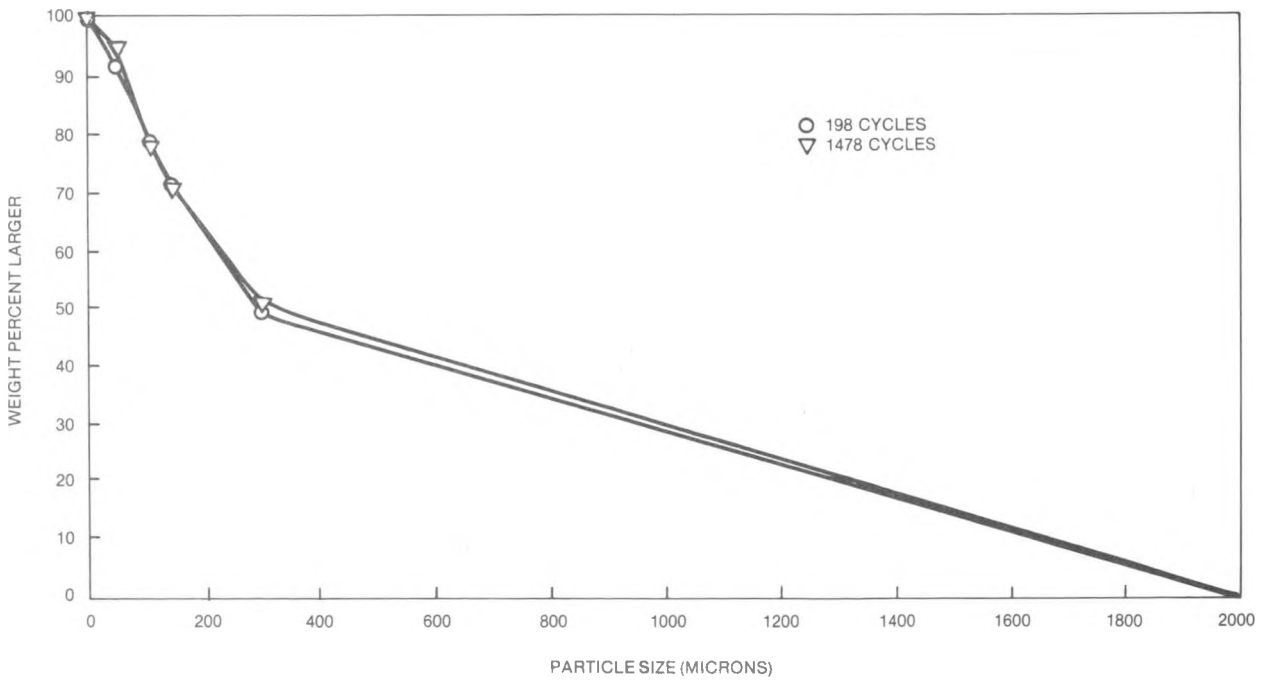

Figure 71. Comminution Effect Upon Alloy 14A

4.5 Alloy 23A ($Mg_{0.8}Al_{0.1}La_{0.1}$)

Alloy 23A ($Mg_{0.8}Al_{0.1}La_{0.1}$) was crushed to -10 mesh (~2000 micron) and then loaded into the pressure vessel. The total number of cycles recorded on this alloy was 1235.

Sampling results from this alloy yielded some unusual developments (see Table 26). In the previous studies of long term cyclic effects on various hydride alloys, the hydrogen content deteriorated over the span of cycles. This was not the case with Alloy 23A. The first three samples* of Alloy 23A actually showed a progresive increase in the hydrogen/metal ratio. A possible explanation for this phenomenon may be that the alloy was comminuting, and that, initially, the alloy may not have been fully activated. Part of this is verified by the comminution effect summarized in Figure 72. Sample #4 resulted in a decrease in the hydrogen content and commminution showed that the percentage of large particles also decreased. This was an expected circumstance because more surface area exposed to contamination results in a decrease in the H/M ratio. Sample #5, however, increased in hydrogen content. This can probably be explained by the greater percentage of large particles in this particular sample, hence less tendency for contamination and subsequent deterioration of H/M ratio.

Table 26

Cyclic Effects Upon Alloy 23A

Sample Number	Cycle Number	H/M	% H_2 Absorbed
1	270	0.73	1.98
2	610	0.86	2.35
3	836	1.83	4.86
4	1032	1.20	3.25
5	1235	1.51	4.06

*The samples themselves did not each go through "increasing cycles". They served as "milestones along the way".

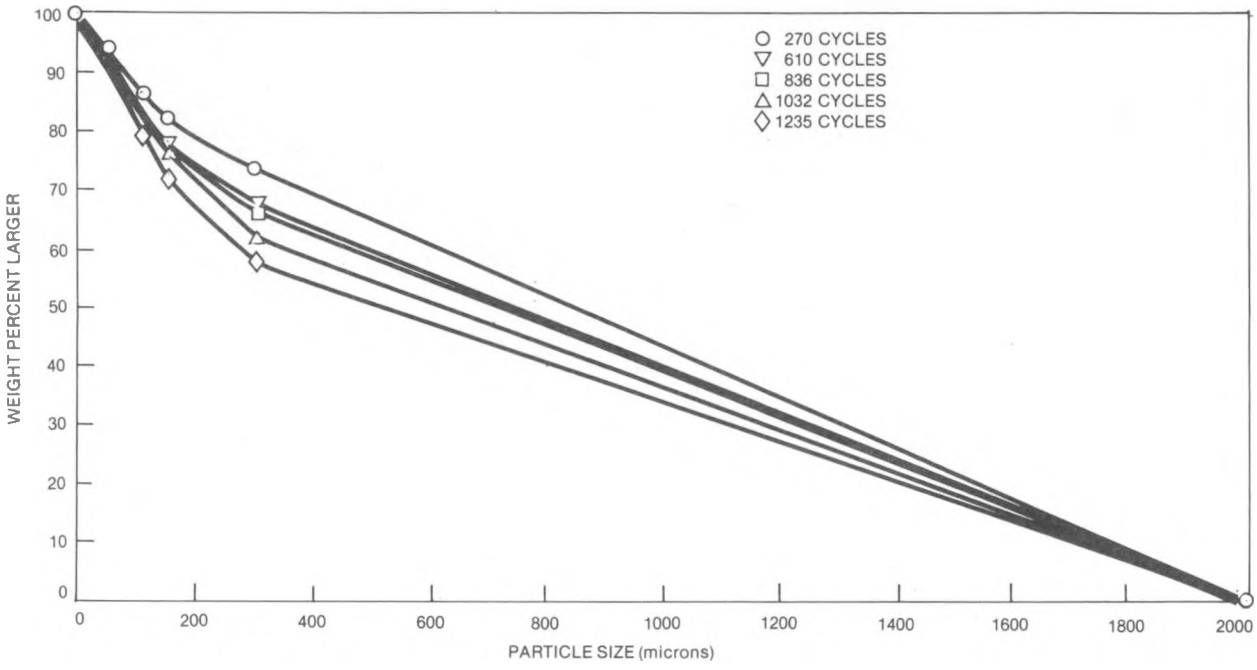

Figure 72. Comminution Effect Upon Alloy 23A

4.6 Alloy 14L ($Mg_{0.7}Li_{0.1}Ni_{0.1}Sn_{0.1}$)

The final alloy tested was Alloy 14L, $Mg_{0.7}Li_{01}Ni_{0.1}Sn_{0.1}$. This alloy was crushed to -10 mesh (~2000 micron) and loaded into the pressure vessel for cycling. Only 795 cycles were recorded on this alloy due to the failure of a strategic heater-control thermocouple. Two samples were taken and these results are shown in Table 27.

Table 27

Cyclic Effects Upon Alloy 14L

Sample Number	Cycle Number	H/M	% H_2 Absorbed
1	520	0.874	2.42
2	795	0.751	2.09

The effect of comminution of the alloy for the two samples is illustrated in Figure 73.

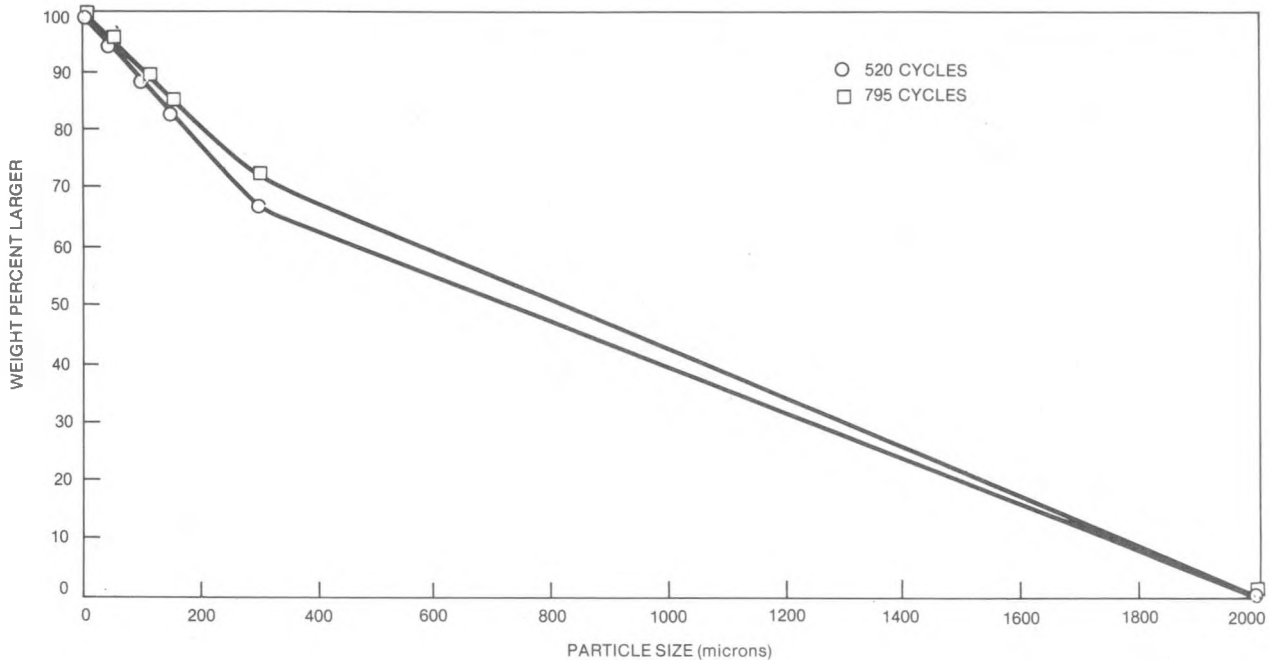

Figure 73. Comminution Effect Upon Alloy 14L

The alloy exhibited the expected deterioration of hydrogen content over an increasing number of cycles along with comminution of the hydride particles. If further testing had been possible on this alloy, it is believed that this trend would have continued.

5

SUMMARY AND CONCLUSIONS

5.1 SUMMARY

The extensive research efforts of the authors on magnesium-base hydride alloys have resulted in the development of a number of alloys using substantially less nickel than previously investigated materials, or no nickel at all (nickel is considered a strategic material).

In the Mg-Cu-Ni family of alloys, the $Mg_{0.845}Cu_{0.1}Ni_{0.05}Y_{0.005}$ (Alloy 149) composition exhibits improved hydride properties over the Mg-25Ni alloy hydride reported by Reilly, et al. (Ref. 23) with a nickel content of less than 10 weight percent.

Among the Mg-Al alloys, modifications of $Mg_{17}Al_{12}$ and Mg-10Al with ternary additions of rare earths and yttrium resulted in alloys exhibiting more rapid kinetics, plateau pressures greater than one and one-half times, and hydrogen contents about a factor of three greater than the binary alloys hydrided under the same conditions. Rare-earth additions to the Beta-(Mg_2Al_3 and Mg_5Al_8) and Epsilon-(Mg_4Al_5) phases substantially reduced the time required for activation, and greatly enhanced the reactivity (T) and hydriding kinetics of these alloys. Mid-plateau pressures in the range of 12 to 14.5 atmospheres at 350°C have also been achieved for these alloy hydrides.

A study was conducted to determine hydriding characteristics of mixtures of low-temperature hydrides (Fe-Mn-Ti and V-Nb) and the higher temperature Mg-base alloy hydrides. These mixed-hydrides provided for hydrogen mass-fraction of up to about four percent, but characteristic high dissociation temperatures were not reduced.

Investigations of sensitivity to impurities (O_2 and N_2) and to the effects of a large number of hydriding-dehydriding cycles of Mg alloy hydrides indicate that the H/M ratio gradually deteriorates (O_2 being more of a problem than N_2). The plateau pressures, on the other hand, remain substantially unchanged.

The hydriding characteristics of the newly developed alloys are summarized and compared with other selected Alloys in Table 28. Figure 74 compares isotherms of nickel-free and nickel-containing magnesium-base alloys and points up the possibility of producing useful hydride alloys without the use of the strategic metal, nickel.

Table 29 compares densities and hydrogen contents of newly selected developed alloys with those of certain reference hydride alloys. The alloys listed were

Table 28

Comparison of Selected Magnesium Alloy Hydrides

Alloy	Composition, Wt. Percent	Mid-Plateau Desorption Pressure in Atm (310°C)	Temperature (°C) of Mid-Plateau Pressure of One Atm[a]	H/M Ratio	Hydrogen Wt. Percent
Mg_2Ni (Ref. Alloy)	55.3Mg-54.7Ni	4.2[a]	253	1.3	3.6[b]
Mg_2Ni-Mg (Ref. Alloy)	74.8Mg-25.2Ni	1.9[a]	287	1.6[b]	5.7[b]
$Mg_{0.62}Al_{0.38}$ (Ref. Alloy)	59.52Mg-40.8Al	1.3	--	0.6	2.3[c]
$Mg_{0.7}Li_{0.1}Ni_{0.1}Sn_{0.1}$	48.0Mg-1.96Li-16.56Ni-33.48Sn	2.4	--	0.8	2.3
$Mg_{0.56}Al_{0.34}Y_{0.1}$	43.5Mg-29.48Al-25.98Y	2.2	286	1.2	3.6[c]
$Mg_{0.8}Al_{0.1}La_{0.1}$	53.97Mg-7.49Al-38.54La	2	--	1.6	4.2[c]
$Mg_{0.335}Al_{0.622}La_{0.044}$	26.25Mg-54.06Al-19.69La	14.5 (350°C)	--	0.6	1.7[d]
$Mg_{0.420}Al_{0.570}Y_{0.042}$	34.83Mg-52.44Al-12.73Y	12.3 (350°C)	--	0.5	2.0[d]
$Mg_{0.386}Al_{0.570}MM_{0.044}$	30.34Mg-49.70Al-19.97MM	12.5 (350°C)	--	0.7	2.3[d]

[a] Calculated from Van't Hoff relationship

[b] Held at >200 psi above dissociation pressure for several days

[c] Held 12 hours at 400°C under 600 psi

[d] Held 60 hours at 400°C under 1000 psi

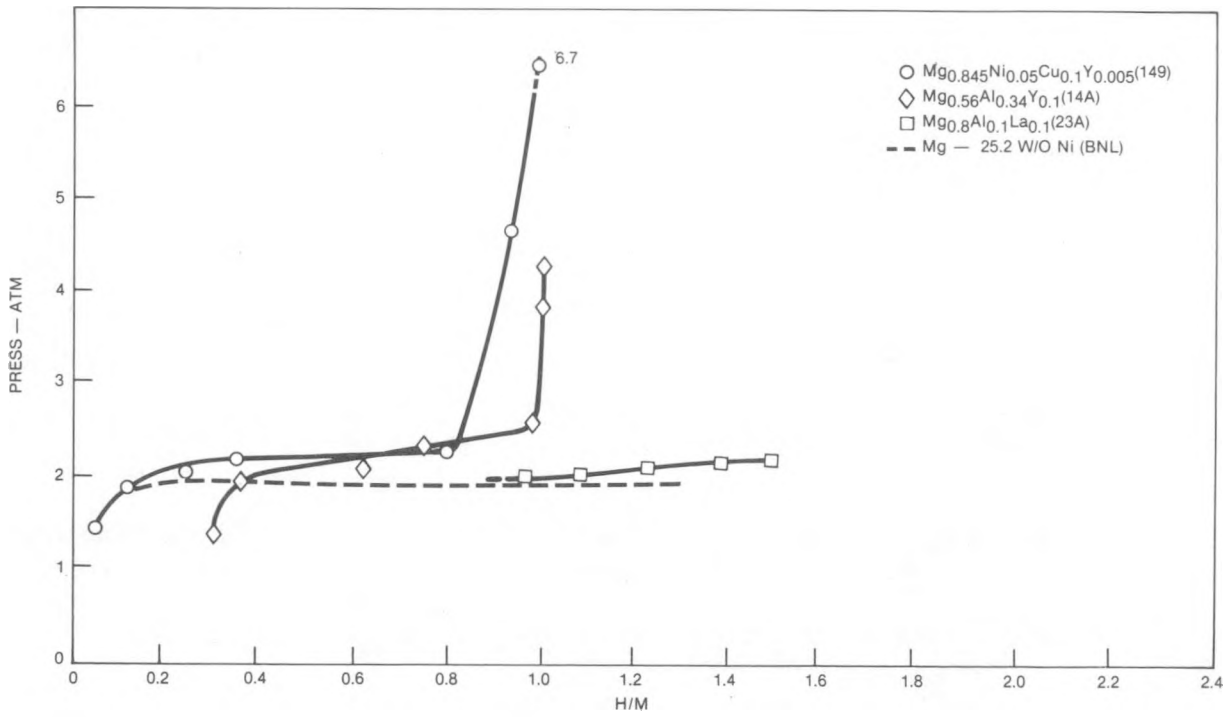

Figure 74. Comparison of Hydride Alloys With and Without Nickel at 310°C

Table 29

Comparative Properties of Hydride Alloys

Alloy	Composition	Alloy Density g/cc	Weight Percent H_2 Absorbed	Section Reference In This Report
	SELECTED NEWLY DEVELOPED ALLOYS			
149	$Mg_{0.845}Ni_{0.05}Cu_{0.1}Y_{0.005}$	2.37	4.42	3.1
14L	$Mg_{0.7}Li_{0.1}Ni_{0.1}Sn_{0.1}$	3.36	2.32	3.2.4
14A	$Mg_{0.56}Al_{0.34}Y_{0.1}$	2.56	3.6	3.3.1
23A	$Mg_{0.8}Al_{0.1}La_{0.1}$	2.41	4.22	3.3.2
	REFERENCE ALLOYS			
Fe-Mn-Ti	$Fe_{0.5}Mn_{0.5}Ti$	5.44	--	--
$LaNi_5$	--	8.43	1.5	--
Mg_2Ni	--	3.44	4.2	Appendix A
Mg	--	1.74*	7.6	--

*ASM Metals Handbook, 8th Edition, Vol. 1, 1961. All other values were measured in the Solar Laboratories.

selected for their hydriding characteristics from among some 200 alloys studied under this program.

5.2 CONCLUSIONS

1. The four most promising candidate new lightweight hydrides developed and investigated in this effort were:

Project Designation	Composition
149	$Mg_{0.845}NI_{0.05}Cu_{0.1}Y_{0.005}$
14L	$Mg_{0.7}Li_{0.1}Ni_{0.1}Sn_{0.1}$
14A	$Mg_{0.56}Al_{0.34}Y_{0.1}$
23A	$Mg_{0.8}Al_{0.1}La_{0.1}$

2. A stated program goal of achieving a dissociation temperature of 200°C or less, with the released hydrogen at one atmosphere or more, was not met.

3. The lowest dissociation temperatures determined for those lightweight hydrides, found to be promising otherwise, was determined to be in the range of 250 to 270°C.

4. These more promising candidate lightweight hydrides investigated had maximum hydrogen weight or mass fractions in the range of 3 to 4.5 percent.

5. The use of "mini-PC isotherms", or pressure-composition curves, at a given temperature determined on the basis of only three to four data points, was found to be an effective and efficient screening means for candidate lightweight hydrides.

6. The combination of conventional optical photomicrographs, plus Scanning Electron Microscope (SEM) and Energy Dispersive X-Ray (EDX) techniques proved to be quite effective in characterizing and generally understanding the nature of the experimentally-investigated hydride materials.

7. Combined alloy hydrides, that is physical mixtures of lightweight and heavier hydrides (e.g., Fe-Mn-Ti) were demonstrated as means of "tailoring" isotherm characteristics. However, no significant improvement in reduced-temperature operation of magnesium-based lightweight materials was observed.

8. Special impurity-effect testing of oxygen and nitrogen contaminants showed:

   - Oxygen, at about 0.1 percent addition reduces the maximum hydrogen fraction of a typical lightweight hydride* about 10 percent; however, plateau pressures were little affected

   - Nitrogen addition did not significantly affect the behavior of a representative lightweight hydride material*

9. For certain magnesium-aluminum based alloys (beta- and epsilon-phases), some of the aluminum is "tied up" in highly stable RE Al_2 compounds. Adding a commensurate unassociated amount of aluminum, by way of compensation, was not found advantageous.

10. Efforts to further diminish the amount of nickel (strategic material) in an already nickel-lean material (viz., Alloy 149, see formula above) by substituting copper for nickel, while increasing yttrium for increased activity (catalytic effect), were not successful. Although the hydrogen content was slightly increased, the plateau pressure was significantly reduced.

---

*Alloy 14A, see formula above.

11. Alloy cycle testing using a special automatic cycling rig proved quite informative in that new information was generated on the behavior of four lightweight hydrides from about 700 to beyond 2000 hydriding/dehydriding cycles.

12. The state-of-knowledge of lightweight hydrides has been substantially broadened by the reported research. However, practical lightweight hydride automotive hydrogen storage systems remain to be designed and tested.

REFERENCES AND BIBLIOGRAPHY

1. Ecklund, E. D. and Kester, F. L. (1976). "Hydrogen Storage on Highway Vehicles: Update '76", Proceedings of the 1st World Hydrogen Energy Conference, Miami Beach, FL.

2. Rohy, D. A., Nachman, J. F., and Duffy, T. E. (1975). "Automotive Storage of Hyrogen Using Modified Magnesium Hydrides", TEC-75/002.

3. King, R. O. and Mogens, R. (1955). "The Oxidation, Decomposition, Ignition and Detonation of Fuel Vapors and Gases, XXVII. The Hydrogen Engine", Canadian Journal of Technology, Vol. 33, 445.

4. Sultan, O. and Shaw, H. (1975). "Study of Automotive Storage of Hydrogen Using Recyclable Liquid Chemical Carriers", TEC-75/003.

5. Rohy, D. A., Nachman, J. F., Hammer, A. N., and Duffy, T. E., Final Report on DOE Contract No. EY-76-C-1167 (1979).

6. Douglass, D. L. (1975). Met. Trans. A, V. 6A.

7. Lundin, C. E. and C. B. Magee (1977). "A Correlation Between the Intersititial Hole Sizes in Intermetallic Compunds and the Thermodynamic Properties of the Hydride Formed From Those Compounds", J. Less Common Metals, V. 56.

8. Teatum, E., et al. (1960). "Compilation of Calculated Data Useful in Predicting Metallurgical Behavior of the Elements in Binary Alloy Systems", LA-2345, Los Alamos Scientific Laboratory.

9. Hansen, M. (1958). Constitution of Binary Alloys, McGraw-Hill Book Co., Inc. New York.

10. Air Products & Chemicals, Inc. (May 1979). "Development of New Hydrogen Storage Systems for Automotive Hydrogen Fuel Storage", Final Report on BNL Contract No. 435582-S.

11. Reilly, J. J., R. H. Wiswall and C. H. Waide (1974). Final Report EPA Grant R802579, Brookhaven National Laboratory, Upton, New York.

12. Air Products & Chemicals, Inc. (1979). Final report on BNL Contract No. 485875-S.

13. Mintz, M. H., Z. Gavra, and G. Kimmel (1980). Proc. Int. Symp. on the Properties and Applications of Metal Hydrides, Colorado Springs, Colorado, April 7-11, 1980; J. Less Common Metals, V. 74.

14. Rohy, D. A. and J. F. Nachman (1979). Annual Task Report on DOE Contract DE-AC037851059.

15. van Mal, H.H., K.H.J. Buschow, and A. R. Miedema (1974). J. Less Common Metals, V. 35.

16. Magee, C. B. (1979). Denver Research Institute, University of Denver, Denver, Colorado, Personal Communication.

17. Glassner, A. (1958). "The Thermodynamic Properties of the Oxides, Fluorrides, and Chlorides to 2500°K", ANL-5750, Argonne National Laboratory, 485875-S.

18. Moffat, William G. (1978). The Handbook of Binary Phase Diagrams, Vol. 3 General Electric Company.

19. Gschneidner, K. A. (1961). Rare Earth Alloys, D. Van Nostrand Co., New York.

20. Gavra, Z., et al. (to be published). "Effects of Nickel and Indium Ternary Additions on the Hydrogenation of Magnesium-Aluminum Intermetallic Compounds", Nuclear Centre Negev and the Ben-Gurion Univ. of the Negrv.

21. Eisenberg, F. G., D. A. Zagnoli and J. J. Sheridan III (1980). Proceedings of International Symposium of the Properties and Applications of Metal Hydrides, Colorado Springs, Colorado, April 7-11, 1980; J. Less Common Metals, V. 73.

22. Vigeholm, B., et al., "Magnesium Hydrogen Storage", Proceedings of the International Symposium on the Properties and Applications of Metal Hydrides, Colorado Springs, Colorado, April 7-11, 1980, V. II.

23. Reilly, J. J. and R. H. Wiswall (1978). Inorg. Chem. V. 7.

ADDITIONAL PUBLICATIONS AND PRESENTATIONS DERIVED FROM THIS CONTRACT EFFORT

1. Rohy, D. A., Nachman, J. F., and Argabright, T.A., "Lightweight Hydrides for Automotive Storage of Hydrogen, 16th IECEC Conference, Atlanta, GA, 1981.

2. Nachman, J. F. and Rohy, D. A., "Magnesium Alloy Hydries", published in Metal Hydrogen Systems, ed. T. Nejat Veziroglu, Pergamon Press, 1982, pp. 557-600.

3. Rohy, D. A., et al., "Automotive Storage of Hydrogen Using Modified Magnesium Hydrides", Summary Report, March 1977, contract ERDA EY-76-C-1167.

4. Rohy, D. A., et al., "Automotive Storage of Hydrogen Using Modified Magnesium Hydrides, Summary Report, November 1977, Contract ERDA EY-76-C-1167.

5. Rohy, D. A., et al., "Automotive Storage of Hydrogen Using Medified Magnesium Hydrides, Summary Report, March 1979, Contract DOE EY-76-C-1167.

6. Rohy, D. A. and Nachman, J. F., "Development of Lightweight Hydrides", Annual Report, October 1979, contract DOE DE-AC03-78CS-52059.

7. Rohy, D.A. et al., "Automobile Hydrogen Storage With Magnesium Hydride", May 1978 Contractors Coordinating Meeting, Troy, MI.

8. Rohy, D. A. and Nachman, J. F., "Development of Lightweight Hydrides", October 1978 Contractors Coordinating Meeting, Dearborn, MI.

9. Rohy, D.A. et al., "Automotive Hydrogen Storage With Magnesium Hydride", October 1976 Contractors Coordinating Meeting, Ann Arbor, MI.

10. Rohy, D.A. et al., "Automotive Hydrogen Storage With Magnesium Hydride", May 1976 Contractors Coordinating Meeting, Ann Arbor, MI.

11. Rohy, D. A., et al., "Development of Lightweight Hydrides", October 1979 Contractors Coordinating Meeting, Dearborn, MI.

12. Rohy, D. A., et al., "Development of Lightweight Hydrides", October 1981 Contractors Coordinating Meeting, Dearborn, MI.

APPENDIX A

REVIEW OF OTHER PUBLISHED MAGNESIUM ALLOY HYDRIDE WORK

Magnesium-Nickel Alloys

Mg reacts with Ni to form intermetallic compounds, Mg_2Ni and $MgNi_2$. Mg_2Ni reacts with H_2 at a temperature of 325°C and a pressure of 300 psia, while $MgNi_2$ does not react with H_2 even at temperatures of 350°C and pressures of 400 psia (Ref. 1).

Figure A-1 shows the pressure-composition isotherms for the Mg_2Ni-H_2 system. The compound Mg_2Ni, similar to Mg_2Cu, is readily hydrided, except that a ternary hydride is formed as shown in equation (1).

$$Mg_2Ni + 2H_2 \rightleftharpoons Mg_2NiH_4 \qquad (1)$$

The crystal structure of this ternary hydride was determined by Reilly and coworkers (Ref. 1) to be tetragonal. More recent thermodynamic and crystallographic studies of Mg_2NiH_4 by Gavra and Mintz (Ref. 2) and Mintz, et al., (Ref. 3) indicate the existence of two allotropic forms of this compound. One is the orthorhombic form which is stable at ambient temperatures. At 210-245°C the low temperature form transforms to a cubic CaF_2-type structure. However, the hydrogen composition remains the same for both allotropic modifications.

A Van't Hoff plot of dissociation temperature versus reciprocal of the absolute temperature (Ref. 1) gives the following relationship:

$$P_{atm} = -3360/T + 6.389 \qquad (2)$$

The $\Delta H_{298°K}$ of Mg_2NiH_4 calculated from the dissociation pressure data equals -15.4 ± 1 kcal/mole of H_2.

Figure A-2 shows pressure-composition isotherms for an alloy composition of 72.9 weight percent Mg and 25.2 weight percent Ni. The presence of an excess of Mg produces an isotherm with two pressure plateaus. The length of the plateau region represents the proportional amount of excess Mg with respect to Mg_2Ni.

Mg_2Ni promotes the hydriding of Mg because of the absence of a compact oxide layer as with pure Mg, and the presence of catalytically active metal (Ref. 4).

In studying the formation of hydrides by reaction of high-pressure (300-800 psi) hydrogen at 400°C and 450°C with Mg-25Ni, Douglass (Ref. 5) found that the reaction kinetics can be described by the Johnson-Mehl relationship, Figure A-3. The plot log of time for 50 percent reaction versus reciprocal temperature gave an activation energy of 8400 cal/mole. Hydriding occurred preferentially in the magnesium matrix, with the entire magnesium matrix being converted to MgH_2 before hydriding of the Mg_2Ni phase took place.

Douglass (Ref. 5) suggests that the rate-controlling step in hydriding may be the interfacial reaction in which hydrogen atoms transfer across the metal/hydride interface. Experimental determination of Kirkendall marker movements

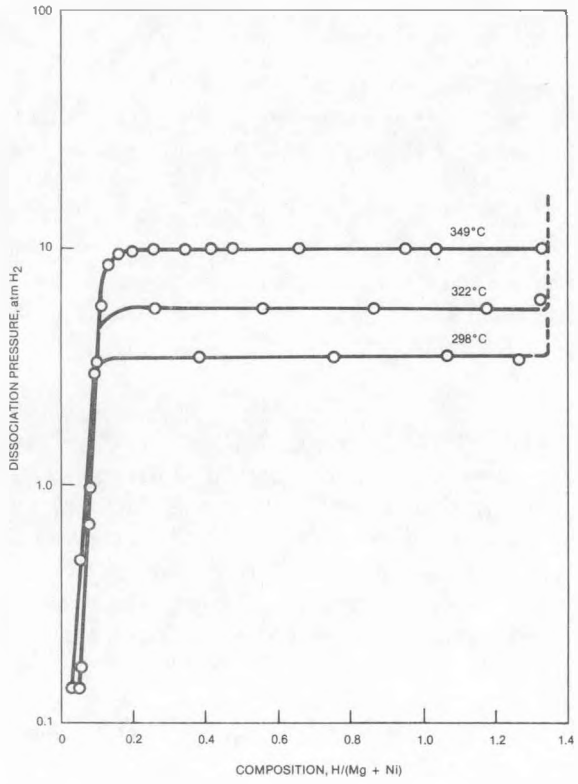

Figure A-1.

Pressure-Composition Isotherm for the Mg_2Ni-H_2 System (Ref. 1)

Figure A-2.

Pressure-Composition Isotherm for the Mg_2Ni-Mg-H_2 System (Ref. 1)

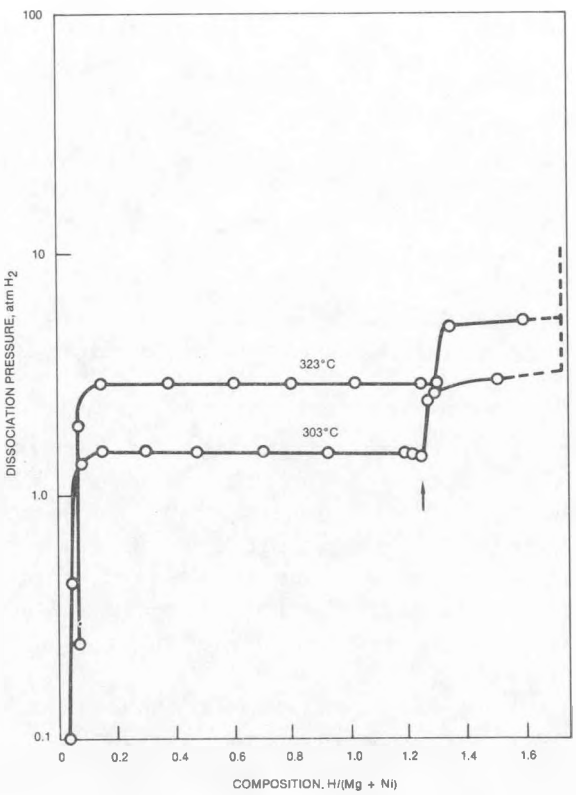

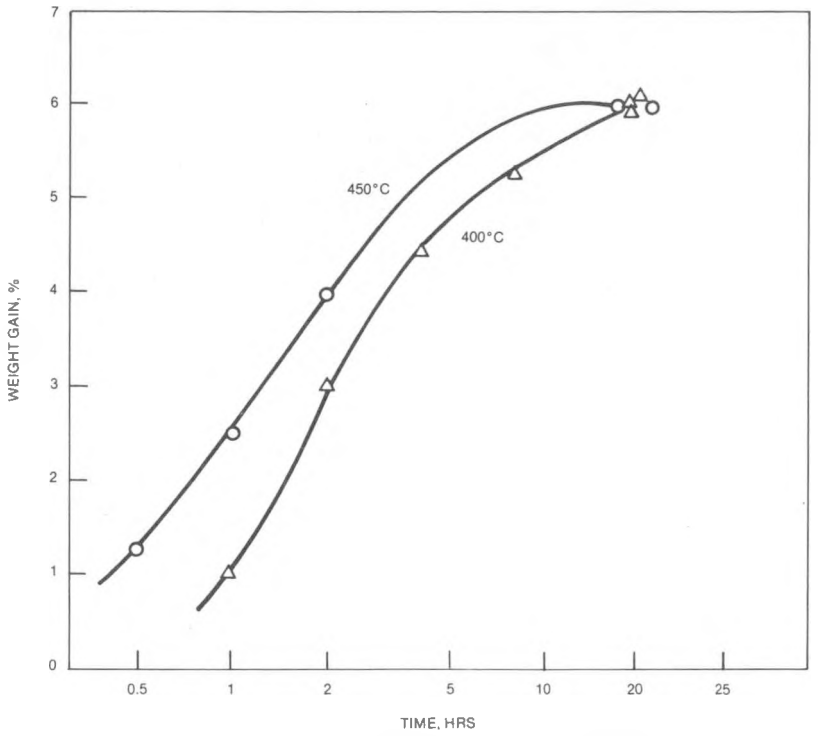

Figure A-3. Hydriding Kinetics of Mg-25Ni (Ref. 5)

by Luz, Genossar and Rudman, (Ref. 6) indicates that the H^- anion rather than the Mg^{2+} cation is the diffusing species during the hydriding of Mg.

In their study of the effects of nickel plating on the hydriding-dehydriding kinetics of Mg, Eisenberg, et al. (Ref. 7) found that electroless plating had little effect on activation, hydrogen capacity, and absorption kinetics, but, the effect on desorption kinetics was quite great. However, the rate appears to decay with cycling because of agglomeration of the surface nickel crystallites.

Magnesium-Copper Alloys

Magnesium copper hydrides have been studied by Reilly and Wiswall (Ref. 8). Of the two intermetallic compounds, Mg_2Cu and $MgCu_2$ in the Mg-Cu system, their work indicates that only Mg_2Cu hydrides rapidly at 300°C and pressures of approximately 300 psia. Hydriding of the intermetallic compound Mg_2Cu (Ref. 8) proceeds reversibly by the following reaction:

$$2Mg_2Cu + 3H_2 \rightleftharpoons 3MgH_2 + MgCu_2 \qquad (3)$$

Figure A-4 represents pressure-composition isotherms with an excess of Mg. Two plateaus are exhibited, with the lower plateau due to the formation of MgH_2 and the upper due to the reaction of Mg_2Cu with H_2 as indicated in equation (3).

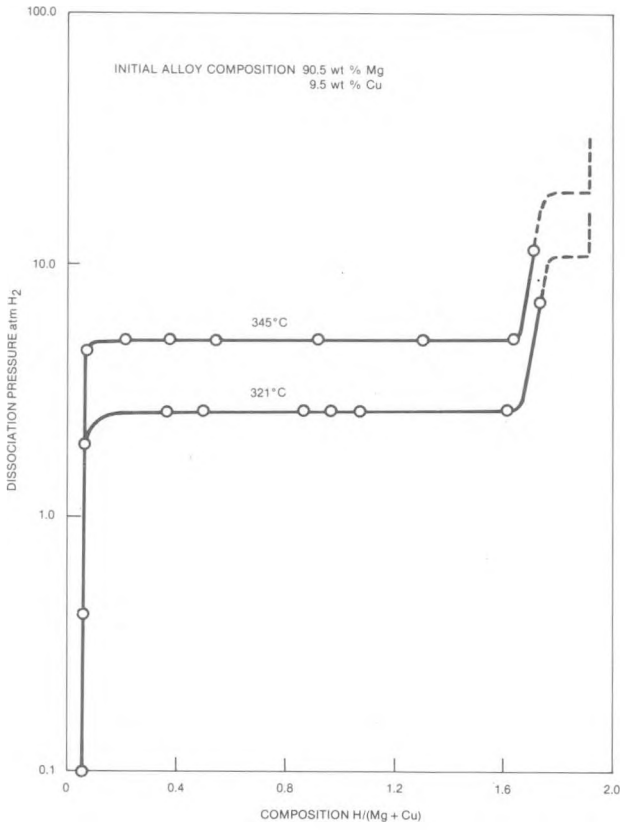

Figure A-4.

Pressure-Composition Isotherms for the System 90.5 wt. % Mg-9.5 wt. % Cu-H_2 (Ref.8)

Since only MgH_2 is present, no ternary hydrides are formed during this reaction (Ref. 8). Figure A-5 shows the pressure-composition isotherms for the Mg_2Cu-H_2 system at three different temperatures. A Van't Hoff plot of dissociation pressure versus reciprocal of the absolute temperature yields the following relationship:

$$\log P_{atm} = -3809/T + 7.437 \qquad (4)$$

The heat of formation for reaction (3) calculated from these data equals -17.4 ± 1.0 kcal/mole of H_2 (Ref. 8).

The presence of Mg_2Cu serves as a catalyst for hydriding reaction (3), as considerably higher pressures are required to hydride Mg by itself (Ref. 8). According to Genossar and Rudman (Ref. 6) and others (Ref. 4), maintaining an unoxidized external surface appears to be necessary for chemisorption and/or transfer of atomic hydrogen into the interior. The Mg_2Cu provides an unoxidized surface because oxides of copper are readily reduceable by hydrogen. Maximum hydrogen absorption by Mg_2Cu expressed in H/M ratio is 1.02, and in weight percent is 2.72 (Ref. 8).

Magnesium-Rare Earth/Yttrium Alloys

Earlier discussions of the Solar authors' investigations of varying alloying additions to magnesium alloys show the beneficial effect of adding rare-earth

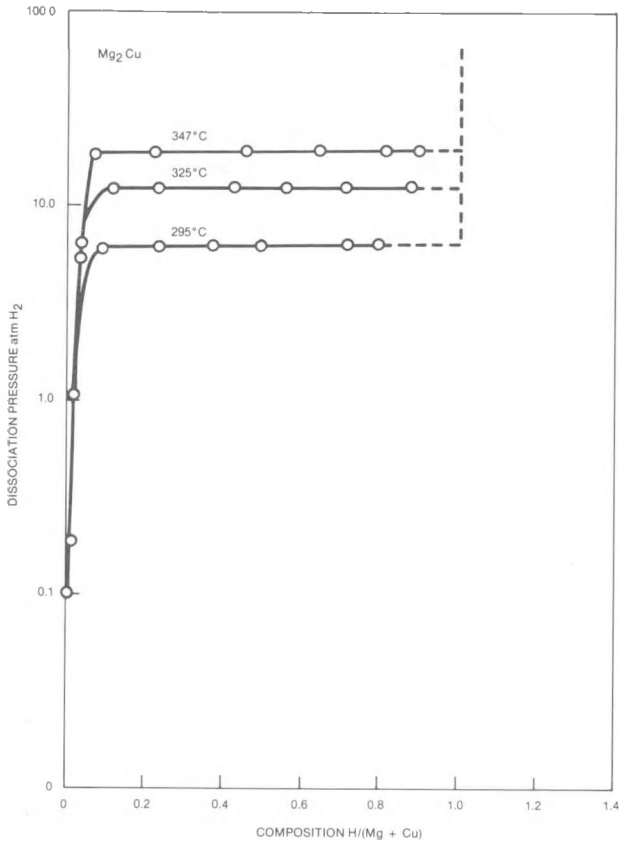

Figure A-5.

Pressure-Composition Isotherms for the Mg_2Cu-H_2 System (Ref. 8)

or yttrium on hydriding kinetics and hydrogen capacity. Other investigators have studied hydriding of such intermetallic compounds as $CeMg_9$, $CeMg_{12}$, La_2Mg_{17}, Ce_2Mg_{41} and observed increased hydriding rates and improved H_2 capacities. These studies are discussed below.

In their search for new hydride materials, Reilly, et al. (Ref. 9) investigated the hydriding characteristics of Mg_9Ce and Mg_9R.E.(mischmetal). These intermetallic compounds absorbed 4.1 and 4.4 weight percent hydrogen, respectively. No comments were made by these investigators regarding activation or kinetics of hydriding and dehydriding.

Buchner and coworkers (Ref. 10) studied the hydriding charcteristics of the Mg-MgY system with respect to vehicular applications. They reported the kinetics of hydriding and dehydriding as being substantially faster than that of MgH_2. The PC isotherms for this system are shown in Figure A-6. The heat of formation is comparable to that of MgH_2. Darriet, Pezat and coworkers (Ref. 11) studied the hydriding behavior of $Mg_{12}Ln$, $Mg_{17}Ln$ and Ln_5Mg_{41} intermetallic compounds, where Ln = La, Ce, or mischmetal. In hydriding of the $Mg_{12}Ln$ type phases, initialy an irreversible decomposition of the alloy is reported to take place as follows:

$$Mg_{12}Ln + 27/2\ H_2 \quad LnH_3 + 12\ MgH_2 \qquad (5)$$

The following reaction then reportedly takes place during the absorption-desorption cycles:

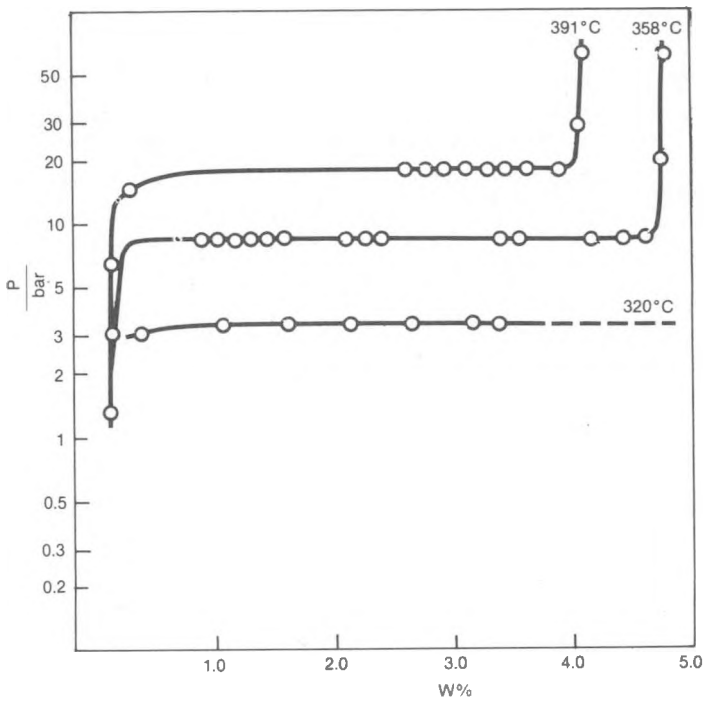

Figure A-6.

Concentration-Pressure-Isotherms for Mg-Y Alloys (Ref. 10)

$$LnH_3 + 12MgH_2 \rightleftharpoons 12Mg + LnH_x + (27 - x)/2H_2 \quad (6)$$

Figure A-7 shows the pressure-composition isotherms for $Mg_{12}Ce$ at temperatures of 325, 360, and 380°C. Hydrogen absorption rate versus temperature is given in Figure A-8 for a pressure of 30 bar. Even at room temperature a significant amount of hydrogen is absorbed. Pressure enhances adsorption initially, but after about an hour absorption appears to be the same regardless of the pressure. At 325°C and a pressure 30 bar $Mg_{12}Ce$ absorbs 4.7 percent hydrogen. Desorption is strongly dependent upon temperature as shown in Figure A-9. Approximately 90 percent of the hydrogen is recovered at a temperature of about 340°C. Similar results are obtained with $Mg_{12}La$ and mischmetal Mg_{12}.

$Mg_{17}La_2$ was the only phase of the $Mg_{17}Ln_2$ type structure Darriet, et al. (Ref. 11) could isolate. This compound behaves similarly to the $LnMg_{12}$ alloys during hydriding, taking place in two consecutive steps. Under a pressure of 3 MPa at 325°C and one hour 4.7 percent hydrogen is absorbed, after 20 hours 5.5 percent is absorbed.

Similarly, $Mg_{41}Ce_5$ exists only with cerium. Mechanism of hydriding involves the irreversible disproportionation of $Mg_{41}Ce_5$ as with the above compound (Ref. 11). Hydrogen absorption is similar to $Mg_{17}La_2$ at about 5.5 percent.

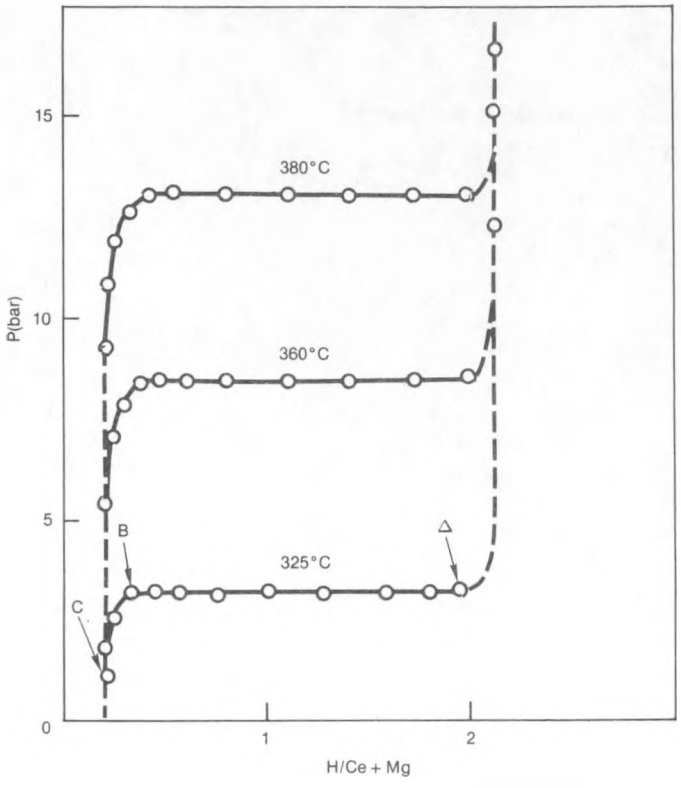

Figure A-7.

Isotherms for $CeMg_{12}$ (Ref. 11)

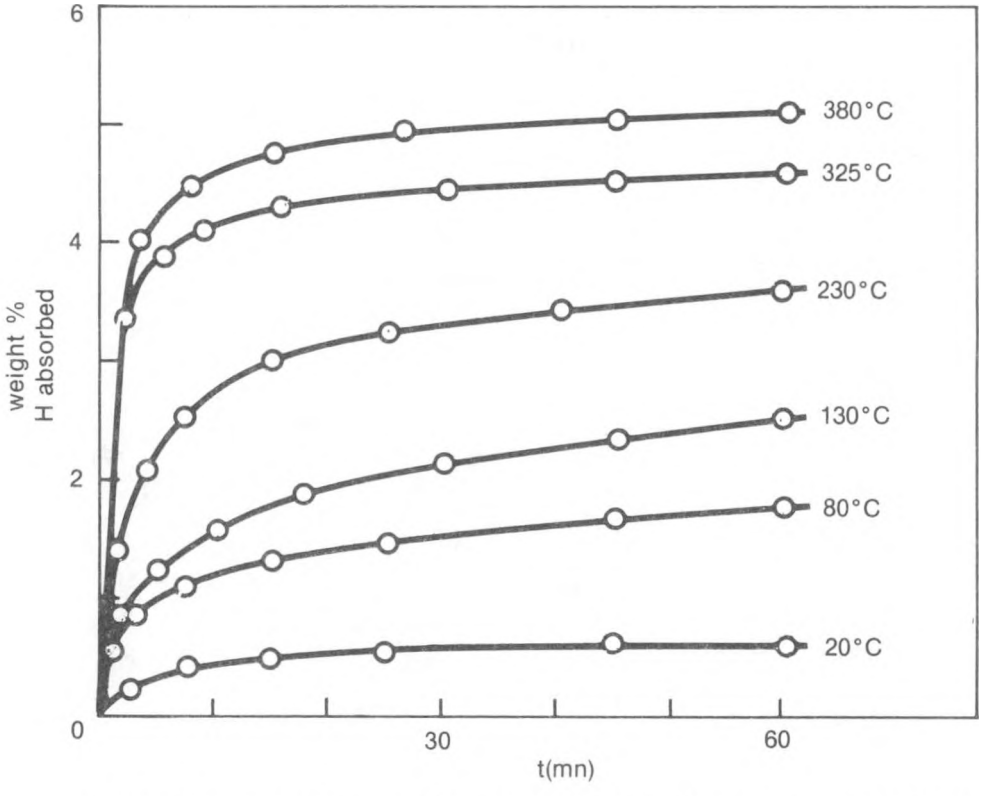

Figure A-8. Hydrogen Absorption Data Versus Temperature (Ref. 11)

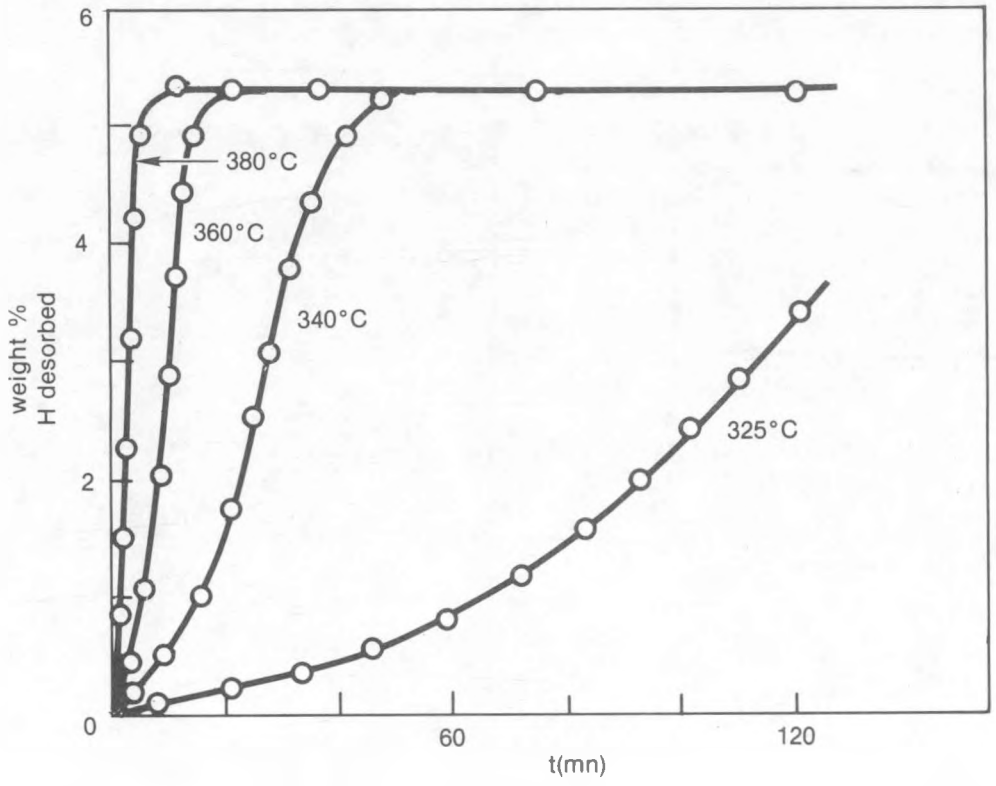

Figure A-9. Desorption of Hydrogen From $CeMg_{12}$ Under Pressure of 0.2 MPa (Ref. 11)

References

1. Reilly, J. J. and Wiswall, R. H., Inorg. Chem. V. 7 (1968).

2. Gavra, Z., Mintz, M. H., Kimmel G., and Hadari, Z., Inorg. Chem., V. 18 (1979).

3. Gavra, Z., et al., "Effects of Nickel and Indium Ternary Additions on the Hydrogenation of Magnesium-Aluminum Intermetallic Compounds", Nuclear Centre Negev and the Ben-Gurion Univ. of the Negrv (to be published).

4. Seiler, A., Schlapbach, L. Von Waldlarch, Th. Shaltiel, D. and Studin, F., Proc. Int. Symp. on the Properties and Applications of Metal Hydrides, Colorado Springs, Colorado, April 7-11, 1980; J. Less Common Metals, V. 73.

5. Douglass, D. L., Met. Trans. A., V. 6A (1975)

6. Genossar, J. and Rudman, P. S., "Hydrogen in Metals" (6-9 March 1979), Munster, West Germany.

7. Eisenberg, F. G., Zagnoli, D. A. and Sheridan, J. J. III, Proc. Int. Symposium of the Properties and Applications of Metal Hydrides, Colorado Springs, Colorado, April 7-11, 1980; J. Less Common Metals, V.73.

8. Reilly, J. J. and Wiswall, R. H., Inorg. Chem., V. 6 (1967).

9. Reilly, J. J., Wiswall, R. H. and Waide, C. H., Final Report EPA Grant R802579, Brookhaven National Laboratoty, Upton, New York (1974).

10. Buchner, H., Bernauer, O. and Straub, W., "Development of High-Temperature Hydrides for Vehicular Applications", Proceedings 2nd World Hydrogen Energy Conference, Zurich, Switzerland, August 21-24, 1978, V. 3, Ed. T. N. Veziroglu and W. Seifritz (1978).

11. Darriet, B., Pezat, A., Hbika, A, and Hagenmuller, P. Int. J. Hydrogen Energy, V. 5 (1980).

* U. S. GOVERNMENT PRINTING OFFICE 1982 381-060/4115